NON-CODING RNA REGULATION OF COLON CANCER STEM CELL FATE AND METASTASIS

A Dissertation

Presented to the Faculty of the Graduate School

of Cornell University

In Partial Fulfillment of the Requirements for the Degree of

Doctor of Philosophy

by

Lihua Wang

August 2017

NON-CODING RNA REGULATION OF COLON CANCER STEM CELL FATE AND METASTASIS

Lihua Wang, PhD
Cornell University, 2017

ABSTRACT

Colorectal cancer (CRC) is a leading cause of cancer related death. Colon cancer stem cells (CCSCs) play important roles in CRC tumorigenesis and metastasis. The role of non-coding RNAs such as microRNAs and long non-coding RNAs (lncRNAs) in regulating cancer progression and stem cell renewal and differentiation are being increasingly appreciated. The aim of my study is to understand how non-coding RNAs regulate CRC initiation and metastasis.

In Chapter 1, we identified that Lnc34a, a previously unidentified LncRNA, is enriched in CCSCs to create a spatial imbalance in microRNA miR-34a expression, leading to the initiation of asymmetric cell division. Lnc34a recruits Dnmt3a via PHB2 and HDAC1 to methylate and deacetylate the miR-34a promoter simultaneously, hence epigenetically silencing miR-34a expression independent of its upstream regulator p53. Lnc34a levels affect CCSC self-renewal and colorectal cancer (CRC) growth in xenograft models. Lnc34a is upregulated in late-stage CRCs, contributing to epigenetic miR-34a silencing and CRC proliferation.

In Chapter 2, we describe that miR-34a regulates asymmetric division of normal intestinal stem cells (ISCs). Proinflammatory stress triggers asymmetric division of ISCs that normally undergo symmetric division. Silencing of miR-34a in ISCs inhibits asymmetric

division and increases inflammation-induced ISC proliferation. These findings suggest that miR-34a provides a safeguard mechanism against excessive stem cell proliferation under inflammation, which is common during tumorigenesis.

In Chapter 3, we demonstrate that miR-34a deficiency leads to colon tumorigenesis after *Citrobacter rodentium* infection. miR-34a targets both immune and epithelial cells to restrain inflammation-induced reparative regeneration. miR-34a targets the Interleukin 6 receptor (IL-6R) to suppress T helper 17 (Th17) cell differentiation, targets the Interleukin 23 receptor (IL-23R) to block Th17 cell expansion, targets chemokine CCL22 production to hinder Th17 cell recruitment to the colon epithelium, and targets the Interleukin 17 receptor D (IL17RD) in colon stem cells to inhibit IL17-induced stem cell proliferation. This study highlights the importance of microRNAs in protecting tissue integrity during pro-inflammatory response despite their lack of function in regular tissue homeostasis.

In Chapter 4, we show that the microRNA miR-1269a promotes CRC metastasis and forms a positive feedback loop with TGF-β signaling. miR-1269a is upregulated in late-stage CRCs and strongly associated with risk of CRC relapse and metastasis. Consistent with clinical observations, miR-1269a significantly increases the ability of CRC cells to invade and metastasize *in vivo*. TGF-β activates miR-1269 via Sox4, while miR-1269a enhances TGF-β signaling by targeting Smad7 and HOXD10, hence forming a positive feedback loop to promote metastasis. Stage II CRC patients with high miR-1269a expression in resected tumors have significantly higher rate of relapse and worse prognosis. Our findings suggest that miR-1269a is a potential marker to guide adjuvant chemotherapy decisions for CRC patients and a potential therapeutic target to deter metastasis.

BIOGRAPHICAL SKETCH

Lihua Wang was born in the city of Xiangcheng in China's central Henan province. As a child, Lihua coped with the difficulties of being raised in an impoverished household and learned how to help the family to overcome their difficulties. She worked in the field planting wheat, corn, soybean and potatoes while also taking care of the goats and pigs at home. Through these experiences, she built a diligent, independent and perseverant character which helped her to overcome future challenges. Also, she realized that only by gaining knowledge and obtaining an education she could improve her quality of life and the quality of life of her family.

Through hard work and moral support from her entire family, Lihua was admitted to Dalian University of Technology to study biochemical engineering. She was ranked sixth out of 210 peers, was recommended to continue her education in graduate school, and got an exemption from the entrance examination and tuition fees. She graduated with both bachelor's and a master's degrees in biochemical engineering in July 2004.

After graduation, she first worked at TIANGEN, a biotech company in Beijing. She developed a peptide synthesis platform and various real-time PCR related products. In recognition of her great performance, she was awarded the "Excellent Employee of the Year" award, the only person in the R&D department to receive such an honor.

From 2007 to 2009, Lihua worked as an operational director at Quintara Bioscience, a Californian sequencing company. Her family then moved to Ithaca, New York at the end of 2009. During 2010 to 2011, she worked as a lab technician at Cornell University before joining Dr. Xiling Shen's laboratory as a PhD student in the Department of Biological and

Environmental Engineering at Cornell University. She focused her research on the roles of non-coding RNA (microRNA and long non-coding RNA) in colon cancer tumorigenesis and metastasis.

Lihua would like to thank the PhD program at Cornell University for her academic training, which helped her learn how to articulate scientific ideas and perform rigorous scientific research. She also learned to mentor undergraduate students throughout her PhD studies. Lihua will continue to work forward to an independent academic career after her PhD experience.

To my family, advisor, colleagues and friends for their endless love and support

ACKNOWLEDGMENTS

I would like to express my gratitude to all those who have helped me in my life. First and foremost, I would like to thank my advisor, Professor Xiling Shen, for his mentorship throughout my graduate study. He inspired my passion to pursue the research in an academic lab. He offered me valuable suggestions and encouragement to overcome the difficulties that occurred during my research. I especially appreciate his patience. While preparing research manuscripts for publication, he has spent an incredible amount of time reading and editing each word and providing me constructive advice. Finally, I thank him for his generous financial support, allowing me to finish the research.

I would also like to thank Professor Robert Weiss, Professor Andrew Grimson and Professor Minglin Ma for serving on my graduate committee. Their generous advice, suggestions, and comments have contributed greatly to my research progress.

My husband Pengcheng Bu has been my great supporter throughout my PhD study. He constantly encouraged me to pursue my academic career. When I gave birth to my second son in the middle of my graduate studies, he was extremely supportive for me to complete my PhD study.

I have learned a lot from the members of the Shen lab. I give my deep thanks to Nikolai Rakhilin, who always sacrifice his own time to help everyone. During my PhD study, he not only spent a lot of his time helping me order reagents but also helped me with my writing and presentation. I also thank Kai-Yuan Chen for helping me with the computational work, including RNA-seq, TCGA, and ATAC-seq analyses. I would like to thank Preetish K. L. Murthy for helping me with histology work and sharing reagents with

me. Additionally, I would like to thank Kun Xiang, Yitian Xu, Yiwei Ai, and Robert Mince who have worked closely with me and contributed to my study.

I feel proud of all the undergraduate students who I have mentored or worked with over the past five years. Sara King (BS, Biological Science, Cornell University) demonstrated exceptional work ethic and research talents while working closely with me for three years. Gary Zhou (BS, Biological and Medical Engineering, Duke University) was an amazing undergraduate student and has helped me significantly with my scientific research. Both impressed me with their strong commitment to research in our lab despite huge pressure from endless homework and classes.

TABLE OF CONTENTS

BACKGROUND

1 Colorectal cancer (CRC)

Colorectal cancer (CRC) is the third most commonly diagnosed cancer and the fourth leading cause of cancer-related death worldwide. There are more than one million new cases diagnosed annually, and the 5-year survival rate for metastatic CRC is around 14% [1]. The rate of CRC incidence continues to rise. New cases of CRC are estimated to increase by more than 2.2 million by 2030 [2]. There are unmet needs to improve our understanding of the mechanism of CRC tumorigenesis and metastasis.

CRC progress through sequential genetic mutations such as APC, KRAS and p53 [3]. As mutations accumulate, adenomas turn into invasive carcinomas, then metastasize to distal organs such as the liver and lung. The role of transformed stem cells in CRC tumorigenesis has been demonstrated [4]. A growing body of evidence also supports the theory that chronic inflammation plays an important role in CRC initiation [5].

Non-coding RNAs (ncRNAs) occupy the bulk of the human genome. Increasingly, studies have shown that non-coding RNAs play important role in the regulation of many diseases including cancer initiation and metastasis. Many ncRNAs serve as prognostic markers for cancer, and some microRNA mimics or inhibitors are currently in clinical trials to test their efficacy as chemotherapeutic agents [6]. Understanding the roles of colon stem cells, inflammation, and ncRNAs in CRC may lead to future CRC prevention and therapies.

2 Colon Stem cell and CRC

Intestine crypt

The small intestine and colon are lined with a single layer of epithelial cells. The intestinal epithelium is one of the most dynamic and fastest regenerating tissues in the body, replacing itself every 3 – 5 days. The intestinal crypt has a tubular shape and harbors stem cells and their proliferating progeny, which are responsible for driving epithelial homeostasis and regeneration. Epithelial regeneration relies on a small population of adult stem cells at the crypt base intercalated with Paneth cells, which continuously generate highly proliferating transit-amplifying (TA) cells that occupy the remainder of the crypt [7, 8].

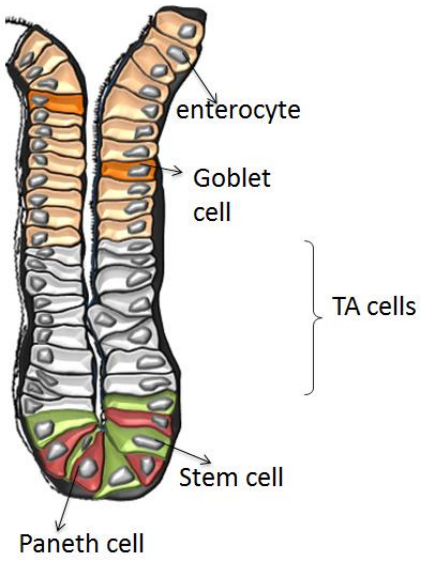

Figure 1. the organization of epithelium in the intestine [8].

The nascent TA cells differentiate into various absorptive or secretory cell lineages on the villi such as enterocytes, tuft cells, goblet cells and enteroendocrine cells. These differentiated cells migrate upwards towards the base of the villi. Paneth cells are the only differentiated intestinal cell type that does not move upward out of the crypt but instead migrates downward to reside at the bottom of the crypt for up to 6-8 week [7, 8].

Intestine/colon stem cell niche

The activity and function of intestinal stem cells (ISCs) are regulated by factors produced by neighboring Paneth cells. These Paneth cells, found in close association with the Leucine-rich repeat-containing G-protein coupled receptor 5 (Lgr5) + ISCs at the crypt base, provide an important source of various niche factors including epidermal growth factor (EGF), Wnt3A, and Notch ligand [9]. Recent studies suggest that Paneth cells are not the sole niche component of ISCs. Ablation of Paneth cells by Diphtheria toxin receptor (DTR) did not affect crypt architecture, maintenance, or proliferation of ISCs [10]. It was also reported that lack of Wnt3, which is normally secreted by Paneth cells to support intestinal stem cell self-renewal, could not block the maintenance of intestinal stem cells in mice. This observation indicated the existence of redundant, non-epithelial sources of Wnt and other key niche signals [10]. Recent studies indicate that the stroma cells located beneath the intestinal crypts may contribute to the maintenance of the intestinal/colon stem cell niche for its self-renewal. For example, IL-22, produced by RORϒt + innate lymphoid cells in the intestine's lamina propria, was shown to maintain epithelial integrity and protect stem cells against damage which plays important role in graft-versus-host disease [11]. Additionally, IL-22 was confirmed to promote organoid growth by activating the Stat3 pathway in Lgr5+ ISCs and by signaling to stem cells that express the IL-22 receptor [11].

Paneth cells are absent from the colon, and the colonic stem cell niche is poorly characterized. Using multicolor, fluorescence-activated cell sorting technology and gene expression analysis of selected populations of single cells, the Clark lab found that cKit/CD117+ goblet cells expressed Dll1, Dll4, and epidermal growth factor analogously

to Paneth Cells. Additionally, goblet cells formed a regular pattern with Lgr5+ stem cells at the crypt base, like the organization of the intestinal crypt. Based on these findings, cKit/CD117+ goblet cells probably provide niche components for Lgr5+ stem cells [12]. However, the major Wnt source in the colon has yet to be identified.

Colon cancer stem cell

Cancer stem cells are a small population of cancer cells that retain some of the phenotypic characteristics of normal stem cells, including the abilities to self-renew and to differentiate into new progenies. Cancer stem cells could originate from the accumulation of mutations during stem cell development [13] or from mutations in adult stem cells or projector cells [14]. Differentiated tumor cells might also become cancer stem cells by dedifferentiation [15].

Although it is still largely unclear, it has been suggested that mutations, which occur in normal intestine/colon stem cells, cause the stem cells to become malignant. The mutant stem cells then divide symmetrically or asymmetrically to generate other cancer stem cells or differentiated progenies for tumor progression. For example, the deletion of APC in Lgr5+ intestine/colon stem cells caused stem cell transformation and the development of microadenoma. In contrast, the loss of APC in a transit-amplifying cell rarely causes adenoma formation [3]. Specific markers have been identified in colon cancer stem cells including CD133, CD44, and ALDH1 [16-19]. These markers are correlated with stem cell phenotypes such as self-renewal, differentiation and tumorigenesis.

Cancer stem cells can initiate and sustain cancer progression. Many cancer stem cells are resistant to chemotherapy and persist in the tumor mass even after tumor regression, leading to tumor relapse and metastasis [20]. Therefore, understanding cancer stem cells

and developing new therapeutic approaches will benefit patient survival and improve quality of life.

Symmetric division and asymmetric division

Stem cells can divide symmetrically to generate two stem cell daughters or asymmetrically to generate one stem cell and one differentiated cell. By using asymmetric division, stem cells can maintain a constant number of stem cells to prevent overgrowth of the stem cell population. Thus, making asymmetric division necessary to maintain tissue homeostasis. During embryogenesis and wound recovery, the stem cells utilize a symmetric division strategy to rapidly proliferate instead of their asymmetric strategy used to maintain healthy, developed tissue. By dynamically switching between asymmetric and symmetric division strategies, the stem cell population can respond to a wider variety of conditions [21]. Therefore, stem cells use a symmetric division strategy to generate two daughter cells which can generate more stem cells and differentiated cells.

Asymmetric division as tumor suppressor

Stem cells proliferate via symmetric division, which doubles their number after each division. However, it increases the risk of tumorigenesis. On the other hand, asymmetric division does not increase the number of stem cells, hence reducing the risk. Drosophila neuroblasts undergo asymmetric division to keep the self-renewal and tissue homeostasis under the regulation of PINS, aPKC and lethal giant larvae (lgl) [22]. Once this regulatory machine is disrupted, neuroblasts switch from asymmetric division to symmetric division and can form tumors [22, 23]. After receiving mutated copies of *raps, Numb, Pros* or *Mira* brought in Larval brains transplantation, neuroblast division changed

from asymmetrical to symmetrical. Neuroblast division alteration caused about 20% of the brains to develop tumors [23]. Asymmetric division also occurs in other human cancer types including breast, glioma, colorectal, and lung cancer [24-28]. Furthermore, asymmetric division frequency is negatively correlated with their proliferative capacity [29].

miR-34a regulates the balance between asymmetry and symmetry in CCSCs

Our group previously discovered that CCSCs undergo both symmetric and asymmetric division [30]. miR-34a expression levels balance cell division mode and tumorigenic capability. A low miR-34a level increases the frequency of symmetric division, promotes CCSC self-renewal, and leads to tumor formation and growth. Analysis of CCSCs from different stages of colon cancer showed that cancer stem cells from the early stages of colon cancers have higher miR-34a expression, which leads to a higher frequency of asymmetric cell division.

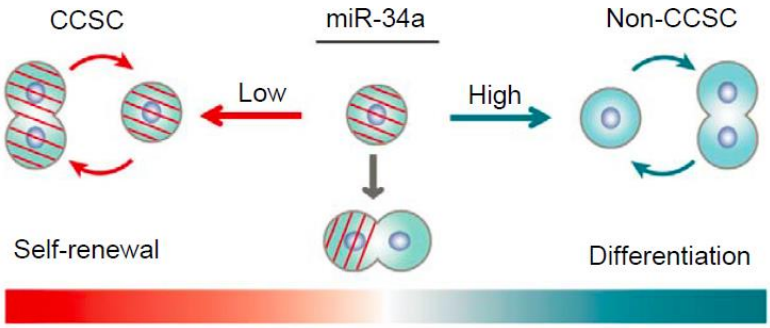

Figure 2. miR-34a regulates CCSC fate [30].

In contract, cancer stem cells from late stages of colon cancers display the opposite trend. Mechanistically, miR-34a directly targets Notch1 to generate a bimodal Notch1 distribution, which produces binary cell fate decisions [30]. However, it is still unknown

whether normal intestine/colon stem cells divide asymmetrically in certain conditions and whether miR-34a regulates normal stem cell division as it does in CCSCs.

3 Inflammation and CRC

Chronic inflammation has been regarded as one of the most significant risk factors in CRC development [5, 31]. Patients with inflammatory bowel diseases (IBD) appear to have a high risk for developing colitis-associated CRC (CAC) with high mortality rate [32]. Although the clinical presentations of IBD usually do not show a clear onset of cancer, the fundamental role of inflammation in CAC progress can be inferred from clinical samples that show the association of tumor-associated inflammation and early stage cancer development in the gut [33].

Th17 cell in CRC

Inflammation often activates T helper cells including Th1, Th2 and Th17 cells [34]. Different T helper cells have distinct roles in their contribution to colon cancer progression. Systemic analysis of T helper cell enrichment and CRC prognosis revealed that CRC patients with high Th17 cell enrichment in CRC had a poor prognosis. In contrast, enrichment of Th1 cells benefits the patient survival. However, Th2 levels had little prognostic value [35]. Th17 cells were first identified in 2005. Since then, Th17 cells have been revealed to have significant roles in the pathogenesis of inflammatory and autoimmune diseases [36]. Recent studies have shown that Th17 cells are also heavily involved in the regulation of tumorigenesis. Th17 cells have been found in many different types of human tumors such as breast cancer [37], colon cancer [38], and liver cancer [39]. The level of tumor infiltrating Th17 cells is closely correlated with tumor progression and prognosis.

In mice, IL-6 and TGF-ß initiate the differentiation of CD4+ T cells into Th17 cells. IL-23 finalizes the Th17 cell differentiation process and maintains the differentiated Th17 cells [40]. Th17 cells mediate inflammatory responses through selective migration and accumulation at specific sites. Th17 cells express chemokine receptors such as CCR4 and CCR6. Many cells including tumor cells secrete the corresponding chemokines and attract Th17 cells to their sites [41, 42]. For example, cervical cancer secretes CCL20 (the ligand of CCR6) and CCL22 (the ligand of CCR4), which recruits TH17 cells in the cervical cancer sites and promote cancer growth [43].

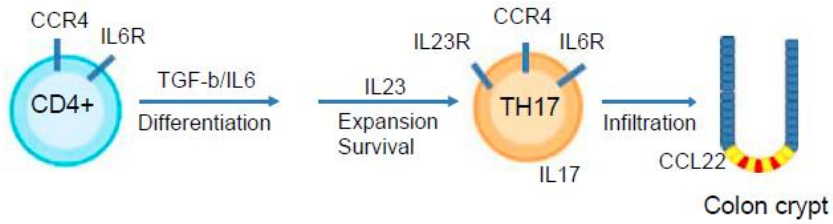

Figure 3. Th17 cell differentiation and infiltration.

IL-17 in CRC

Th17 cells secrete various cytokines including IL-17A, IL-17F, IL2 and TNFα [1]. Among those, IL-17 (IL-17A) is the predominant cytokine that Th17 cells produce, as Th17 cells were named after their production of IL-17. IL-17 belongs to the IL-17 family consisting of six members from ILA17A to IL-17F [44]. IL-17 is an important cytokine that facilitates the host response against bacterial infection due to its role in the induction of other important cytokines, chemokines, and antimicrobial peptides [45]. Increasing recent evidence supports the theory that IL-17 acts as promoter for CRC initiation and progression. For example, ablation of IL-17, either by knockout from the host or treatment with anti-IL-17 antibody, significantly reduces intestinal tumor initiation and progression due to the

disruption of the immune responses [46, 47]. The IL-17 receptor (IL-17R) family includes IL-17RA, IL-17RB, IL-17RC, IL-17RD, and IL-17RE. IL-17 is primarily thought to bind a homodimer of IL-17RA or IL-17RC or a heterodimer of IL-17RA and IL-17RC. IL-17RD was previously thought as an orphan receptor that is not involve in IL-17 mediating signaling. A recent study showed that IL-17RD associates with IL-17RA to mediate IL-17 signaling [48]. However, it is largely unclear whether the interaction of IL-17 and its receptors is altered by varying physiological and pathological conditions in different tissue or cell types.

4 Non-coding RNA and colon cancer

Human genome sequencing revealed that only 2% of the human genome codes for proteins. This leaves 98% of the human genome, which is often called “junk DNA” or “dark genes” [49]. Increasing evidence has shown that these “junk DNA” can be transcribed into microRNA (miRNA), small nucleolar RNA (snoRNA), and long non-coding RNA (lncRNA). Most of these non-coding RNAs play a vital function in regulation of carcinogenesis, stem cell reprogramming, aging, cancer metastasis, and metabolism [49]. Several non-coding RNAs have been identified as biomarkers for diagnosis of disease. Specifically, miR-34a mimics has entered phase 2 clinical trials after the first demonstration of its anticancer activity in 2002 [50]. The rapid progress from discovery to application reflects its importance in human cancer.

miRNA

miRNAs are short non-protein coding RNA containing19-25 nucleotides. miRNA genes are estimated to account for 2-5% of the human genome, but regulate up to 20% of all human genes [49]. The sequences are first transcribed by Pol II/III to form a pri-miRNA,

which contains hundreds of nucleotides forming a stem and a terminal loop structure with flanking segments. Next, pri-miRNA is cleaved into pre-miRNA by the Drosha protein complex. Pre-miRNA is a hairpin RNA around 60-70bp long with 2bp overhangs at its 3' end. Pre-miRNA is then transported from the nucleus to the cytoplasm by exportin-5. A cytoplasmic endonuclease RNase III, Dicer, helps generate a miRNA duplex containing the mature miRNA guide and its complementary passenger strand (miRNA*). The left single strand is integrated into the RNA-induced silencing complex (RISC), a ribonucleoprotein effector containing a catalytic endonuclease core, an Argonaute protein, and binds to the cognate site within the 3`-untranslated regions (3UTR) of the targeted mRNA. The targeted mRNA will be degraded or silenced when the seed region (the 5`-end region of mature miRNA, around 6-8bp) of mature miRNA is complementarily matched with the 3 UTR of mRNA [50]. Increasing evidence has shown that miRNAs exert an important influence on cell development, metabolism, and carcinogenesis [51].

miRNAs in CRC

miRNAs have shown great promise for clinical applications. Due to their stability and robust expression pattern, miRNA has been used as biomarkers and prognostic indicators [52]. Many miRNAs have been discovered to be associated with CRC development, metastasis, and invasion in the past decades. For example, the Let-7 family targets the oncogenes including KRAS, c-Myc, CDC34, CDC25A, CDK6, HMGA2, Lin28, and Lin28b to inhibit migration, invasion, and angiogenesis [52, 53]. miR-21 is one of the more famous oncogenes. High miR-21 expression is correlated with the clinical CRC stage and is markedly increased in chemotherapy-resistant colon cancer. miR-21 also modulates stemness in CRC by regulating TGF-ßR2 [54] and targets PTEN and PDCD4

to promote tumor progression, invasion, and metastasis [55]. miR-21 is a candidate biomarker for advanced CRC diseases [54, 55].

miR-34a

miR-34a belongs to the miR-34 family that consists of three members: miR-34a, miR-34b and miR-34c. miR-34a is transcribed from the human chromosome 1. In contrast, miR-34b and miR-34c are transcribed from the same primary transcript on the human chromosome 11 [50, 56]. miR-34a is widely expressed in the body, e.g., in the brain, while miR-34b and miR-34c are mainly expressed in the lungs [56]. The miR-34 family is highly conserved throughout evolution [56].

upregulated by p53, miR-34a is a key tumor suppressor. By silencing targets such as c-Met, Bcl-2, MDM4 and E2F3, miR-34a has been proved to play important roles in the regulation of the cell cycle and cell proliferation [57]. In addition, increasing evidence has indicates that miR-34a is also heavily involved in tumor initiation and progression, and stem cell self-renewal and differentiation [58]. We have previously shown that miR-34a is asymmetrically distributed in differentiated daughter cells during colon cancer stem cell (CCSC) division [30]. High levels of miR-34a promoted CCSC differentiation, while inhibition of miR-34a expression enhanced CCSC self-renewal. However, it is completely unclear how miR-34a asymmetric distribution is regulated. Although perturbation of p53 expression level could alter CCSC division, p53 is distributed symmetrically during CCSC division, suggesting other factors may play role in regulation of miR-34a distribution.

miR-34a expression is also epigenetically regulated. It has been reported that miR-34a is silenced in human cancers including breast, lung, colon, kidney, bladder and pancreatic carcinoma because of the methylation of CpG islands in the miR-34a promoter region

[59]. The miR-34a promoter becomes more methylated in late-stage CRC, consistent with its lower expression. However, it is largely unknown how the miR-34a promoter is methylated.

Long non-coding RNA

Long non-coding RNAs (lncRNAs) are non-protein coding transcripts with lengths greater than 200bp. In recent years, lncRNAs have gained widespread attentions because they play important roles in various diseases including tumorigenesis and cancer biology [60]. Expression profiles of lncRNAs have been compared between tumors and their corresponding tissues of origin, which showed marked alteration in all types of cancer [61]. The Cancer Genome Atlas (TCGA) analyzed alterations at transcriptional, genomic, and epigenetic levels of lncRNAs and protein-coding genes in 5,037 human tumor specimens across 13 cancer types, and found that lncRNAs were highly cancer-type specific compared with protein-coding genes [61]. Therefore, lncRNAs may serve as potential diagnostic and prognostic biomarkers. Elucidation of lncRNA-related functions and mechanisms will increase our understanding of cancer.

LncRNAs play important roles in the regulation of tumorigenesis and tumor progression. For example, HOTAIR lncRNA targets PRC2 to alter histone H3 lysine 27 methylation, leading to increased cancer invasiveness and metastasis [62]. Currently, high expression of HOTAIR has been associated with poor prognosis in breast cancer [62], liver [63], colorectal cancer [64], gastrointestinal cancer [65], and pancreatic cancer [66]. MALAT1 (metastasis-associated lung adenocarcinoma transcript) is highly associated with lung cancer metastasis [67]. Mechanistically, MALAT1 alters the activity of the polycomb2 protein to active the target genes from a repressive status. Activation of these target

genes drives tumor growth and metastasis. LincRNA-p21 can serve as a repressor in p53-dependent transcriptional responses through interaction with heterogeneous nuclear ribonucleoprotein K (hnRNP-K), which explains why p53 activation cannot induce tumor cell apoptosis [68].

LncRNA and epigenetics

Epigenetic regulation seems to be an important mechanism for lncRNA to regulate gene expression. DNA in the form of chromatin can be packaged around histone proteins in the nucleus, and these histones can be modified by acetylation, methylation, sumoylation, and ubiquitylation. Histone modifications induce structural variations in chromatin (i.e. conversion of loosely-packed euchromatin to tightly-collapsed heterochromatin) and affect gene expression through altered chromatin accessibility. Futhermore, the effects of this process can persist for several generations independent of DNA sequence.

The major function of lncRNAs is to recruit protein factors for the regulation of chromatin by methods such as DNA methylation and histone modifications. LncRNAs may function in cis strategies, acting on linked genes near the RNA synthesis sites. Alternatively, lncRNAs can act in trans strategies, regulating genes located in distant domains or chromosome. It has been shown that lncRNAs interact with chromatin-modifying complexes [69, 70]. For example, HOTAIR and Xist/RepA regulate gene expression by recruiting PRC2 [71]. LncRNA Air interacts with H3K9 histone methyltransferase G9a to modulate gene activity [72]. LncRNAs can also act as a scaffold that can assemble multiple proteins onto the promoter of the gene, allowing the complex to modify the chromatin [73]. For example, LncRNA HOTAIR binds polycomb repressive complex 2 (PRC2) on its 5’ domains and binds LSD1/CoREST/REST complex on its 3’ domains to

tether these two distinct complexes for a RNA-mediated assembly of PRC2 and LSD1 to guide histone H3 lysine 27 methylation and lysine 4 demethylation for HOX silence [73]. Beyond histone modifications, lncRNAs can also epigenetically regulate DNA methylation at CpG dinucleotides, which is crucial for the stable repression of genes. LncRNA Tsix represses Xist by recruiting Dnmt3a to methylate and silence the Xist promoter [74]. Kcnq1ot1 recruits Dnmt1 to affect the methylated regions [75]. Besides recruiting epigenetic complexes to regulate gene expression, lncRNAs can function as molecular decoys for transcription factors to affect the process of transcription by competing for transcription factor binding sites or by influencing the cellular localization of transcriptional factors (TFs) [76].

Crosstalk between lncRNA and microRNA

Simultaneous dysregulation of lncRNAs, miRNAs, and their downstream targets has been observed in multiple types of cancers [77]. For example, MALAT1 has two binding sites for miR-125b. MALAT1 is negatively correlated with miR-125b in bladder cancer. Overexpression of miR-125b can inhibit MALAT1 expression while simultaneously blocking cell proliferation, migration and inducing apoptosis. Also, MALAT1 can reverse the roles of miR-125b mimics in bladder cancer [77]. LncRNA-ROR (Regulator of Reprogramming, core regulator of hESC self-renewal and differentiation) can bind to miR-145 to suppress the latter's function. LncRNA-ROR can reverse microRNA-mediated reprogramming core TFs' suppression including Nanog, Sox2 and Oct4 [78]. Another example is that lncRNA SIRT1-AS can bind to the SIRT1's 3-UTR, which blocks miR-29c binding sites on the SIRT1 [79]. The interaction will increase the expression level of SIRT1 and subsequently increase cell proliferation and survival. miR-34a has also been reported

to directly target HOTAIR to suppress prostate cancer progression [80]. LncRNA H19 has been found to promote epithelial to mesenchymal transition (EMT) in multiple cancer types including colorectal, ovarian, and gastric cancers. It has been suggested that H19 reduces the activity of miR-138 and miR-200a in colon cancer [81].

REFERENCES

1. Cancer Facts & Figures 2017 - American Cancer Society
2. Arnold, M., et al., Global patterns and trends in colorectal cancer incidence and mortality. Gut, 2017. 66(4): p. 683-691
3. Drost, J., et al., Sequential cancer mutations in cultured human intestinal stem cells.Nature, 2015. 521(7550): p. 43-7.
4. Barker, N., et al., Crypt stem cells as the cells-of-origin of intestinal cancer. Nature, 2009. 457(7229): p. 608-611.
5. Wang, K. and M. Karin, Tumor-Elicited Inflammation and Colorectal Cancer. Adv Cancer Res, 2015. 128: p. 173-96.
6. Christopher, A.F., et al., MicroRNA therapeutics: Discovering novel targets and developing specific therapy. Perspect Clin Res, 2016. 7(2): p. 68-74
7. van der Flier, L.G. and H. Clevers, Stem cells, self-renewal, and differentiation in the intestinal epithelium. Annu Rev Physiol, 2009. 71: p. 241-60.
8. Chen KY, Srinivasan T, Tung KL, et.al., A Notch positive feedback in the intestinal stem cell niche is essential for stem cell self-renewal. Mol Syst Biol. 2017 Apr 28;13(4):927. doi: 10.15252/msb.20167324.
9. Sato, T., et al., Paneth cells constitute the niche for Lgr5 stem cells in intestinal crypts. Nature, 2010.
10. Farin, H.F., J.H. Van Es, and H. Clevers, Redundant Sources of Wnt Regulate Intestinal Stem Cells and Promote Formation of Paneth Cells. Gastroenterology, 2012. 143(6): p. 1518-+
11. Lindemans, C.A., et al., Interleukin-22 promotes intestinal-stem-cell-mediated epithelial regeneration. Nature, 2015. 528(7583): p. 560-4.
12. Rothenberg, M.E., et al., Identification of a cKit(+) colonic crypt base secretory cell that supports Lgr5(+) stem cells in mice. Gastroenterology, 2012. 142(5): p. 1195-1205 e6.
13. Wang, Y., et al., Expression of mutant p53 proteins implicates a lineage relationship between neural stem cells and malignant astrocytic glioma in a murine model. Cancer Cell, 2009. 15(6): p. 514-26.
14. Burgess, D.J., STEM CELLS Competitive behaviour of cancer mutations. Nature Reviews Cancer, 2014. 14(1)
15. Friedmann-Morvinski, D. and I.M. Verma, Dedifferentiation and reprogramming: origins of cancer stem cells. Embo Reports, 2014. 15(3): p. 244-253.
16. Ginestier, C., et al., ALDH1 is a marker of normal and malignant human mammary stem cells and a predictor of poor clinical outcome. Cell Stem Cell, 2007. 1(5): p. 555-67.
17. Kozovska, Z., V. Gabrisova, and L. Kucerova, Colon cancer: Cancer stem cells markers, drug resistance and treatment. Biomedicine & Pharmacotherapy, 2014. 68(8): p. 911-916.
18. Sahlberg, S.H., et al., Evaluation of Cancer Stem Cell Markers CD133, CD44, CD24: Association with AKT Isoforms and Radiation Resistance in Colon Cancer Cells. Plos One, 2014. 9(4).

19. Shmelkov, S.V., et al., CD133 expression is not restricted to stem cells, and both CD133+ and CD133- metastatic colon cancer cells initiate tumors. J Clin Invest, 2008. 118(6): p. 2111-20.
20. Acharyya, S., et al., A CXCL1 paracrine network links cancer chemoresistance and metastasis. Cell, 2012. 150(1): p. 165-78.
21. Inaba, M. and Y.M. Yamashita, Asymmetric stem cell division: precision for robustness. Cell Stem Cell, 2012. 11(4): p. 461-9.
22. Lee, C.Y., K.J. Robinson, and C.Q. Doe, lgl, pins and aPKC regulate neuroblast self-renewal versus differentiation. Nature, 2006. 439(7076): p. 594-598.
23. Caussinus, E. and C. Gonzalez, Induction of tumor growth by altered stem-cell asymmetric division in Drosophila melanogaster. Nature Genetics, 2005. 37(10): p. 1125-1129.
24. Pece, S., et al., Biological and molecular heterogeneity of breast cancers correlates with their cancer stem cell content. Cell, 2010. 140(1): p. 62-73.
25. Pine, S.R., et al., Microenvironmental modulation of asymmetric cell division in human lung cancer cells. Proc Natl Acad Sci U S A, 2010. 107(5): p. 2195-200.
26. Dey-Guha, I., et al., Asymmetric cancer cell division regulated by AKT. Proc Natl Acad Sci U S A, 2011.
27. Lathia, J.D., et al., Distribution of CD133 reveals glioma stem cells self-renew through symmetric and asymmetric cell divisions. Cell Death Dis, 2011. 2: p. e200.
28. O'Brien, C.A., et al., ID1 and ID3 Regulate the Self-Renewal Capacity of Human Colon Cancer-Initiating Cells through p21. Cancer Cell, 2012. 21(6): p. 777-92.
29. Bu, P., et al., Asymmetric division: a marker for cancer stem cells in early stage tumors? Oncotarget, 2013. 4(7): p. 948-9.
30. Bu, P., et al., A microRNA miR-34a-Regulated Bimodal Switch Targets Notch in Colon Cancer Stem Cells. Cell Stem Cell, 2013. 12(5): p. 602-15.
31. Feagins, L.A., R.F. Souza, and S.J. Spechler, Carcinogenesis in IBD: potential targets for the prevention of colorectal cancer. Nature Reviews Gastroenterology & Hepatology, 2009. 6(5): p. 297-305.
32. Lakatos, P.L. and L. Lakatos, Risk for colorectal cancer in ulcerative colitis: Changes, causes and management strategies. World Journal of Gastroenterology, 2008. 14(25): p. 3937-3947.
33. Grivennikov, S.I., F.R. Greten, and M. Karin, Immunity, Inflammation, and Cancer. Cell, 2010. 140(6): p. 883-899.
34. Alex, P., et al., Distinct Th1/Th2/Th17 profiles identified in gene and cytokine expression signatures from patients with inflammatory bowel disease. Gastroenterology, 2007. 132(4): p. A698-A699.
35. Tosolini, M., et al., Clinical impact of different classes of infiltrating T cytotoxic and helper cells (Th1, th2, treg, th17) in patients with colorectal cancer. Cancer Res, 2011. 71(4): p. 1263-71.
36. Tesmer, L.A., et al., Th17 cells in human disease. Immunological Reviews, 2008. 223: p. 87-113.
37. Zhu, X., et al., IL-17 expression by breast-cancer-associated macrophages: IL-17 promotes invasiveness of breast cancer cell lines. Breast Cancer Res, 2008. 10(6): p. R95.

38. Su, X., et al., Tumor microenvironments direct the recruitment and expansion of human Th17 cells. J Immunol, 2010. 184(3): p. 1630-41.
39. Zhang, J.P., et al., Increased intratumoral IL-17-producing cells correlate with poor survival in hepatocellular carcinoma patients. J Hepatol, 2009. 50(5): p. 980-9.
40. Dong, C., Regulation and pro-inflammatory function of interleukin-17 family cytokines. Immunol Rev, 2008. 226: p. 80-6.
41. Lim, H.W., et al., Human Th17 cells share major trafficking receptors with both polarized effector T cells and FOXP3+ regulatory T cells. J Immunol, 2008. 180(1): p. 122-9.
42. Acosta-Rodriguez, E.V., et al., Surface phenotype and antigenic specificity of human interleukin 17-producing T helper memory cells. Nat Immunol, 2007. 8(6): p. 639-46.
43. Yu, Q., X.M. Lou, and Y. He, Preferential recruitment of Th17 cells to cervical cancer via CCR6-CCL20 pathway. PLoS One, 2015. 10(3): p. e0120855.
44. Rouvier, E., et al., CTLA-8, cloned from an activated T cell, bearing AU-rich messenger RNA instability sequences, and homologous to a herpesvirus saimiri gene. J Immunol, 1993. 150(12): p. 5445-56.
45. Kao, C.Y., et al., IL-17 markedly up-regulates beta-defensin-2 expression in human airway epithelium via JAK and NF-kappa B signaling pathways. Journal of Immunology, 2004. 173(5): p. 3482-3491.
46. Oshiro, K., et al., Interleukin-17A is involved in enhancement of tumor progression in murine intestine. Immunobiology, 2012. 217(1): p. 54-60.
47. Chae, W.J., et al., Ablation of IL-17A abrogates progression of spontaneous intestinal tumorigenesis. Proceedings of the National Academy of Sciences of the United States of America, 2010. 107(12): p. 5540-5544.
48. Zhili, R., et al., IL-17RD (Sef or IL-17RLM) interacts with IL-17 receptor and mediates IL-17 signaling. Cell Research (2009) 19:208–215.
49. Forman, J.J., A. Legesse-Miller, and H.A. Coller, A search for conserved sequences in coding regions reveals that the let-7 microRNA targets Dicer within its coding sequence. Proceedings of the National Academy of Sciences of the United States of America, 2008. 105(39): p. 14879-14884.
50. Li, X.J., Z.J. Ren, and J.H. Tang, MicroRNA-34a: a potential therapeutic target in human cancer. Cell Death Dis, 2014. 5: p. e1327.
51. Hatfield, S. and H. Ruohola-Baker, microRNA and stem cell function. Cell Tissue Res, 2008. 331(1): p. 57-66.
52. Bouchie, A., First microRNA mimic enters clinic. Nat Biotechnol, 2013. 31(7): p. 577.
53. Yu, F., et al., let-7 regulates self-renewal and tumorigenicity of breast cancer cells. Cell, 2007. 131(6): p. 1109-23.
54. Yu, Y.J., et al., MicroRNA-21 induces stemness by downregulating transforming growth factor beta receptor 2 (TGF beta R2) in colon cancer cells. Carcinogenesis, 2012. 33(1): p. 68-76.
55. Medina, P.P., M. Nolde, and F.J. Slack, OncomiR addiction in an in vivo model of microRNA-21-induced pre-B-cell lymphoma. Nature, 2010. 467(7311): p. 86-90.
56. Concepcion CP1, Han YC, Mu P, et.al., Intact p53-dependent responses in miR-34-deficient mice. PLoS Genet. 2012;8(7): e1002797. doi: 10.1371/journal.pgen.1002797. Epub 2012 Jul 26.

57. Misso, G., et al., Mir-34: a new weapon against cancer? Mol Ther Nucleic Acids, 2014. 3: p. e194.
58. Liu, C. and D.G. Tang, MicroRNA regulation of cancer stem cells. Cancer Res, 2011. 71(18): p. 5950-4.
59. Lodygin, D., et al., Inactivation of miR-34a by aberrant CpG methylation in multiple types of cancer. Cell Cycle, 2008. 7(16): p. 2591-600.
60. Kung, J.T., D. Colognori, and J.T. Lee, Long noncoding RNAs: past, present, and future. Genetics, 2013. 193(3): p. 651-69.
61. Yan, X., et al., Comprehensive Genomic Characterization of Long Non-coding RNAs across Human Cancers. Cancer Cell, 2015. 28(4): p. 529-40.
62. Gupta, R.A., et al., Long non-coding RNA HOTAIR reprograms chromatin state to promote cancer metastasis. Nature, 2010. 464(7291): p. 1071-6.
63. Yang, L., et al., ncRNA- and Pc2 methylation-dependent gene relocation between nuclear structures mediates gene activation programs. Cell, 2011. 147(4): p. 773-88.
64. Kogo, R., et al., Long noncoding RNA HOTAIR regulates polycomb-dependent chromatin modification and is associated with poor prognosis in colorectal cancers. Cancer Res, 2011. 71(20): p. 6320-6.
65. Niinuma, T., et al., Upregulation of miR-196a and HOTAIR drive malignant character in gastrointestinal stromal tumors. Cancer Res, 2012. 72(5): p. 1126-36.
66. Kim, K., et al., HOTAIR is a negative prognostic factor and exhibits pro-oncogenic activity in pancreatic cancer. Oncogene, 2013. 32(13): p. 1616-25.
67. Ji, P., et al., MALAT-1, a novel noncoding RNA, and thymosin beta4 predict metastasis and survival in early-stage non-small cell lung cancer. Oncogene, 2003. 22(39): p. 8031-41.
68. Huarte, M., et al., A large intergenic noncoding RNA induced by p53 mediates global gene repression in the p53 response. Cell, 2010. 142(3): p. 409-19.
69. Khalil, A.M., et al., Many human large intergenic noncoding RNAs associate with chromatin-modifying complexes and affect gene expression. Proc Natl Acad Sci U S A, 2009. 106(28): p. 11667-72.
70. Kanhere, A., et al., Short RNAs Are Transcribed from Repressed Polycomb Target Genes and Interact with Polycomb Repressive Complex-2. Molecular Cell, 2010. 38(5): p. 675-688.
71. Rinn, J.L., et al., Functional demarcation of active and silent chromatin domains in human HOX loci by noncoding RNAs. Cell, 2007. 129(7): p. 1311-23.
72. Nagano, T., et al., The Air noncoding RNA epigenetically silences transcription by targeting G9a to chromatin. Science, 2008. 322(5908): p. 1717-20.
73. Tsai, M.C., et al., Long noncoding RNA as modular scaffold of histone modification complexes. Science, 2010. 329(5992): p. 689-93.
74. Sado, T., Y. Hoki, and H. Sasaki, Tsix defective in splicing is competent to establish Xist silencing. Development, 2006. 133(24): p. 4925-31.
75. Mohammad, F., et al., Kcnq1ot1 noncoding RNA mediates transcriptional gene silencing by interacting with Dnmt1. Development, 2010. 137(15): p. 2493-9.
76. Hung, T., et al., Extensive and coordinated transcription of noncoding RNAs within cell-cycle promoters. Nat Genet, 2011. 43(7): p. 621-9.

77. Han, Y.H., et al., Hsa-miR-125b suppresses bladder cancer development by down-regulating oncogene SIRT7 and oncogenic long non-coding RNA MALAT1. Febs Letters, 2013. 587(23): p. 3875-3882.
78. Wang, Y., et al., Endogenous miRNA sponge lincRNA-RoR regulates Oct4, Nanog, and Sox2 in human embryonic stem cell self-renewal. Dev Cell, 2013. 25(1): p. 69-80.
79. Liu, J., W. Wu, and J. Jin, A novel mutation in SIRT1-AS leading to a decreased risk of HCC. Oncol Rep, 2015. 34(5): p. 2343-50.
80. Chiyomaru, T., et al., Genistein inhibits prostate cancer cell growth by targeting miR-34a and oncogenic HOTAIR. PLoS One, 2013. 8(8): p. e70372.
81. Liang, W.C., et al., The lncRNA H19 promotes epithelial to mesenchymal transition by functioning as miRNA sponges in colorectal cancer. Oncotarget, 2015. 6(26): p. 22513-25.

Chapter 1

A Long Non-Coding RNA Targets MicroRNA miR-34a to Regulate Colon Cancer Stem Cell Asymmetric Division

This section is adapted from the following publication:

Lihua Wang[*], [*], Pengcheng Bu[*], Yiwei Ai, Tara Srinivasan, Huanhuan Joyce Chen, Kun Xiang, Steven M. Lipkin, Xiling Shen. A large non-coding RNA regulates colon cancer stem cell asymmetric division. **eLife**. 2016; 10.7554/eLife.14620.

* co-first author

Author contributions: Lihua Wang, Pengcheng Bu, Steve Lipkin and Xiling Shen conceived the concept, designed the experiments, and co-wrote the manuscript. Steve Lipkin contributed clinical samples. Lihua Wang, Pengcheng Bu and Yiwei Ai performed the molecular experiments and some of the animal-related experiments. Tara Srinivasan performed immunofluorescence on the tissue samples. Kun Xiang and Huanhuan Joyce Chen performed the rest of the animal-related experiments.

INTRODUCTION

A downstream target of p53, the microRNA miR-34a is a well-known tumor suppressor in various types of cancer [1,2]. Among its many functions, miR-34a has been shown to limit self-renewal of cancer stem cells [3,4]. miR-34a mimics such as MRX34 are among the first microRNA mimics to reach clinical trial for cancer therapy [5,6]. Besides cancer, miR-34a has been shown to regulate stem cell differentiation, somatic stem cell reprogramming, cardiac aging, neurodegeneration, ciliogenesis, bone resorption, and metabolism [7-13].

Loss of p53 function can lead to downregulation of miR-34a. However, miR-34a expression also tends to be silenced due to aberrant CpG methylation of its promoter in many types of cancer, including breast, prostate, lung, colon, kidney, bladder, pancreatic, and ovarian cancer [14-16]. Methylation of the miR-34a promoter is inversely correlated with miR-34a expression and is positively correlated with progression of colorectal cancer (CRC) [17]. However, it is completely unclear how miR-34a is silenced by epigenetic modification.

Normal stem cells often divide asymmetrically to produce one daughter cell like itself for self-renewal and another daughter cell unlike itself to go down a path of differentiation [18]. Asymmetric division allows stem cells to maintain self-renewal while generating a heterogeneous population for cellular diversity [19]. Tumor cells are usually heterogeneous and have a wide range of potential for tumorigenesis, proliferation, and metastasis. Recent studies have reported that cancer cells, including colorectal, glioma, lung and breast cancer cells, can also divide asymmetrically, generating progenies with different proliferation capabilities [3, 20-25]. The frequencies of symmetric vs. asymmetric

divisions are associated with cancer proliferation and progression. Disruption of asymmetric division in favor of symmetric self-renewal alters the balance between self-renewal and differentiation, which has been linked to neoplastic transformation and tumor growth [25, 26].

Here, we discovered that a novel lncRNA, Lnc34a, directly targets the miR-34a promoter for epigenetic silencing by recruiting the DNA methyltransferase Dnmt3a via Prohibitin-2 (PHB2) and Histone Deacetylase 1 (HDAC1). Asymmetric distribution of Lnc34a during colon cancer stem cell (CCSC) division leads to asymmetric daughter cell fate. Its suppression leads to differentiation while its abundance leads to CCSC proliferation via symmetric self-renewal. Lnc34a tends to be upregulated in late-stage CRC, associated with miR-34a silencing. The ability of lncRNA to target microRNA provides RNA circuitry more ways to increases the complexity of the regulatory network.

RESULTS

A lncRNA overlapping with miR-34a promoter

We performed RT-PCR with 10 pairs of primers to scan for potential transcripts overlapping the miR-34a promoter and its downstream sequence. A 293-base pair (bp) transcript fragment was amplified. Rapid amplification of cDNA ends (RACE) further identified a full-length, 693bp transcript (Figures 1A and 1B). Northern blot confirmed the existence and size of the transcript in seven CRC cell lines and two colon cancer stem cell (CCSC) lines (Figures 1D, 2A and 2B). The CCSCs were isolated from two early-stage CRC specimen, and were functionally validated by serial sphere formation, tumor initiation, and marker staining [3]. The original frozen stocks from the first passage were used in the study. The transcript is composed of two exons, spanning nearly 15.3 kilobases (kb), and does not contain a valid Kozak sequence. The full-length transcript has no protein coding potential according to the Coding Potential Calculator (CPC) and Coding Potential Assessment Tool (CPAT) [27, 28]. We named the transcript Lnc34a.

To analyze Lnc34a expression in CRC cells, RT-qPCR was performed in 9 commonly used CRC cell and the two CCSC lines. Consistent with the Northern blot measurement, Lnc34a levels were significantly higher in the CCSC sphere cells (Figures 1C and 2C). Cellular fractionation assays show enrichment of Lnc34a in the nuclear fraction (Figures 2D and 2E), and RNA fluorescence in situ hybridization (RNA FISH) indicates that Lnc34a is mainly in the nucleus (Figure 2F). RNA FISH specificity was validated when the same RNA-FISH probe did not detect Lnc34a after Lnc34a was knocked down by lentiviral short-hairpin RNA (shRNA) vectors in CCSC spheres (Figure 3A).

Lnc34a asymmetry

Notably, RNA-FISH showed that a small population among the CCSC sphere cells did not express Lnc34a, although the majority did (Figure 2F). We then separated the sphere cells into two populations based on the expression levels of ALDH1, a CCSC marker [29]. Flow analysis confirmed that ALDH1+ cells also express high levels of CD133, another CCSC marker (Figure 4A). RT-qPCR showed that, in both sphere cultures (CCSC1 and CCSC2), ALDH1+ cells have much higher Lnc34a expression levels than the ALDH1- cells (Figures 5A and 5B). We then performed the pair-cell assay by plating single cells and allowing them to progress through one cell division [30]. α-tubulin staining was used to identify dividing cells (Figure 5C). Co-staining revealed that Lnc34a was asymmetrically distributed and enriched in the ALDH1+ (CCSC) daughter cells, which were also CD133+ (Figures 4B, 4C, 5C and 5D).

Lnc34a asymmetry in dividing cell pairs was confirmed in vivo by RNA-FISH and tubulin staining of xenograft tumors derived from subcutaneously injected CCSCs (Figures 5E and 5F). We investigated Lnc34a asymmetry in 23 early-stage (stage I/II) and 22 late-stage (stage III/IV) human CRC specimens (Table 1). Lnc34a asymmetry in dividing cell pairs is more strongly associated with early-stage CRC, while late-stage CRC mostly has symmetric Lnc34a levels in dividing pairs (Figures 5G and 5H).

To investigate whether Lnc34a regulates CCSC division symmetry, we first knocked down Lnc34a using lentiviral shRNAs, which have been reported to knock down certain nuclear lncRNAs efficiently [31-34]. Among the five tested shRNAs against Lnc34a, two showed efficient suppression of Lnc34a (shLnc34a1 and shLnc34a2; Figure 3B). Lnc34a knockdown decreased asymmetric division while increasing symmetric, ALDH1-/ALDH1-

division (Figure 5I). We then ectopically expressed Lnc34a using lentiviral vectors. Higher level of ectopic Lnc34a was detected in the nucleus than in the cytoplasm (Figure 3C). Ectopic Lnc34a expression also decreased asymmetric division, but increased symmetric, ALDH1+/ALDH1+ division instead (Figure 5J). The phenotype was rescued by ectopic miR-34a expression, suggesting that Lnc34a regulates symmetry through miR-34a (Figure 5J). The same trend was observed with CD133 staining (Figures 4C and 4D). Therefore, ectopic Lnc34a seems to promote symmetric CCSC self-renewal, while Lnc34a silencing promotes differentiation.

Pair-cell BrdU incorporation assay showed that, when cultured in proliferative medium (DMEM with 10% FBS), the Lnc34a+ daughter cell starts incorporating BrdU and enters into the next division immediately, whereas the Lnc34a- daughter cells do not incorporate BrdU (Figure 5K). Therefore, the Lnc34a+ daughter cell has higher proliferative capacity.

Lnc34a enhances CCSC self-renewal and tumorigenesis

Serial sphere propagation assays were performed to evaluate the effect of Lnc34a on CCSC self-renewal. CCSCs containing a control vector exhibited stable sphere formation capability through 3 generations of sphere propagation. Lnc34a knockdown strongly suppressed sphere formation capability, which was completely lost after 3 generations of passage (Figures 6A and 6B). In contrast, ectopic Lnc34a expression increased sphere numbers and sizes significantly. Ectopic miR-34a abrogated the effect of Lnc34a on sphere formation regulation, suggesting that Lnc34a promotes CCSC self-renewal by targeting miR-34a (Figures 6A and 6C).

Next, we used the mouse xenograft model to examine whether Lnc34a influences tumor growth. All five mice in the control group (injected with sphere cells containing the control

vector) developed tumors. However, only three mice injected with sphere cells expressing shLnc34a1 and two mice injected with sphere cells expressing shLnc34a2 formed tumors, which were smaller than those of the control group (Figures 6D and 6E). All 5 mice injected with sphere cells ectopically expressing Lnc34a developed tumors, which were notably bigger than those in the control group. Ectopic miR-34a expression abrogates the effect of ectopic Lnc34a on tumor growth, resulting in similar tumor sizes as the control group (Figures 6F and 6G). Furthermore, we performed FACS on disassociated xenograft tumor cells. Lnc34a knockdown decreased the ALDH1+ CCSC population in the xenograft tumors (Figure 6H), while ectopic Lnc34a enriched the ALDH1+ CCSC population in the tumors (Figure 6I). Taken together, Lnc34a contributes to CCSC self-renewal and tumorigenesis.

Lnc34a suppresses miR-34a expression.

Opposite to Lnc34a, miR-34a is downregulated in ALDH1+ CCSCs and upregulated in ALDH1- non-CCSCs (Figures 7A and 7B). Knockdown of Lnc34a significantly increased miR-34a expression levels, while ectopic Lnc34a expression decreased miR-34a levels (Figures 7C and 7D). Therefore, Lnc34a suppresses miR-34a expression. RNA FISH showed that Lnc34a and miR-34a are mutually exclusive in the same daughter compartment and are present in opposite daughter compartments in more than 70% of CCSC1 and around 80% of CCSC2 dividing pairs (Figures 7E and 7F). On the other hand, we only observed symmetric distribution of p53, the other miR-34a upstream regulator (Figure 8). Therefore, Lnc34a provides a potential mechanism that accounts for asymmetric miR-34a levels in daughter pairs.

Bisulfite sequencing was then performed to evaluate miR-34a promoter methylation in ALDH1+ CCSCs and ALDH1- non-CCSCs isolated from spheres. 93.3% of tested CpG islands were methylated in CCSCs. In contrast, methylation rate was as low as 2.2% in non-CCSCs (Figure 7G). Knockdown of Lnc34a diminished overall miR-34a promoter methylation in sphere cells (Figure 7H), whereas ectopic Lnc34a expression significantly enhanced miR-34a promoter methylation, compared with the control vector (Figure 7I). Besides methylation (Figure 7J), ectopic Lnc34a expression decreased acetylated histones H3 and H4 (Figure 7K). Taken together, the data suggests that Lnc34a silences miR-34a expression in CCSCs by promoting methylation and histone deacetylation of the miR-34a promoter. The effect of ectopic Lnc34a suggests that Lnc34a might act both in cis and in trans, as have been observed for various lncRNAs such as Evf-2, and some cis-acting lncRNAs to act in trans [32, 35-40].

Lnc34a also silences miR-34a in common CRC cell lines. Ectopic Lnc34a expression suppressed miR-34a expression and promoted methylation and deacetylation of the miR-34a promoter in CRC cell lines Caco-2 and HT29 (Figure 9).

Lnc34a, miR-34a, and promoter methylation are correlated with CRC progression.

RT-qPCR performed in 23 early-stage (stage I/II) and 22 late-stage (stage III/IV) CRC specimens showed that Lnc34a expression is correlated with CRC progression. Overall, Lnc34a expression is lower in early-stage CRC and increases in late-stage CRC (Figures 8L and 10A). miR-34a expression follows a reverse trend (Figures 8M and 10A). Consistent with Lnc34a methylation of the miR-34a promoter, bisulfite sequencing revealed that the miR-34a promoter is more methylated in late-stage CRC than in early-stage CRC (Figures 8N and 10B).

Lnc34a interacts with epigenetic regulators

To understand the mechanisms via which Lnc34a regulates miR-34a expression, we performed an RNA pull-down assay with biotin-labeled Lnc34a, followed by mass spectrometry (MS), to search for potential Lnc34a-associated proteins. The DNA methyltransferase Dnmt3a, Histone Deacetylase 1 (HDAC1), and Prohibitin 2 (PHB2) were identified to be associated with Lnc34a (Figure 11A and Table 2). RNA immunoprecipitation (RIP) using specific antibodies against Dnmt3a, HDAC1 and PHB2 further confirmed the interactions (Figure 11B). In contrast, RNA pulldown and RIP did not detect any interaction between Lnc34a and Dnmt1, an enzyme that plays important roles in maintaining methylation during DNA replication (data not shown).

To investigate how Lnc34a interacts with Dnmt3a, HDAC1 and PHB2, we performed RIP while knocking down each of the proteins. Knockdown of PHB2 abolished the interaction between Lnc34a and Dnmt3a but had no effect on the interaction between Lnc34a and HDAC1 (Figure 11C). Knockdown of Dnmt3a did not affect the interaction of Lnc34a with either PHB2 or HDAC1 (Figure 11D). Knockdown of HDAC1 did not interrupt Lnc34a and Dnmt3a interaction and only had limited effect on Lnc34a and PHB2 interaction (Figure 11E). These data suggest that Lnc34a interacts with PHB2 and HDAC1 and recruits Dnmt3a through PHB2.

We then serially truncated Lnc34a and performed RNA pull-down assays to map HDAC1 and PHB2 binding to Lnc34a. The 1-267bp fragment is sufficient to bind HDAC1, and the 560-693bp fragment is sufficient to bind PHB2 (Figure 11F). Interaction between the fragments and their cognate proteins were further validated by the electrophoretic mobility shift assay (EMSA). Incubation of labeled RNA probes Lnc34a:1-267bp with recombinant

HDAC1 and Lnc34a:560-690bp with recombinant PHB2 resulted in specific gel retardation, while unlabeled RNA probes of the same fragments competitively disrupted those binding (Figure 11G). All three fragments are needed for full suppression of miR-34a expression (Figure 11H). Although the 267-560bp fragment does not interact with either HDAC1 or PHB2, the *in vitro* interaction assay shows that it directly binds to the miR-34a promoter (Figure 11I). Therefore, Lnc34a binds to the miR-34a promoter via the 267-560bp sequence and recruits HDAC1 and Dnmt3a/PHB2 via the two flanking (1-267bp and 560-690) sequences (Figure 11J).

We then knocked down PHB2, Dnmt3a, and HDAC1 respectively, followed by RT-qPCR measurements of miR-34a expression. Knockdown of PHB2, Dnmt3a, or HDAC1 upregulated miR-34a expression (Figures 11I-11K). Inhibition of HDAC activity by SAHA and TSA also increased miR-34a expression (Figures 11L and 11M). The data suggest that these epigenetic regulators influence miR-34a expression levels.

DISCUSSION

The abundance of lncRNA in the human genome is being increasingly appreciated, but our understanding of their diverse functions is still lagging [39,41]. We demonstrate that a lncRNA, Lnc34a, can initiate CCSC asymmetric division by targeting miR-34a. Previously, lncRNAs like HOTAIR and Xist have been shown to cause histone H3 lysine 27 methylation or lysine 4 demethylation [42-44]. Here, Lnc34a binds to the miR-34a promoter via its middle fragment, and recruits PHB2/Dnmt3a and HDAC1 via its flanking sequences to methylate and deacetylate the promoter, silencing miR-34a expression. This process reminds us of the ordered steps of protein-mediated DNA methylation—a DNA binding protein first interacts with the promoter, via which DNA methyltransferases are further recruited [45-47].

Lnc34a promotes CCSC self-renewal, and Lnc34a asymmetry leads to cell fate asymmetry in CCSC division. This effect is mediated by miR-34a, which has been shown to target factors of Notch and Wnt signaling pathways, both of which are essential for CCSC self-renewal [3, 48, 49]. In late-stage CRC, Lnc34a expression and miR-34a promoter methylation is upregulated, while miR-34a expression is downregulated. Lnc34a demonstrates that lncRNA can target microRNA for cellular control. Given that lncRNAs occupy the majority of the genome [50], lncRNA/microRNA circuitry can potentially increase the complexity of regulatory networks.

p53 is a well-known upstream regulator of miR-34a, and loss of p53 function certainly downregulates miR-34a. However, the discovery of Lnc34a demonstrates an alternative, epigenetic mechanism that cancer cells can utilize to silence miR-34a without having to mutate p53. Although p53 knockout has been reported to reduce asymmetric division in

mammary stem cells [26], p53 is not known to be a major regulator of differentiation and is symmetric during CCSC division. Lnc34a provides normal and cancer cells a way to decouple mir-34a mediated cell fate decisions from p53, which may be present in both undifferentiated and differentiated cells.

METERIALS AND METHODS

CCSC culture and sphere formation analysis

Human CRC cell lines Colo205, SW480, HT29, SW620, LS174T, DLD1, Caco-2 were purchased from ATCC and cultured in RPMI-1640 medium. No mycoplasma contamination was detected. Human CCSCs were isolated and cultured as described previously [3]. Briefly, CCSCs were isolated from patient tumors by FACS based on markers CD44, CD133 and ALDH1 and functionally validated by serial sphere formation, tumor initiation, and self-renewal assays. For this study, original frozen stocks for the first passage were used. The CCSCs have not been authenticated by STR profiling. No mycoplasma contamination was detected. CCSCs were cultured as spheres in ultralow-attachment flasks (Corning) in DMEM/F12 (Invitrogen), supplemented with nonessential amino acids (Fisher), sodium pyruvate (Fisher), Penicillin-streptomycin (Fisher), N2 supplement (Invitrogen), B27 supplement (Invitrogen), 4 μg/mL heparin (Sigma), 40 ng/mL epidermal growth factor (Invitrogen), and 20 ng/mL basic fibroblast growth factor (Invitrogen) at 37 °C and 5% CO2.

To measure tumor sphere formation, single CCSCs were plated in 24-well ultra-low attachment plates (Corning) at 1,000 cells per well. Tumor spheres were counted after 2 weeks in culture by an inverted microscope (Olympus).

Clinical specimens

45 frozen CRC specimens of different clinical stages were acquired from Weill Cornell Medical College (WCMC) Colon Cancer Biobank. The CRC stage was determined according to the TNM staging system. The clinical data for the patients are summarized

in Figure 1-source data 1. The studies followed informed consent and approval of the IRB committee at Weill Cornell Medical College.

Immunofluorescence

Pair-cell assay for CCSC division were performed as described previously [30]. Briefly, spheres were dissociated and the single cells were plated on an uncoated glass culture slide (Corning) and allowed to divide once. After being fixed and blocked, the cells were incubated with anti-ALDH1 (clone H-4, 1:100, Santa Cruz), anti-CD133 (1:200, Abcam) and anti-α-tubulin (1:500, Abcam) antibodies overnight at 4 °C. For the BrdU incorporation assay, sphere cells were cultured in proliferative medium (DMEM with 10% FBS) for 24 hours. Single cells were then plated and allowed to divide once in proliferative medium (1st division). After treatment with BrdU (Sigma) for 3 hours, the cells were fixed in cold 70% ethanol, incubated in 2 M HCl for 1 hour, washed, and switched to 100 mM $Na_2B_4O_7$ for 2 minutes. After being blocked in 10% normal goat serum for 1 hour, the cells were then incubated with anti-BrdU (1:200, Sigma) antibody at 4 °C overnight. The cells were then incubated with fluorescence-conjugated secondary antibody or streptavidin (Invitrogen) for 1 hour at room temperature. After counterstaining with DAPI (Invitrogen), the slides were observed under a fluorescent microscope (Olympus).

RNA FISH

RNA FISH was performed as described previously [51]. In this study, Digoxigenin (DIG)–labeled locked nucleic acid (LNA) probe (Exiqon) against miR-34a or Biotin-labeled LNA probe against Lnc34a (Exiqon) were used for RNA FISH. RNA expression was detected by Rhodamine Red labeled secondary antibody or Alexa Fluor 488 conjugated

streptavidin (Invitrogen). Anti-tubulin was used to identify dividing cells and DAPI (Invitrogen) was used for nucleic counterstaining.

Lnc34a cloning, shRNAs, Northern blot and Bisulfite sequencing

A 293 bp fragment was amplified using primers: 5`-GGTGGAGGAGATGCCGC-3` and 5`-ACCTGGGTGCATGCTGGGACG-3`. To identify the full length of Lnc34a, 3`RACE and 5`RACE was performed using kit with the primers: 5`-GCAGGACTCCCGCAAAATCTC-3` and 5`- CTCAGTCCGTGCGAAAGTTTG-5` respectively. The full length of Lnc34a was then amplified using the primers: 5`-TTAACCAGTCGGCCTTCCTCGCC-3` and 5`-TGAGATTAACCGACTTTCCCAAG-3`, then cloned into pGEM-T (Promega) for sequencing. The full length of Lnc34a was cloned into pMSCV PIG vector (Addgene) for ectopic Lnc34a expression study. shRNAs against Lnc34a were designed using Invitrogen online tool and cloned in pMSCV PIG vector. shRNAs against PHB2, Dnmt2a, and HDAC1 were purchased from Sigma. The knockdown efficiency was validated by RT-qPCR. Northern blot was performed using NorthernMax® Kit (Invitrogen) according to the manufacturer's instructions. The probes were generated using PCR DIG Probe Synthesis Kit (Roche) with the primers: 5`-TAGCCGAGCAAAACCCC-3` and 5`- ATGTGGGACACGGATGAGA-3`. Bisulfite sequencing was performed using EZ DNA methylation kit (Zymo). 9 sequencing runs were carried out for each condition.

Flow cytometry

Flow cytometry were performed as described previously [3].CD133 expression was detected using anti-CD133 (clone C24B9, 1:50, Cell Signaling) and ALDH1 levels were analyzed using the Aldeflour kit. The samples were analyzed using a BD LSR II flow

cytometer. The raw FACS data were analyzed with the FlowJo software to gate cells according to their forward (FSC) and side (SSC) scatter profiles.

Quantitative real-time RT-PCR analysis

Total RNA was extracted from the cells using the TRIzol Reagent (Invitrogen). cDNA was synthesized using the High Capacity cDNA Archive Kit (Applied Biosystems). Quantitative PCR was carried out using the TaqMan MicroRNA Assay (Applied Biosystems) to detect miR-34a levels and the SYBR Green System (Applied Biosystems) to detect another gene expression. The miR-34a primer and U6 primer were purchased from Applied Biosystems. Other primer sequences include: Lnc34a, 5'-GGAGGCTACACAATTGAACAGG-3' and 5`-AGTCCGTGCGAAAGTTTGC-3`; actin, 5`-CGCGAGAAGATGACCCAGAT-3` and 5`-ACAGCCTGGATAGCAACGTACAT-3`; The expression of each gene was defined from the threshold cycle (Ct), and the relative expression levels were calculated using the 2-△△Ct method after normalization to the actin expression level.

RNA pull-down assay, mass spectrometry, and electrophoretic mobility shift assay (EMSA)

Full length of Lnc34a cDNA and its truncations were cloned into pGEM-3ZF (+). Biotin-labeled RNAs were transcribed from the linearized pGEM-3ZF plasmid in vitro using a biotin labeling mix (Roche) and T7 polymerase (Promega). The biotinylated RNA was heated to 90°C for 2 minutes, incubated on ice for 2 minutes, and then shifted to RT for 20 mins with RNA renature buffer (10mM tris-HCL pH7.0, 0.1M KCL, 10mM MgCl2 to allow proper secondary structure formation. The cell lysates were freshly prepared using RIPA buffer (Millipore) with proteinase inhibitor (Roche). After preclearing using

Dynabeads M-270 streptavidin (Invitrogen), the cell lysates were diluted in binding buffer and incubated with the folded RNA for 2 hours at 4°C. Dynabeads M-270 streptavidin were then added into the mixture and incubated for 1 hour at 4°C. After washing, the RNA-binding protein complexes were released from the Dynabeads. The retrieved proteins were collected for Mass Spec and Western blotting validation. RNA-EMSA was performed using a LightShift Chemiluminescent RNA EMSA Kit (Thermo Scientific) according to the manufacturer's instructions.

RNA immunoprecipitation (RIP) and chromatin immunoprecipitation (ChIP) assays

RIP assays were performed using a RIP RNA-binding protein immunoprecipitation kit (Millipore) according to the manufacturer's instructions. Antibodies against PHB2 (Bethl), HDAC1 (Bethl), and Dnmt3a (Abcam) were added into the cell lysates. Lnc34a was retrieved from the complexes and evaluated by RT-qPCR. ChIP was performed using a ChIP assay kit (Millipore) as described previously [3]. Antibodies against acetylated histones H3 and H4 (Millipore) were used to evaluate histone modifications associated with the miR-34a promoter. Enrichment of miR-34a promoter fragments was quantified by RT-qPCR with the primers: 5'-CACCTGGTCCTCTTTCCTTT-3' and 5'-TCCTCCTTCCTGCTCGT -3'.

Western blot

Cells were lysed in RIPA lysis buffer supplemented with cocktail protease inhibitor (Roche). Proteins were separated by SDS-PAGE and transferred onto a Hybond membrane (Amersham). The membranes were incubated with primary antibodies either anti-PHB2 (1:1000, Bethl), anti-Dnmt3a (1:500, Abcam), anti-HDAC1(1:1000, Bethl) or anti-Actin (1:1000, Abcam) in 5% milk/TBST buffer (25 mM Tris pH 7.4, 150 mM NaCl,

2.5 mM KCl, 0.1% Triton-X100) overnight, followed by incubation with horseradish peroxidase (HRP)-conjugated anti-mouse or anti-rabbit IgG (Santa Cruz) for 1 hour. The target proteins were detected on membrane by enhanced chemiluminescence (Pierce).

Statistical analysis

Data were expressed as mean ± standard deviation of three biological repeats. Student t-tests were used for comparisons, with $p<0.05$ considered significant.

Acknowledgements

We thank other lab members of the Shen laboratory for the helpful discussions, ordering and equipment's training. This work was supported by NIGMS R01GM95990, R01GM114254, NSF 1350659, R01 Ca098626, NSF 1137269, DARPA 19-1091726, and NYSTEM C029543.

Ethics

Human subjects: Frozen CRC specimens of different clinical stages were acquired from Weill Cornell Medical College (WCMC) Colon Cancer Biobank. The studies followed informed consent and approval of the IRB committee at Weill Cornell Medical College.

Animal experimentation: All animal experiments were approved by The Cornell Center for Animal Resources and Education (CARE) and followed the protocol (2009-0071 and 2010-0100).

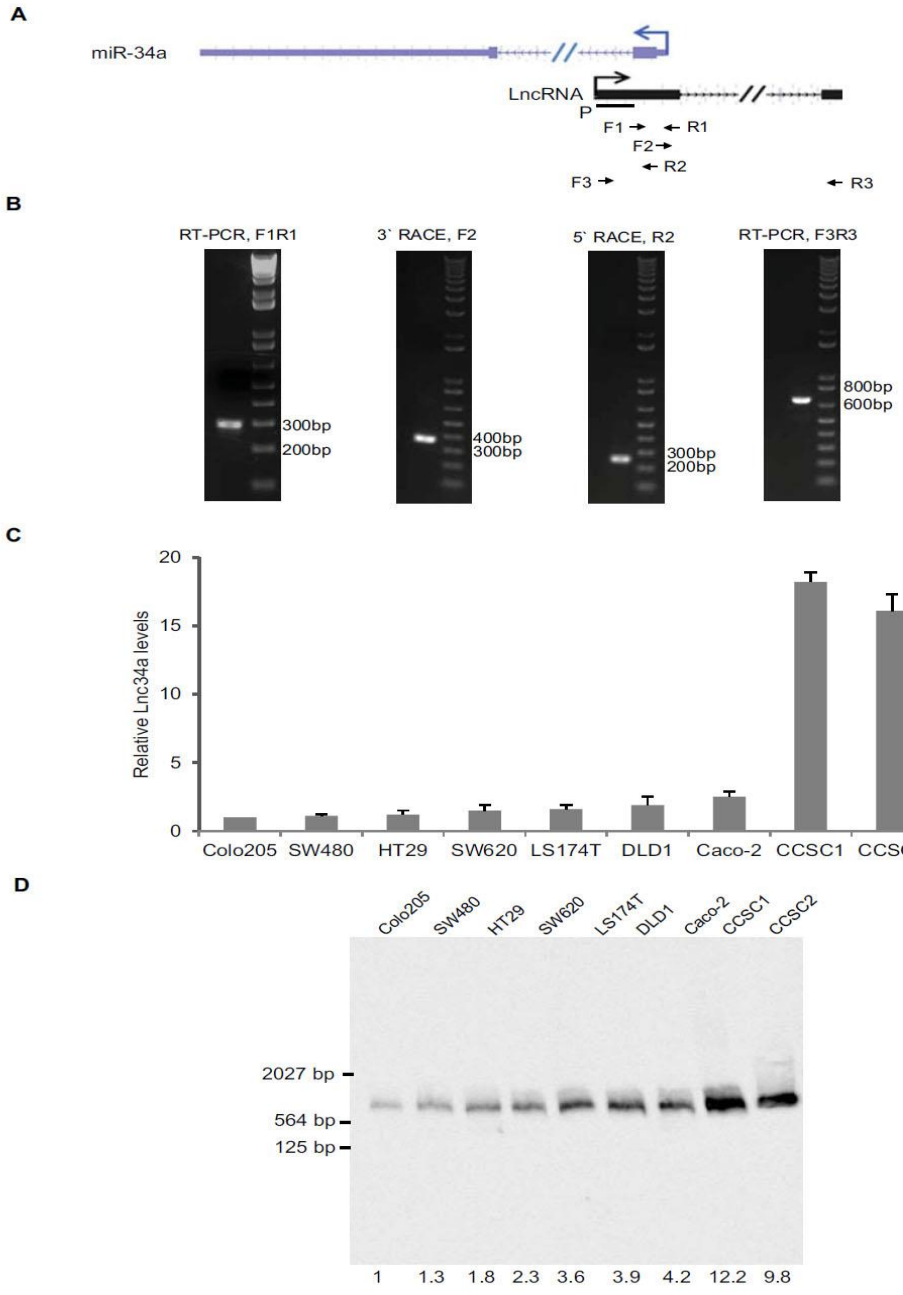

Figure 1. **Identification of Lnc34a.**

(A) Schematic illustration of Lnc34a and miR-34a gene structures. Primers for RT-PCR and rapid amplification of cDNA ends (RACE) were shown. (B) RT-qPCR and RACE that amplified Lnc34a. (C) RT-qPCR detection of Lnc34a expression in CRC cell lines. (D) Northern blot detection of Lnc34a in CRC cell lines and CCSCs. The quantification of each band was carried out using Image J.

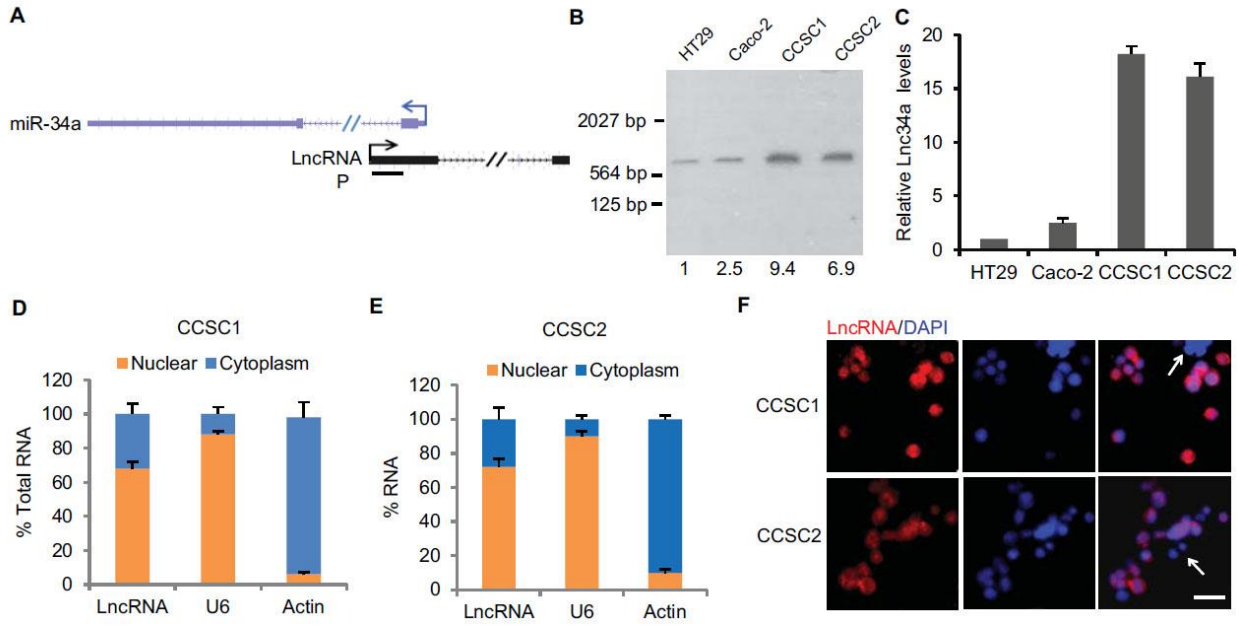

Figure 2. **Characterization of Lnc34a.**

(A) Schematic illustration of Lnc34a (shown in black) and miR-34a (shown in blue) gene structure. Lnc34a and miR-34a contain two exons and are transcribed in different directions. P, probe for Northern blot in (B). (B) Northern blot detection of Lnc34a with the probe shown in (A), quantified by Image J. (C) RT-qPCR detection of Lnc34a expression in colon cancer stem cells (CCSC1 and CCSC2) and well-established colon cancer cell lines (HT29 and Caco-2). (D, E) RT-qPCR detection of Lnc34A level in cellular fractions from CCSC1 (D) and CCSC2 (E) sphere cells. U6 and actin are the nuclear and cytoplasm controls, respectively. (F) Lnc34a expression in CCSC sphere cells detected by RNA-FISH. Scale bar, 20μm.

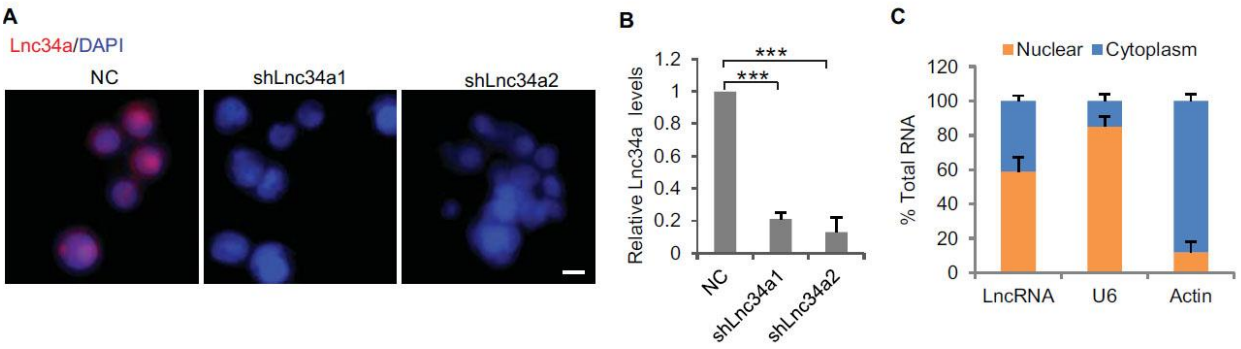

Figure 3. **RNA FISH specificity and Lnc34a knockdown efficiency.**

(A) Knockdown of Lnc34a abolished RNA FISH signals. (B) RT-qPCR showing Lnc34a knockdown efficiencies by shLnc34a1 and shLnc34a2. (C) RT-qPCR detection of Lnc34a level in cellular fractions from CCSC1with Lnc34a ectopic expression.

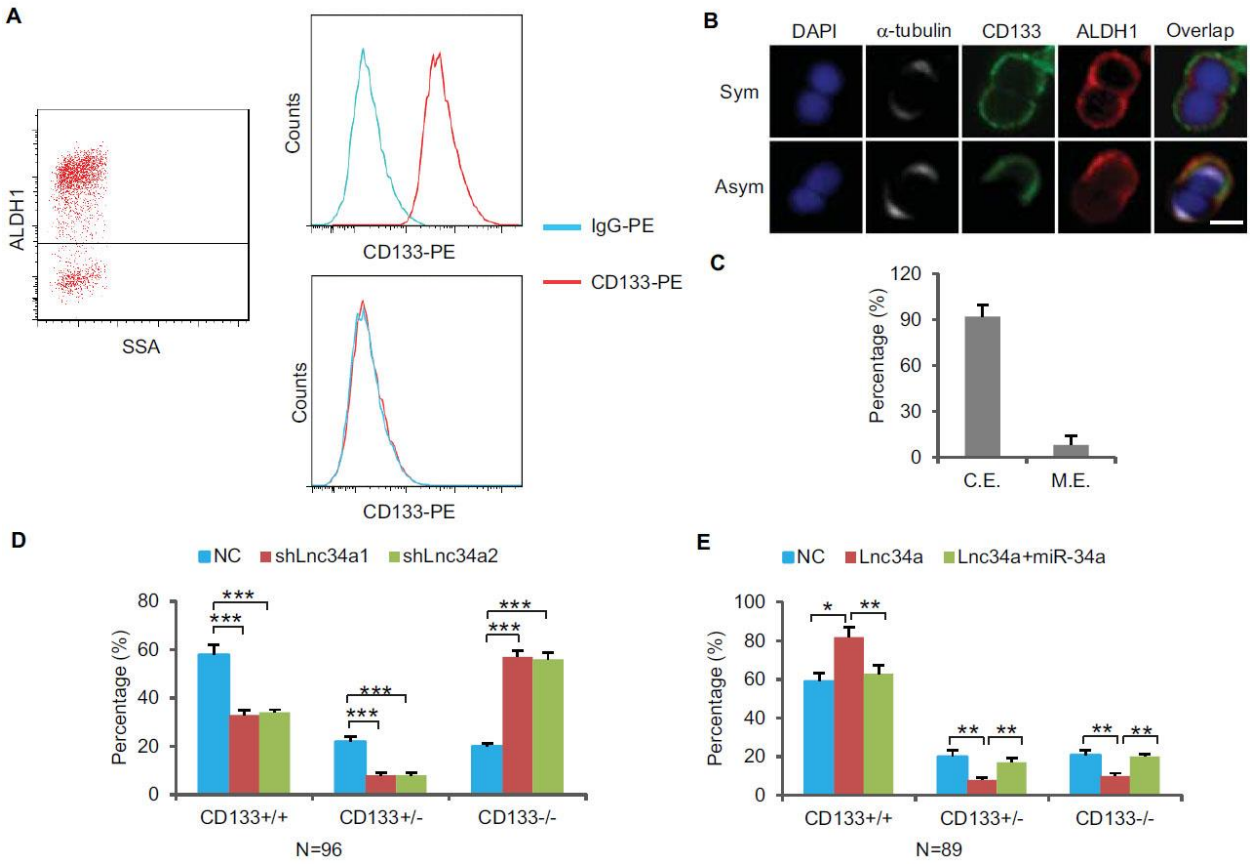

Figure 4. **CCSCs co-express ALDH1 and CD133.**

(A) FACS showing ALDH1+ sphere cells are CD133+. (B) Co-immunofluorescence of ALDH1 and CD133 showing ALDH1 and CD133 are expressed in the same daughter cell during CCSC division. (C) Percentages of CCSC divisions wherein miR-34a and ALDH1 are coexpressed (C.E.) or mutually exclusive (M.E.). (D, E) Effect of Lnc34a knockdown (D) and ectopic Lnc34a and miR-34a expression (E) on mode of division based on CD133 staining of dividing cell pairs.

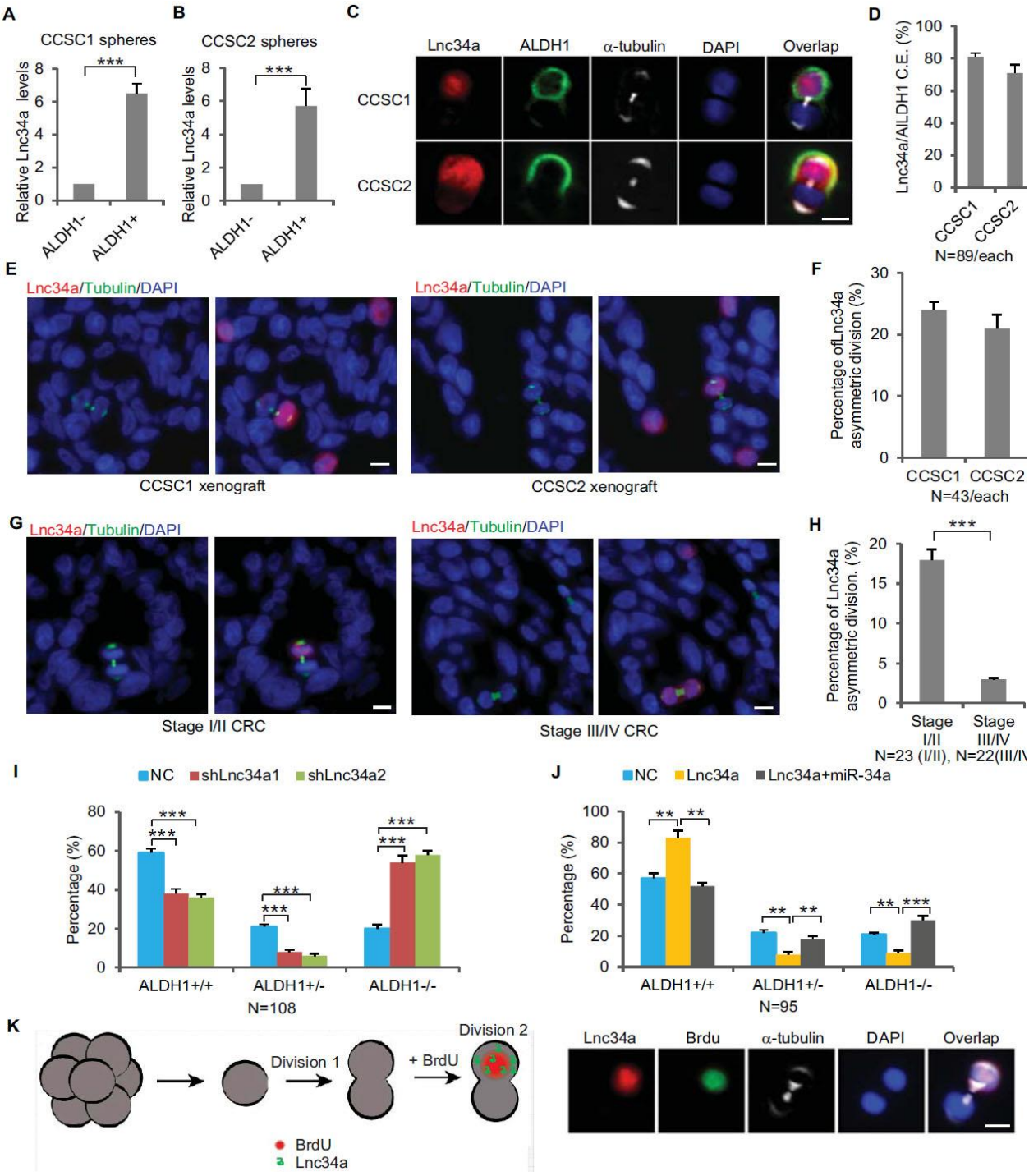

Figure 5. **Lnc34a Asymmetry in CCSC division.**

(A, B) RT-qPCR detection of lnc34a in ALDH1+ and ALDH1- populations isolated from spheres of two independent patient-derived lines, CCSC1 (A) and CCSC2 (B). Lnc34a is high in ALDH1+ (CCSC) but low in ALDH1- (non-CCSC) cells. (C) Representative images of Lnc34a distribution in dividing pairs. α-tubulin staining is consistent with the telophase

(final phase of mitosis) configuration of microtubules – the midbody at the division plane during cytokinesis and asters at the poles. ALDH1 identifies the CCSC daughter. (D) Quantification of Lnc34a/ALDH1 co-expression (C.E.) in daughter compartments of dividing pairs as shown in (C). (E) Representative images of Lnc34a asymmetry in dividing pairs in xenograft tumors derived from CCSC1 and CCSC2. Dividing pairs are identified by tubulin staining. (F) Percentage of Lnc34a asymmetry in dividing pairs in CCSC xenografts as shown in (E). (G) Representative images of asymmetric and symmetric Lnc34a distribution in dividing pairs in early- and late-stage human CRC specimens. (H) Percentage of Lnc34a asymmetry in dividing pairs in human CRC specimens. (I) Effect of Lnc34a knockdown on mode of division based on ALDH1 staining of dividing cell pairs. Lnc34a knockdown decreased asymmetric (ALDH1+/ALDH1-) division and symmetric self-renewal (ALDH1+/ALDH1+), and increased differentiation (ALDH1-/ALDH-). (J) Effect of ectopic Lnc34a expression on mode of division. Ectopic Lnc34a increased symmetric self-renewal (ALDH1+/ALDH+), and reduced asymmetric division (ALDH1+/ALDH1-) and differentiation (ALDH1-/ALDH1-). The effect of ectopic Lnc34a expression was abrogated by ectopic miR-34a expression. (K) Pair-cell BrdU incorporation assay showing asymmetric proliferative potential. Left, schematic representation of the experimental approach. Single sphere cells were allowed to divide once (1st division). Cells were then treated with BrdU for 3 hours to label cells that were re-entering the 2nd division. Right, representative images showing that the Lnc34a+ cells were more proliferative and incorporated BrdU. Scale bar, 8μm. Error bars denote s.d. of triplicates. *, $p<0.05$; **, $p<0.01$; ***, $p<0.001$. p-value was calculated based on Student's t-test.

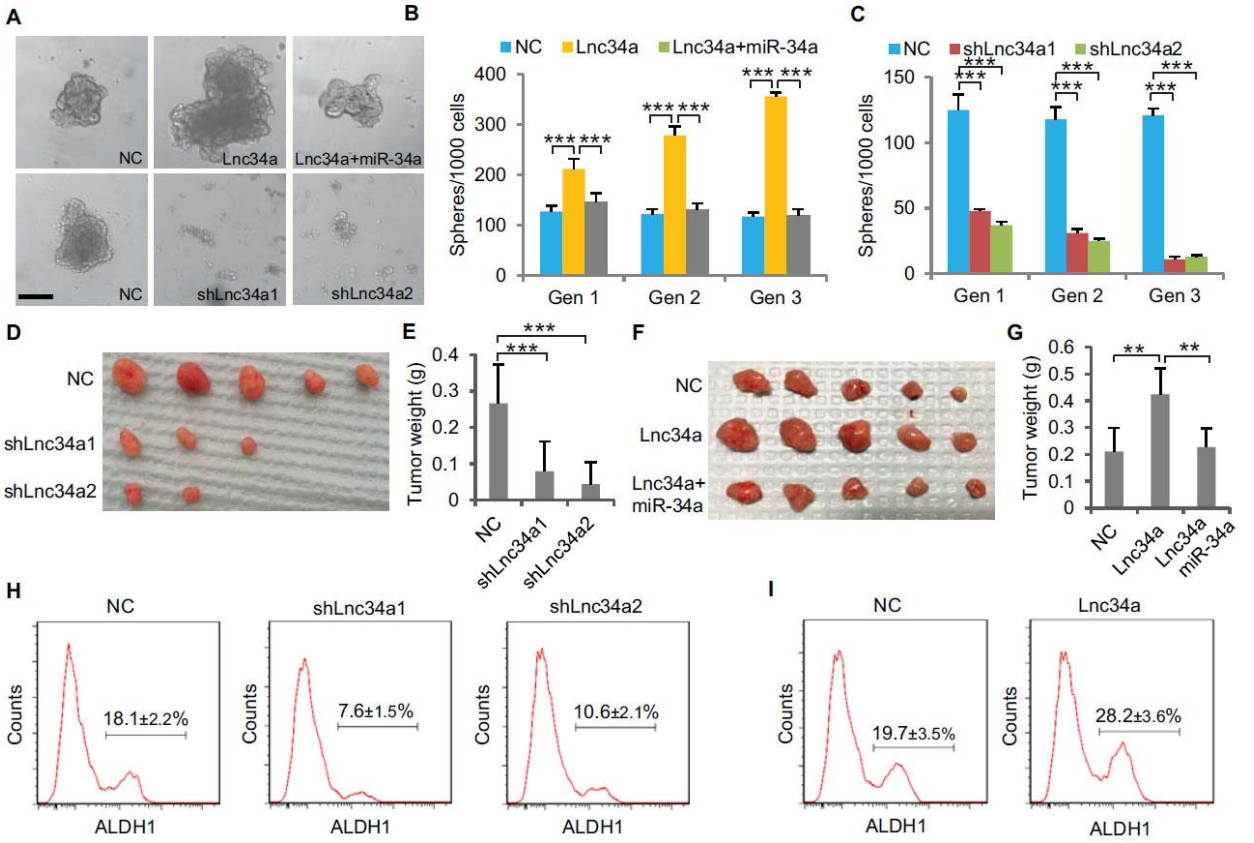

Figure 6. **Lnc34a promotes CCSC self-renewal and tumor formation.**

(A) Representative images of CCSC spheres with Lnc34a knockdown (shLnc34a1 and shLnc34a2), ectopic Lnc34a expression (Lnc34a), and ectopic Lnc34a/miR-34a expression. (B, C) Sphere formation during serial passages after Lnc34a knockdown (B) and ectopic Lnc34a and miR-34a expression (C). Equal number of cells was passaged for 3 generations to form spheres. (D, E) Knockdown of Lnc34a (shLnc34a1 and shLnc34a2) reduced tumorigenicity, shown by images (D) and weights of xenograft tumors (E). (F, G) Ectopic Lnc34a expression (Lnc34a) enhances tumorigenicity, which can be abrogated by ectopic miR-34a expression. (H, I) FACS plots identifying ALDH1+ (CCSC) populations in xenograft tumors with Lnc34a knockdown (H) or ectopic Lnc34a expression (I). Scale bar, 50□m. Error bars denote s.d. of triplicates. **, p<0.01; ***, p<0.001. p-value was calculated based on Student's t-test.

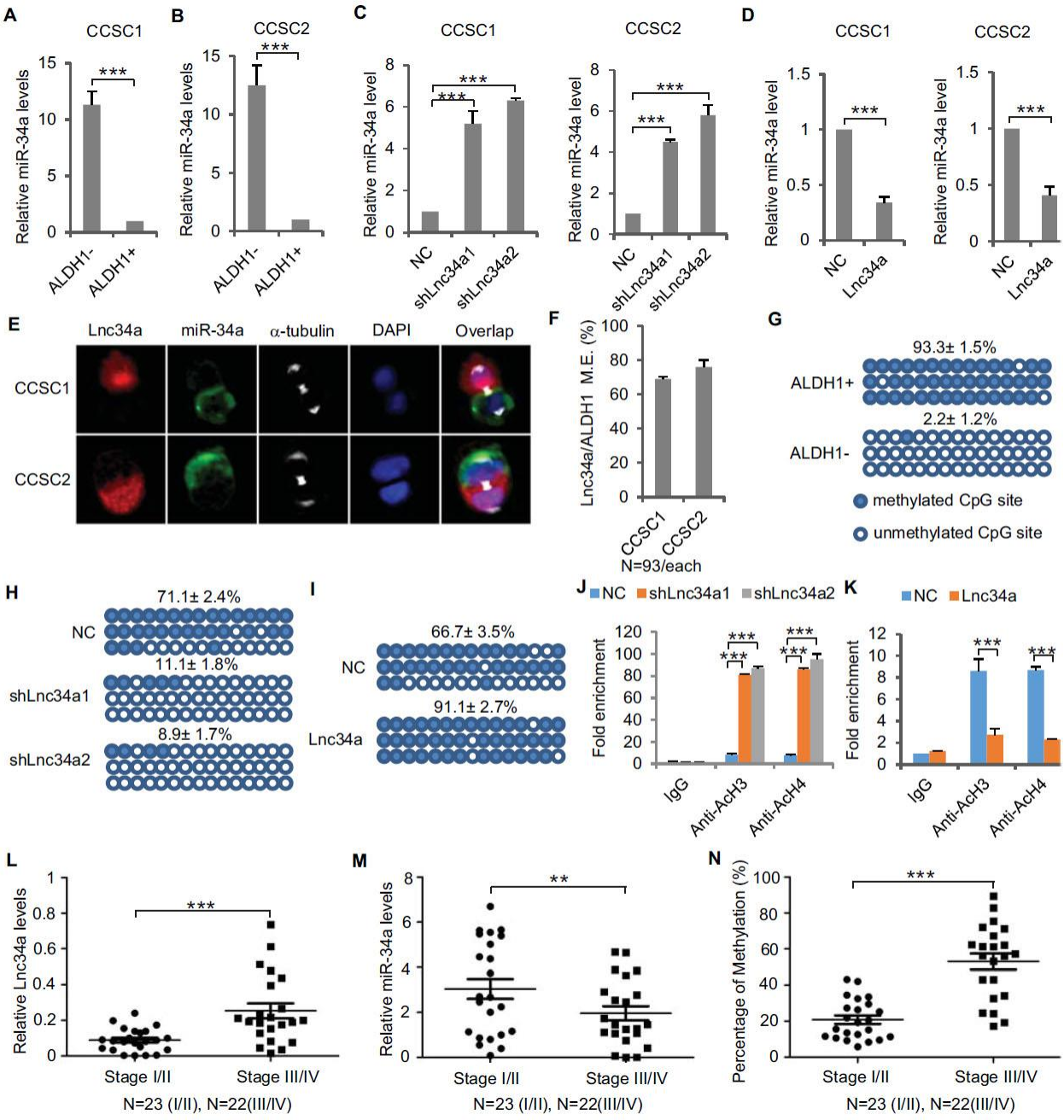

Figure 7. **Lnc34a epigenetically silences miR-34a promoter.**

(A, B) RT-qPCR of miR-34a levels in CCSC1 (A) and CCSC2 (B). (C, D) RT-qPCR of miR-34a levels in CCSC1 (C) and CCSC2 (D) spheres with Lnc34a knockdown (shLnc34a1 and shLnc34a2) or ectopic expression (Lnc34a). NC is the control vector. (E) Representative images of Lnc34a and miR-34a asymmetry in CCSC1 and CCSC2 sphere cells. (F) Quantification of (E). Lnc34a and miR-34a distributions are mutually exclusive (M.E.) during most CCSC divisions. (G) Bisulfite sequencing analysis showing miR-34a promoter methylation status in ALDH1+ (CCSC) and ALDH1- (non-CCSC) cells isolated from sphere cells. PCR products amplified from bisulfite-treated genomic DNA were cloned and sequenced to reveal the methylation status of individual CpG sites.

Percentages of the methylated CpG sites (filled circles) among all scored sites are indicated. (H) Lnc34a knockdown decreased miR-34a promoter methylation in sphere cells. (I) Ectopic Lnc34a expression increased miR-34a promoter methylation in sphere cells. (J, K) ChIP-qPCR with antibodies against acetylated histones H3 and H4. Lnc34a knockdown decreased miR-34a promoter acetylation (J), while ectopic Lnc34a expression increased acetylation (K). (L) RT-qPCR measurements of Lnc34a expression in early- and late-stage CRC specimens. (M) RT-qPCR measurements of miR-34a expression in early- and late-stage CRC specimens. (N) Bisulfite sequencing analysis of miR-34a promoter methylation status in early- and late-stage CRC specimens. Scale bar, 8μm. Error bars denote s.d. of triplicates. **, $p<0.01$; ***, $p<0.001$. p-value was calculated based on Student's t-test.

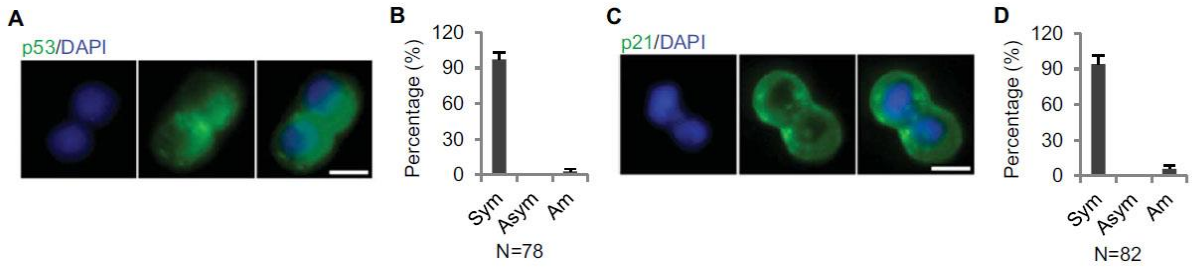

Figure 8. **p53 symmetry**.

(A) Representative immunofluorescence images showing symmetric distribution of p53 during CCSC division. (B) Percentage of p53 division type. (C) Representative immunofluorescence images showing symmetric distribution of p21 during CCSC division. (D) Percentage of p21 division type. Sym, symmetric segregation; Asym, asymmetric segregation; Am, ambiguous.

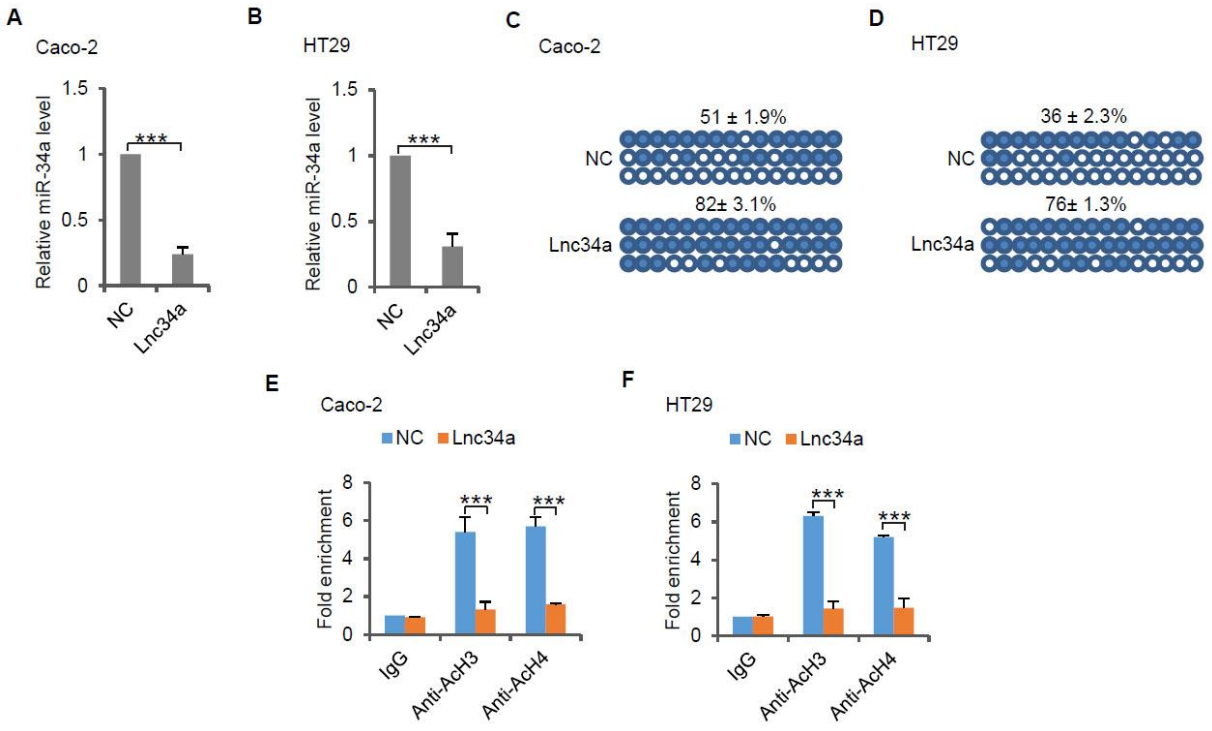

Figure 9. Lnc34a epigenetically silences miR-34a promoters in Caco-2 and HT29 cells.

(A, B) RT-qPCR of miR-34a levels in CRC lines Caco-2 (A) and HT29 (B). Ectopic Lnc34a expression suppressed miR-34a expression. (C, D) Bisulfite sequencing analysis showing ectopic Lnc34a expression increased miR-34a promoter methylation in Caco-2 (C) and HT29 (D). (E, F) ChIP-qPCR with antibodies against acetylated histones H3 and H4. Ectopic Lnc34a expression decreased miR-34a promoter acetylation in Caco-2 (E) and HT29 (F).

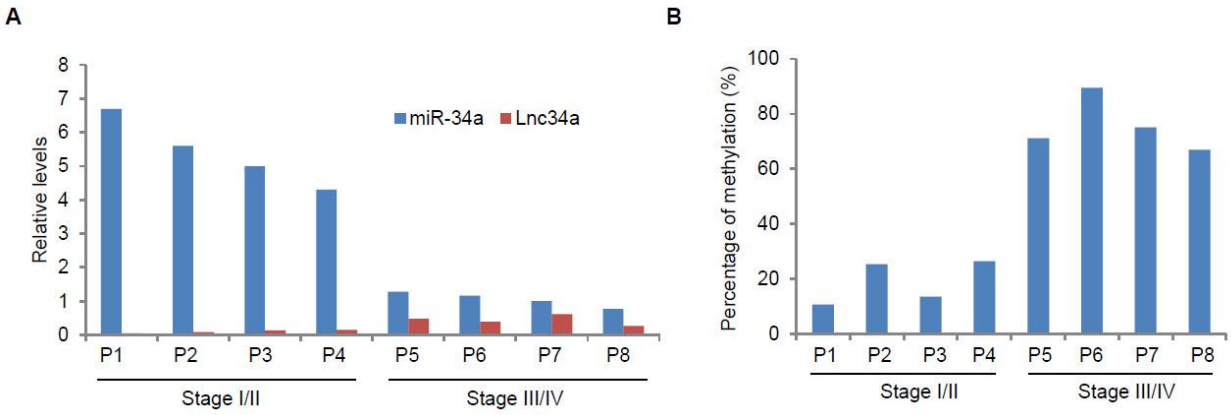

Figure 10. **Lnc34a, miR-34a, and promoter methylation levels in CRC specimens.**

(A) RT-qPCR showing Lnc34a and miR-34a expression in individual CRC specimens. Levels are normalized to corresponding actin levels. (B) Bisulfite sequencing analysis of miR-34a promoter methylation in the same CRC specimens shown in (A).

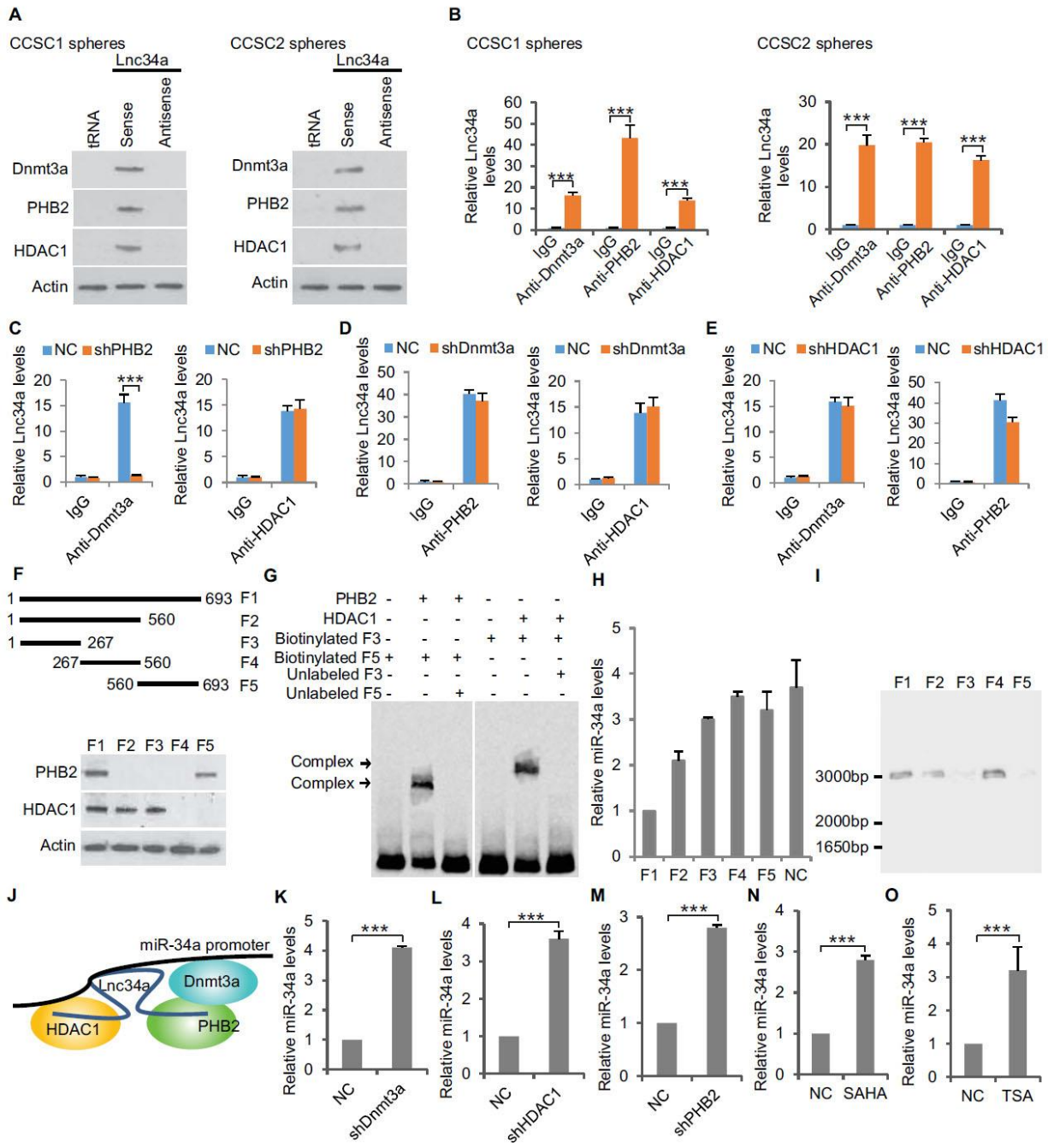

Figure 11. Lnc34a recruits epigenetic regulators.

Western blot following RNA-pull down showing Lnc34a interaction with PHB2, Dnmt3a and HDAC1 in CCSC1 (left) and CCSC2 (right) sphere cells. RNA-pull down was performed using CCSC lysates with biotin-labeled Lnc34a, antisense and tRNA. Actin was used for input control. (B) RNA immunoprecipitation (RIP) showing Lnc34a interaction with PHB2, Dnmt3a and HDAC1 in CCSC1 (left) and CCSC2 (right) sphere cells. (C) RIP showing PHB2 knockdown disrupts Lnc34a interaction with Dnmt3a, but has no effect on Lnc34a interaction with HDAC1. (D) RIP showing Dnmt3a knockdown does not affect Lnc34a interaction with PHB2 or HDAC1. (E) RIP showing HDAC1

knockdown has limited effect on Lnc34a interaction with PHB2 or Dnmt3a. (F) Mapping PHB2 and HDAC1 interaction domains on Lnc34a. Upper panel, schematic illustration of full-length Lnc34a and the truncated fragments for RNA put-down. Lower panel, Western blot of PHB2 and HDAC1 from RNA put-down of the fragments. (G) EMSA showing Lnc34a/PHB2 (left) and Lnc34a/HDAC1 (right) interactions. (H) RT-qPCR of miR-34a levels after expressing full-length or truncated fragments of Lnc34a. (I) In vitro interaction assay binding of the truncated fragment (267-560bp) to the DNA containing the miR-34a promoter sequence. (J) Schematic illustration of Lnc34a interaction with PHB2, Dnmt3a and HDAC1. (K, L, M) RT-qPCR showing knockdown of Dnmt3a (K), HDAC1 (L), and PHB2 (M) increased miR-34a expression in sphere cells. (N, O) RT-qPCR showing treatments with HDAC inhibitor SAHA (N) or TSA (O) increased miR-34a expression in sphere cells. Error bars denote s.d. of triplicates. ***, $p<0.001$. p-value was calculated based on Student's t-test.

Table 1. Information of CRC patients.

Patient	Gender	Age at visit	Stage	Differentiation	Lymph nodes
P1	M	44	I	Moderate	N0
P2	M	61	I	Moderate	N0
P3	M	85	I	NA	N0
P4	F	84	I	Moderate	N0
P5	F	65	I	Moderate	N0
P6	M	79	I	NA	N0
P7	F	88	I	Moderate	N0
P8	F	63	I	Moderate	N0
P9	M	61	I	Moderate	N0
P10	M	54	I	Moderate	N0
P11	M	85	I	NA	N0
P12	M	70	I	Poor	N0
P13	M	66	I	NA	N0
P14	M	81	I	NA	N0
P15	M	52	I	Well	N0
P16	F	57	IIA	Moderate	N0
P17	F	70	IIA	NA	N0
P18	M	43	IIA	NA	N0
P19	F	48	IIA	Moderate	N0
P20	F	68	IIA	Poor	N0
P21	M	81	IIA	Poor	N0
P22	F	92	IIB	Well	N0
P23	M	81	IIB	Poor	N0
P24	F	50	IIIA	Moderate	N1 1-3
P24	M	73	IIIA	Well	N1 1-3
P25	F	54	IIIB	Moderate	N1 1-3
P26	M	62	IIIB	NA	N1 1-3
P27	F	77	IIIB	Poor	N1 1-3
P28	F	71	IIIC	NA	N2 >3
P29	F	50	IIIC	Poor	N2 >3
P30	F	84	IIIC	Moderate	N2 >3
P31	M	85	IIIC	Poor	N2 >3
P32	F	61	IIIC	Poor	N2 >3
P33	F	88	IIIC	Poor	N2 >3
P34	F	70	IIIC	Poor	N2 >3
P35	F	73	IV	Poor	N2 >3
P36	F	73	IV	Moderate	N1 1-3

P37	M	66	IV	Poor	N1 1-3
P38	M	56	IV	Poor	N2 >3
P39	F	68	IV	Poor	N2 >3
P40	F	46	IV	NA	N1 1-3
P41	F	73	IV	Poor	N1 1-3
P42	M	37	IV	Poor	N2 >3
P43	F	21	IV	Moderate	N1 1-3
P45	F	69	IV	Moderate	N1 1-3

Table 2. Potential Lnc34a-associated proteins identified by biotinylated Lnc34a pull-down and mass spectrometry.

Protein accession #	Protein description	Mass of protein	# of peptide matching	Protein coverage (%)
gi5031857	lactate dehydrogenase A	43596	74	19
gi332864	pyruvate kinase 3 isoform 1	67178	61	18.4
gi315429	Chaperonin	73562	35	11.2
gi545355	ras-related nuclear protein	28933	14	9.7
gi13128860	Histone Deacetylase 1 (HDAC1)	55130	9	9.7
gi488543	heat shock 70 protein 1B	81954	34	8.6
gi600585	prohibitin 2 (PHB2)	37859	4	8.51
gi59270	splicing factor, arginine/serine-rich 1 isoform 1	29904	2	8.5
gi892741	cytokine induced apoptosis inhibitor 1	40777	4	8.3
gi45505	tumor-associated calcium signal transducer 1 precursor	41981	4	7.42
gi12751473	DNA (cytosine-5)-methyltransferase 3A isoform a (Dnmt3a)	101585	11	6.1
gi517461	nucleosome assembly protein 1-like 4	50530	12	5.6
gi482558	protein kinase C substrate 80K-H isoform 1	68149	6	4.33
gi213611	Na+/K+ -ATPase alpha 1 subunit isoform a proprotein	127198	14	3.9
gi45505	tumor-associated calcium signal transducer 1 precursor	41981	4	7.42

REFERENCES

1. Chang, T.C., et al., Transactivation of miR-34a by p53 broadly influences gene expression and promotes apoptosis. Mol Cell, 2007. 26(5): p. 745-52.
2. He, L., et al., A microRNA component of the p53 tumour suppressor network. Nature, 2007. 447(7148): p. 1130-4.
3. Bu, P., et al., A microRNA miR-34a-regulated bimodal switch targets Notch in colon cancer stem cells. Cell Stem Cell, 2013. 12(5): p. 602-15.
4. Liu, C., et al., The microRNA miR-34a inhibits prostate cancer stem cells and metastasis by directly repressing CD44. Nat Med, 2011. 17(2): p. 211-5.
5. Bader, A.G., miR-34 - a microRNA replacement therapy is headed to the clinic. Front Genet, 2012. 3: p. 120.
6. Bouchie, A., First microRNA mimic enters clinic. Nat Biotechnol, 2013. 31(7): p. 577.
7. Aranha, M.M., et al., miR-34a regulates mouse neural stem cell differentiation. PLoS One, 2011. 6(8): p. e21396.
8. Boon, R.A., et al., MicroRNA-34a regulates cardiac ageing and function. Nature, 2013. 495(7439): p. 107-10.
9. Choi, Y.J., et al., miR-34 miRNAs provide a barrier for somatic cell reprogramming. Nat Cell Biol, 2011. 13(11): p. 1353-60.
10. Krzeszinski, J.Y., et al., miR-34a blocks osteoporosis and bone metastasis by inhibiting osteoclastogenesis and Tgif2. Nature, 2014. 512(7515): p. 431-5.
11. Liu, N., et al., The microRNA miR-34 modulates ageing and neurodegeneration in Drosophila. Nature, 2012. 482(7386): p. 519-23.
12. Song, R., et al., miR-34/449 miRNAs are required for motile ciliogenesis by repressing cp110. Nature, 2014. 510(7503): p. 115-20.
13. Xu, Y., et al., A metabolic stress-inducible miR-34a-HNF4alpha pathway regulates lipid and lipoprotein metabolism. Nat Commun, 2015. 6: p. 7466.
14. Corney, D.C., et al., Frequent downregulation of miR-34 family in human ovarian cancers. Clin Cancer Res, 2010. 16(4): p. 1119-28.
15. Kong, D., et al., Epigenetic silencing of miR-34a in human prostate cancer cells and tumor tissue specimens can be reversed by BR-DIM treatment. Am J Transl Res, 2012. 4(1): p. 14-23.
16. Lodygin, D., et al., Inactivation of miR-34a by aberrant CpG methylation in multiple types of cancer. Cell Cycle, 2008. 7(16): p. 2591-600.
17. Siemens, H., et al., Detection of miR-34a promoter methylation in combination with elevated expression of c-Met and beta-catenin predicts distant metastasis of colon cancer. Clin Cancer Res, 2013. 19(3): p. 710-20.
18. Neumuller, R.A. and J.A. Knoblich, Dividing cellular asymmetry: asymmetric cell division and its implications for stem cells and cancer. Genes Dev, 2009. 23(23): p. 2675-99.

19. Reya, T., et al., Stem cells, cancer, and cancer stem cells. Nature, 2001. 414(6859): p. 105-11.
20. Dey-Guha, I., et al., Asymmetric cancer cell division regulated by AKT. Proc Natl Acad Sci U S A, 2011. 108(31): p. 12845-50.
21. Lathia, J.D., et al., Distribution of CD133 reveals glioma stem cells self-renew through symmetric and asymmetric cell divisions. Cell Death Dis, 2011. 2: p. e200.
22. O'Brien, C.A., et al., ID1 and ID3 regulate the self-renewal capacity of human colon cancer-initiating cells through p21. Cancer Cell, 2012. 21(6): p. 777-92.
23. Pece, S., et al., Biological and molecular heterogeneity of breast cancers correlates with their cancer stem cell content. Cell, 2010. 140(1): p. 62-73.
24. Pine, S.R., et al., Microenvironmental modulation of asymmetric cell division in human lung cancer cells. Proc Natl Acad Sci U S A, 2010. 107(5): p. 2195-200.
25. Sugiarto, S., et al., Asymmetry-defective oligodendrocyte progenitors are glioma precursors. Cancer Cell, 2011. 20(3): p. 328-40.
26. Cicalese, A., et al., The tumor suppressor p53 regulates polarity of self-renewing divisions in mammary stem cells. Cell, 2009. 138(6): p. 1083-95.
27. Kong, L., et al., CPC: assess the protein-coding potential of transcripts using sequence features and support vector machine. Nucleic Acids Res, 2007. 35(Web Server issue): p. W345-9.
28. Wang, L., et al., CPAT: Coding-Potential Assessment Tool using an alignment-free logistic regression model. Nucleic Acids Res, 2013. 41(6): p. e74.
29. Huang, E.H., et al., Aldehyde dehydrogenase 1 is a marker for normal and malignant human colonic stem cells (SC) and tracks SC overpopulation during colon tumorigenesis. Cancer Res, 2009. 69(8): p. 3382-9.
30. Bultje, R.S., et al., Mammalian Par3 regulates progenitor cell asymmetric division via notch signaling in the developing neocortex. Neuron, 2009. 63(2): p. 189-202.
31. Castel, S.E. and R.A. Martienssen, RNA interference in the nucleus: roles for small RNAs in transcription, epigenetics and beyond. Nat Rev Genet, 2013. 14(2): p. 100-12.
32. Di Ruscio, A., et al., DNMT1-interacting RNAs block gene-specific DNA methylation. Nature, 2013. 503(7476): p. 371-6.
33. Wang, Y., et al., The long noncoding RNA lncTCF7 promotes self-renewal of human liver cancer stem cells through activation of Wnt signaling. Cell Stem Cell, 2015. 16(4): p. 413-25.
34. Xing, Z., et al., lncRNA directs cooperative epigenetic regulation downstream of chemokine signals. Cell, 2014. 159(5): p. 1110-25.
35. Feng, J., et al., The Evf-2 noncoding RNA is transcribed from the Dlx-5/6 ultraconserved region and functions as a Dlx-2 transcriptional coactivator. Genes Dev, 2006. 20(11): p. 1470-84.

36. Gomez, J.A., et al., The NeST long ncRNA controls microbial susceptibility and epigenetic activation of the interferon-gamma locus. Cell, 2013. 152(4): p. 743-54.
37. Jeon, Y. and J.T. Lee, YY1 tethers Xist RNA to the inactive X nucleation center. Cell, 2011. 146(1): p. 119-33.
38. Martianov, I., et al., Repression of the human dihydrofolate reductase gene by a non-coding interfering transcript. Nature, 2007. 445(7128): p. 666-70.
39. Rinn, J.L. and H.Y. Chang, Genome regulation by long noncoding RNAs. Annu Rev Biochem, 2012. 81: p. 145-66.
40. Schmitz, K.M., et al., Interaction of noncoding RNA with the rDNA promoter mediates recruitment of DNMT3b and silencing of rRNA genes. Genes Dev, 2010. 24(20): p. 2264-9.
41. Mercer, T.R., M.E. Dinger, and J.S. Mattick, Long non-coding RNAs: insights into functions. Nat Rev Genet, 2009. 10(3): p. 155-9.
42. Gupta, R.A., et al., Long non-coding RNA HOTAIR reprograms chromatin state to promote cancer metastasis. Nature, 2010. 464(7291): p. 1071-6.
43. Tsai, M.C., et al., Long noncoding RNA as modular scaffold of histone modification complexes. Science, 2010. 329(5992): p. 689-93.
44. Zhao, J., et al., Polycomb proteins targeted by a short repeat RNA to the mouse X chromosome. Science, 2008. 322(5902): p. 750-6.
45. Chu, C., et al., Systematic discovery of Xist RNA binding proteins. Cell, 2015. 161(2): p. 404-16.
46. Serra, R.W., et al., A KRAS-directed transcriptional silencing pathway that mediates the CpG island methylator phenotype. Elife, 2014. 3: p. e02313.
47. Wajapeyee, N., et al., Oncogenic RAS directs silencing of tumor suppressor genes through ordered recruitment of transcriptional repressors. Genes Dev, 2013. 27(20): p. 2221-6.
48. Chen, W.Y., et al., MicroRNA-34a regulates WNT/TCF7 signaling and inhibits bone metastasis in Ras-activated prostate cancer. Oncotarget, 2015. 6(1): p. 441-57.
49. Vermeulen, L., et al., Wnt activity defines colon cancer stem cells and is regulated by the microenvironment. Nat Cell Biol, 2010. 12(5): p. 468-76.
50. Mattick, J.S. and J.L. Rinn, Discovery and annotation of long noncoding RNAs. Nat Struct Mol Biol, 2015. 22(1): p. 5-7.
51. Lu, J. and A. Tsourkas, Imaging individual microRNAs in single mammalian cells in situ. Nucleic Acids Res, 2009. 37(14): p. e100.

Chapter 2

miR-34a and Numb synergize for stem cell asymmetric division in inflammatory or oncogenic intestine and colon

This section is adapted from the following publication:

Pengcheng Bu*, **Lihua Wang***, Kai-Yuan Chen, Tara Srinivasan, Preetish Kadur Lakshminarasimha Murthy, Kuei-Ling Tung, Anastasia Kristine Varanko, Yiwei Ai, Sarah King, Steven M. Lipkin, Xiling Shen.

miR-34a and Numb synergize for asymmetric cell fate determination to control stem cell proliferation. ***Cell Stem Cell***. 2016 18(2):189-202.

* co-first author

Contributions: Pengcheng Bu, Lihua Wang and Xiling Shen conceived the concept, designed the experiments and co-wrote the manuscript. *Pengcheng Bu and *Lihua Wang performed the experiments with the assistance of Tara Srinivasan for the immunofluorescence, Yiwei Ai, and Sarah King for immunohistochemistry. Kuei-Ling Tung and Anastasia Kristine Varanko created miR-34a flox/flox/Lgr5-GFP-IRESCreERT2 mice. Steven M. Lipkin contributed the clinical samples. Kai-Yuan Chen and Preetish Kadur Lakshminarasimha Murthy performed computational simulation.

INTRODUCTION

Cells usually divide symmetrically, producing two identical daughter cells. However, there are prokaryotic and eukaryotic cells that can divide asymmetrically, giving rise to daughter cells with different characteristics [1]. In higher organisms, asymmetric division is a property associated with many types of stem and progenitor cells in embryo, nervous system, skin, mammary gland, blood, etc. To balance proliferation and differentiation as well as aging [2-9]. Asymmetric division manages differentiation and self-renewal simultaneously while keeping the number of stem cells constant, making it an attractive mechanism for tissue homeostasis. On the other hand, symmetric division expands the number of stem cells and often occurs during early embryonic development, tissue regeneration, and repair [10]. These are certainly not fixed rules because stem cells often rely on a spatial niche to regulate their number and behavior [11]. For example, Lgr5+ crypt base columnar (CBC) cells in the intestine predominantly undergo symmetric division and rely on a neutral drift process in the niche to stabilize their number [12,13].

Cancer stem cells or tumor initiating cells of various cancer types undergo both symmetric and asymmetric division [14-21]. Loss of tumor suppressor genes often favors increased symmetric divisions of cancer stem cells, which promote proliferation and tumor growth.

Asymmetric cell division usually relies on imbalance of cell fate determinant proteins in the two cellular compartments to break symmetry, resulting in daughter cells with distinct cell fates. A canonical cell fate determinant in Drosophila neuroblasts and various mammalian stem cells, Numb targets membrane-bound Notch receptors for degradation [22, 23]. Furthermore, Numb is a cell fate determinant for various cancer stem cells, and has been used as a marker for distinguishing symmetric vs. asymmetric division [18].

Recently, emerging evidence suggests that asymmetric distribution of microRNAs can also give rise to asymmetric cell fates [24, 25]. For example, we have shown that miR-34a directly targets Notch to form a cell fate determination switch in colon cancer stem cells (CCSCs). A tumor suppressor in many cancer types, miR-34a regulates differentiation of embryonic and neural stem cells, somatic cell reprogramming, and cardiac aging [26-29]. miR-34a mimics such as MRX34 are among the first microRNA mimics to reach clinical trial for cancer therapy [30,31].

However, this raises the question as to whether microRNA and protein cell fate determinants act independently or coordinate with each other to determine cell fate. The relationship between miR-34a and Numb is intriguing because both target Notch in CCSCs. Here we show that miR-34a directly binds to the 3`UTR of Numb mRNA to suppress Numb expression so that miR-34a, Numb, and Notch form an incoherent feedforward loop (IFFL). Combination of computational analysis and quantitative experiments revealed that the unique regulatory kinetics among miR-34a, Numb, and Notch enable a robust binary switch so that the Notch level is steady and insensitive to precise miR-34a level except for a sharp transition region. The switch enforces bimodality and cell fate bifurcation in the population. Subversion of this IFFL via Numb knockdown degrades Notch bimodality and gives rise to an intermediate subpopulation of cells with ambiguous and plastic cell fate. We further show that this cell fate determination switch plays a role in mouse intestinal stem cells (ISCs). Although Lgr5+ ISCs divide symmetrically in normal tissue homeostasis, we found that excessive proliferation caused by pro-inflammatory stress or APC deficiency triggers asymmetric division, which restrains the number of Lgr5+ ISCs. Silencing of the miR-34a-mediated switch inhibits

ISC asymmetric division and contributes to CCSC-like proliferation in stressed tissue. Hence, the cell fate determinants provide a safeguard mechanism against excessive stem cell proliferation when normal homeostasis is disrupted by inflammation or oncogenic mutation.

RESULTS

miR-34a directly targets Numb.

Using CCSCs derived from patient tumors as we have previously described and characterized [24], we first examined whether miR-34a and Numb spatial distributions are independent or correlated in divided pairs by performing pair-cell assay with immunofluorescence [3, 24] (Figure 1A). During asymmetric CCSC division, miR-34a and Numb are mostly present in the $Notch^{low}ALDH1^{low}$ non-CCSC daughter cells (Figure 1B), consistent with their function as Notch suppressors (Figures 1C and 1D) [24]. According to co-immunofluorescence for mir-34a and Numb, miR-34a and Numb were present in the same daughter cells in 82% of the divided pairs, whereas they were present in different daughter cells in 18% of the divided pairs (Figures 2A and 2B). Expression of Numbl, a Numb homologue involved in neurogenesis, was not detectable in CCSC.

We then examined potential interaction between these two cell fate determinants with the initial hypothesis that one might upregulate the other. We first expressed miR-34a in CCSCs using lentiviral infection and measured Numb expression levels by RT-qPCR and Western blot. Unexpectedly, ectopic miR-34a suppressed Numb expression (Figures 2C and 2D). To investigate whether miR-34a directly targets Numb, we used the microRNA target prediction tool RNA22 to analyze the 3`UTR sequence of Numb and found a putative miR-34a binding site (Figure 2E). The Numb 3`UTR was then cloned into a luciferase reporter, which showed that ectopic miR-34a expression suppressed firefly luciferase activity, whereas mutation in the putative miR-34a seed region in the Numb 3`UTRs abrogated the suppression by miR-34a (Figure 2F). Therefore, miR-34a directly targets Numb mRNA to silence its expression.

miR-34a, Numb, and Notch form an incoherent feedforward loop (IFFL).

It is counterintuitive that miR-34a targets Numb for suppression, considering that both cell fate determinants suppress Notch and promote differentiation. Why does miR-34a suppress Notch directly but upregulate Notch indirectly via Numb? Here, miR-34a, Numb, and Notch form a motif called incoherent feedforward loop (IFFL) (Figure 3A). miR-34a suppresses Notch1 and Numb translation by binding to the 3`UTRs of their mRNA, and Numb suppresses Notch1 by promoting its endocytosis and degradation.

Previous studies have found that IFFL can generate non-monotonic, adaptive, or pulse-like responses in different contexts [32-34], but none of these properties seemed to be particularly relevant to cell fate determination. There have also been computational analyses suggesting that microRNA may reduce noise in IFFL, but those referred to a different topology where the microRNA is suppressed by the protein [35].

To understand how miR-34a and Numb may synergize through this arrangement, we explored the quantitative aspects of this particular IFFL. We previously showed that miR-34a generates a threshold response from Notch due to mutual sequestration while Numb regulates Notch in a graded, continuous way [24, 36, 37], raising the prospect that this IFFL may possess unique properties. A similar setup was used to characterize the newly discovered miR-34a suppression of Numb. We incrementally increased ectopic miR-34a expression level using a Doxycycline-inducible promoter and performed Fluorescence Activated Cell Sorting (FACS) with antibody against Numb. FACS analysis revealed that incremental miR-34a induction gradually suppressed Numb levels in $Numb^{high}$ cells (Figures 3B and 3C).

A computational IFFL model was then constructed by expanding our previously published miR-34a/Notch model to include miR-34a suppression of Numb and Numb suppression of Notch. The model assumes that miR-34a suppression of Notch1 is stronger than its suppression of Numb (which is more gradual), based on the experimental data. Simulation of the model over certain parameter ranges presented an interesting possibility that the IFFL could generate a more robust Notch switch than miR-34a alone (Figure 3D). With IFFL, 'high' and 'low' Notch levels are steady and insensitive to precise miR-34a level except for a narrow transition (threshold) region, which resembles a typical switch used in electronics. In contrast, Notch levels vary more with a wider transition region if there is only miR-34a but no Numb. Intuitively, when miR-34a level increases, Numb level is suppressed accordingly to offset, hence their combined suppression effect on Notch remains roughly constant until the mutual sequestration threshold is reached. Therefore, the IFFL buffers Notch level from miR-34a copy number variation and enforces a sharp transition only around the mutual sequestration threshold. Further simulations of the model suggested that the steepness of the transition is influenced by the relative strength between the direct and indirect paths (Figures 4A and 4B).

The model made a further prediction that IFFL produces better bimodality of Notch levels (and hence cell fate determination) in the population. Intuitively, the narrower transition region of the IFFL minimizes the number of cells with intermediate Notch levels (Figure 3D). Based on previous FACS measurements of Doxycycline-induced miR-34a level distributions in CCSC sphere cells [24], we performed stochastic simulations of IFFL and miR-34a alone (Numb knockdown). The simulations suggested that, even though miR-34a alone could generate Notch bimodality due to mutual sequestration as previously

demonstrated [24], IFFL generates better Notch bimodality with more clearly defined peaks and fewer cells in between, thanks to its more robust switching behavior (Figure 3E).

miR-34a and Numb synergize for a robust Notch bimodal switch.

Experiments were then designed to test whether the presence of Numb enhances miR-34a regulation of Notch as a cell fate switch. First, we measured the response of Notch1 level to incremental miR-34a levels with and without Numb. As previously demonstrated, we used CCSCs stably integrated with a lentiviral vector that drives ectopic miR-34a expression with a Doxycycline-inducible promoter [24] (Figure 5A). CCSCs were then infected with a lentiviral vector expressing short hairpin RNAs (shRNAs) against Numb to knock down Numb. The efficiency of Numb knockdown in CCSCs was verified by western blot (Figure 4C).

CCSCs in separate wells were then treated with incremental dosages (0, 100, 200, 300, 400, and 500 ng/ml) of Doxycycline. RT-qPCR verified that induced miR-34a expression level increased linearly with Doxycycline dosage in CCSCs with or without Numb knockdown (Figures 4D and 4E). Time-series measurements indicated that it took approximately 42 hours for Notch levels to stabilize after doxycycline induction (Figures 4F-4I), so steady-state measurements were performed 48 hours post induction. With Numb, Notch levels remained largely steady until being abruptly turned off by 400 ng/ml Doxycycline induction of miR-34a (Figures 4J, 5B and 5D). In contrast, Notch levels gradually decreased and slowly turned off in response to increasing miR-34a levels when Numb was knocked down (Figures 4K, 5C and 5D). These measurements support the computational hypothesis in Figure 2D that miR-34a and Numb work in synergy to

generate a more robust switch. Without Numb, Notch level is more sensitive to miR-34a variation.

We then tested whether the presence of Numb enhances miR-34a regulation of Notch to be more bimodal as the computational analysis predicted. Again, we induced miR-34a at different levels and measured Notch protein levels in individual cells using flow cytometry with antibody against Notch. In CCSCs with Numb, Notch displayed clear bimodality and individual cells were clustered around the $Notch^{high}$ or $Notch^{low}$ peaks. In contrast, in CCSCs with Numb knockdown, even though Notch level distribution was still overall bimodal due to mutual sequestration, bimodality was degraded by a subpopulation of cells with intermediate Notch levels between high and low (Figure 5E). This result is consistent with the computational prediction in Figure 3E that the IFFL improves Notch bimodality.

Intermediate Notch level leads to ambiguous and plastic cell fate.

The implication of Notch bimodality on cell fate determination was then investigated. We isolated the $Notch^{high}$, $Notch^{low}$ and $Notch^{inter}$ cells by FACS (Figures 6A and 7A) and immediately performed immunofluorescence for the CCSC marker ALDH1 and differentiation marker CK20 (Figure 6B). Consistent with previous reports, $Notch^{high}$ cells are ALDH1+CK20- stem cells and $Notch^{low}$ cells are ALDH1-CK20+ differentiated cells. Interestingly, the cells with intermediate Notch levels ($Notch^{inter}$) expressed both ALDH1 and CK20, reflecting an intermediate state between stem cell and differentiation. RNA-seq transcriptome profiling revealed that $Notch^{inter}$ cells have a distinct gene expression signature between those of $Notch^{high}$ and $Notch^{low}$ cells (Figures 6C and 7B). $Notch^{inter}$ cells express intermediate levels of stem cell and differentiation makers, while $Notch^{high}$ cells express high levels of stem cell markers and $Notch^{low}$ cells express high levels of

differentiation markers (Figures 7C). Gene Set Enrichment Analysis (GSEA) show that pathways commonly associated with CCSCs, such as Notch, Wnt, and MAPK signaling pathways, are upregulated in Notch^{high} cells (Figure 7D).

We then performed serial sphere propagation assay to test these cells' self-renewal ability, which is a measure of their stemness (Figures 6D, 6E, 7E). Notch^{high} cells efficiently formed spheres in 3D Matrigel culture and maintained their sphere formation capability, whereas Notch^{low} cells formed few spheres in the first generation and lost their sphere formation capability after serial propagation. Notch^{inter} cells could also form spheres, but the spheres were far fewer and smaller than those formed by Notch^{high} cells. We then compared tumorigenic capability by subcutaneously injecting 1x10^4 Notch^{high}, Notch^{inter} and Notch^{low} cells respectively into Nude mice. During the observed period (6 weeks), all 6 mice injected with Notch^{high} cells grew tumors, only 2 mice injected with Notch^{inter} cells grew small tumors, and none of the mice injected with Notch^{low} cells grew tumors (Figure 6F). Similar results were observed in mice injected with Notch^{high}, Notch^{inter} and Notch^{low} cells sorted from a second CCSC (CCSC2) line (Figure 7F). Therefore, Notch^{inter} cells have intermediate self-renewal and tumorigenic capability compared to Notch^{high} and Notch^{low} cells, consistent with their intermediate gene expression signature. Since Notch^{inter} cells seem to occupy a state between Notch^{high} CCSC and Notch^{low} non-CCSC, we next examined their plasticity, or ability to convert into CCSC or non-CCSC. When cultured in FBS-free stem cell medium and low-attachment flask, Notch^{inter} cells upregulated the CCSC marker ALDH1, while Notch^{low} cells did not express ALDH1 after 7 days (Figure 6G). This suggests that Notch^{inter} cells may possess the plasticity to dedifferentiate back into stem cells in contrast to Notch^{low} cells. On the other hand,

Notch^{inter} cells are readier to differentiate than Notch^{high} cells. When cultured in differentiation medium, Notch^{inter} cells lost ALDH1 expression within 24 hours, whereas Notch^{high} cells still retained ALDH1 expression (Figure 6H). It took 10 days for most Notch^{high} cells to lose ALDH1 and express CK20. Collectively, these data suggest that Notch^{inter} cells are in an intermediate state that can dedifferentiate into CCSCs or readily commit to differentiation.

We then examined how the presence of the Notch^{inter} cells affects cell division. Pair-cell assay followed by immunofluorescence for ALDH1 and CK20 revealed that Numb knockdown reduced asymmetric division and gave rise to significantly more ambiguous cell division outcomes, wherein one or both daughter cells co-expressed ALDH1 and CK20 (Figures 6I and 6J).

Altogether, the computational analysis and experimental data combined suggest that miR-34a suppresses Numb to form an IFFL, which acts as a robust switch to generate Notch bimodality. Undermining this switch by Numb knockdown results in a subpopulation of cells with intermediate Notch levels. These cells express both stem cell and differentiation markers and show greater plasticity than Notch^{high} and Notch^{low} cells.

miR-34a and Numb are associated with differentiation of mouse intestinal stem cells.

We have previously shown that miR-34a mediated asymmetric cell fate determination is mostly active in CCSCs isolated from early-stage CRC patient specimens and tends to be silenced in CCSCs isolated from late-stage CRC specimens. CCSCs from early-stage specimens form xenograft tumors in mice that maintain histopathology of their primary human CRCs, which still retain reminiscent features of original colon tissue [24]. This

raised the possibility that miR-34a and Numb perform cell fate-related functions in normal tissues, which was initially inherited by early-stage CCSCs but eventually subverted in late-stage CCSCs.

To test this possibility, we first performed immunofluorescence for miR-34a and Numb in cryosectioned mouse intestinal crypts harvested from *Lgr5-EGFP-IRES-CreER^{T2}* transgenic mice [38]. miR-34a and Numb expression are low in GFP-labeled Lgr5+ intestinal stem cells (ISCs) but become higher in more differentiated cells above the stem cell niche (Figures 8A and 8B). On the other hand, Notch1, the target of miR-34a and Numb suppression, was more expressed in Lgr5+ ISCs (Figure 5C), consistent with previous reports that Notch is expressed in ISC and essential for ISC self-renewal [39, 40].

To compare Numb and miR-34a expression levels between ISCs and more differentiated cells, we cultured mouse intestinal cells from *Lgr5-EGFP-IRES-CreER^{T2}* mice in 3D Matrigel, where they grew into crypt-villus like organoids [38] (Figure 8D). The Lgr5+ ISCs (also called CBCs) are capable of both self-renewal and generating other intestinal cell lineages in these organoids. RT-qPCR showed that both Numb and miR-34a expression levels are lower in Lgr5-GFP+ cells than in Lgr5-GFP- cells (Figures 8E and 8F). The difference in expression levels between Lgr5-GFP+ and Lgr5-GFP- cells is greater for miR-34a than for Numb. Flow analysis with RNA FISH probes confirmed low miR-34a expression in Lgr5-GFP+ cells (Figure 9A). Together, the immunofluorescence and RT-qPCR data suggest that miR-34a and Numb expression are associated with more differentiated cells, whereas Notch1 is associated with Lgr5+ ISC.

To validate whether miR-34a and Numb suppress Notch1 in intestinal cells, we infected organoids with lentiviral vectors that express miR-34a or Numb. Transduction and knockdown efficiency was validated by RT-qPCR and Western blot (Figures 9B-9C). Western blot confirmed that ectopic miR-34a and Numb suppressed Notch1 expression in organoid cells (Figures 8G and 8H). Moreover, ectopic miR-34a expression also downregulated Numb expression, consistent with the IFFL (Figure 8I).

We then investigated how miR-34a, Numb and Notch impact ISC cell fate decision. Inhibition of Notch by treating the organoids with the γ-secretase inhibitor DAPT- significantly reduced the Lgr5-GFP+ ISC population in the organoids (Figures 8J, 8N and 9D). Ectopic expression of miR-34a or Numb via lentiviral infection of organoid cells had a similar effect of reducing Lgr5-GFP+ ISCs, consistent with their role of Notch suppression (Figures 8K-8L and 8O-8P). Next, we used a lentiviral vector to express shRNA against Numb in organoids to examine whether knockdown of Numb would impact intestinal cell fate bimodality as it does to early-stage CCSCs. The efficiency of Numb knockdown was validated by Western blot (Figure 9E). Indeed, a subpopulation of cells with intermediate Lgr5 expression levels between $Lgr5^{high}$ ISCs and $Lgr5^{low}$ non-ISCs emerged, and the Lgr5-GFP distribution was no longer bimodal (Figures 8M and 8Q). The effects on ISCs were further validated by measuring the levels of Ascl2, an alternative marker for Lgr5+ ISC [39, 41]. Consistently, inhibition of Notch signaling by DAPT, ectopic miR-34a, or Numb expression reduced Ascl2 levels, whereas Numb knockdown increased Ascl2 levels in organoids (Figures 8R-8Y). Notch inhibition by DAPT, ectopic miR-34a, or Numb expression also increased apoptotic cells shed into the lumen, a

process reminiscent of the shedding of terminally differentiated cells *in vivo* (Figures 9F-9I) [38].

Inflammatory stress induced miR-34a-dependent asymmetric division.

To investigate how loss of the miR-34a-mediated switch may specifically impact ISC cell fate decision, we crossed *miR-34a*$^{flox/flox}$ mice [42] with *Lgr5-EGFP-IRES-CreER*^{T2} mice and then intraperitoneally administered Tamoxifen, which activated Cre to knock out miR-34a in Lgr5+ ISC specifically. miR-34a knockout in Lgr5+ ISCs did not cause noticeable changes to the crypt morphology or the number of Lgr5-GFP ISCs *in vivo* or in derived organoids (Figures 10A-10B). To confirm that miR-34a is not essential for crypt homeostasis, we examined the intestinal crypts from a constitutive miR-34a knockout (miR-34a$^{-/-}$) model [29]. The crypt morphology again seems normal (Figures 10C). This suggests that the miR-34a-mediated switch is not essential for Lgr5+ ISC mediated intestinal homeostasis under normal physiological conditions.

TNFα, a pro-inflammatory cytokine associated with chronic colitis, has been linked to risk of colorectal carcinogenesis [43, 44]. A low dosage (10ng/ml) treatment of TNFα for 3 days caused modest proliferation of Lgr5-GFP+ ISCs, increasing their number from 12% to 19% of the total organoid cell population. The effect of TNFα treatment was amplified by miR-34a knockout. TNFα-induced ISC proliferation became more excessive in organoids derived from *miR-34a*$^{flox/flox}$ mice/*Lgr5-GFP-IRES-CreER*^{T2} mice after miR-34a knockout was induced, causing proliferating Lgr5-GFP+ ISCs to comprise 38% of the organoid cell population (Figure 11A). Consistent with the flow analyses, TNFα and loss of miR-34a greatly increased the expression of Lgr5 and Ascl2, the marker for Lgr5+ ISCs (Figures 11B-11D). Moreover, miR-34a knockout caused TNFα treated organoids to grow

into undifferentiated spheres that resemble CCSC spheres with enrichment of Lgr5-GFP+ ISCs (Figure 11E). BrdU incorporation assay showed that loss of miR-34a led to excessive proliferation in TNFα treated organoids (Figure 11F). Therefore, despite being non-essential for normal tissue homeostasis, the miR-34a-mediated cell fate switch provides a safeguard against excessive ISC proliferation when stem cells regenerate under pro-inflammatory stress.

Lgr5+ ISCs are thought to divide symmetrically in normal conditions [12, 13]. We explored whether the presence of miR-34a has the capability to promote asymmetric division and differentiation to counter excessively proliferating ISCs. We first examined the division of intestinal organoid cells using both the pair-cell assay and direct immunofluorescence on Lgr5-GFP+ doublets freshly isolated by FACS, with antibodies against α or β tubulin to mark mitotic cells. Under normal organoid culture condition, only 4.6% of the Lgr5-GFP+ cells or 3.6% of Ascl2+ cells from *Lgr5-EGFP-CreER^{T2}* organoids divided asymmetrically, while asymmetric division was barely observed in miR-34a deficient Lgr5-GFP+ or Ascl2+ cells from *Lgr5-EGFP-CreER^{T2}/miR-34a$^{flox/flox}$* organoids. Remarkably, 3-day treatment of 10ng/ml TNFα caused 19% of Lgr5-GFP+ cells or 17.3% Ascl2+ cells from *Lgr5-EGFP-CreER^{T2}* organoids to divide asymmetrically. In contrast, miR-34a deficiency reduced such asymmetric division to less than 2% in *Lgr5-EGFP-CreER^{T2}/miR-34a$^{flox/flox}$* organoids (Figures 9J-9K and 11G-11H).

miR-34a dependent asymmetric division *in vivo*

To examine whether inflammation also activates ISC asymmetric division in a miR-34a dependent manner *in vivo*, *Lgr5-EGFP-CreER^{T2}* and *Lgr5-EGFP-CreER^{T2}/miR-34a$^{flox/flox}$* mice were treated with 3% dextran sodium sulfate (DSS) in daily drinking water for 5 days,

followed by 5 days of plain water supply for recovery. Tissues were then harvested and stained. Consistent with previous reports [45-47], DSS upregulated inflammatory factors TNFα, IL-1β, and IL-6 in mouse intestine and colon inflammation (Figures 10D and 10E). Regeneration after DSS-induced tissue damage increased the number of Lgr5-GFP+ ISCs and Lgr5 and Ascl2 expression in the intestine and colon, which was further amplified by loss of miR-34a (Figures 12A-12F and 10F-10G, 12A-12F). DSS treatment caused more proliferation in miR-34a deficient crypts as shown by the number of cells incorporating BrdU (Figures 10H-10I). Crypts were then stained for tubulin to identify dividing cell pairs with microtubule configuration consistent with telophase (the final phase of mitosis) – the midbody at the division plane during cytokinesis and asters at the poles. The cell polarity protein PARD3 was concurrently stained to validate division symmetry. Under stress, more ISCs switch to asymmetric division, from 2% to 13% of all Lgr5-GFP+ divisions and from 1.6% to 9% of all Ascl2+ divisions. Asymmetric division was remarkably decreased to 4% in miR-34a deficient mice (Figures 12G-12H and 13A-13B). Notably, colon stem cells follow the same trend. During recovery from DSS treatment, Lgr5-GFP and Ascl2+ colon stem cells underwent more asymmetric division in a miR-34a dependent manner (Figures 12I-12J and 13C-13D).

We then tested whether asymmetric division can also be triggered by ISC proliferation due to genetic mutation. APC deficiency causes ISC proliferation and is an initiation step for adenomas and 90% of CRC [48]. We crossed transgenic mice carrying *Lgr5-EGFP-CreER^{T2}* and *APC$^{flox/flox}$* alleles, and co-immunofluorescence for Lgr5-GFP and Tubulin confirmed that APC$^{-/-}$ intestinal tissues derived from *Lgr5-EGFP-CreER^{T2}/APC$^{flox/flox}$* mice induced with Tamoxifen *in vivo* contain asymmetric LGR5+/LGR5- or Ascl2+/Ascl2-

division pairs (Figures 13E-13H). Hence ISC proliferations in APC-deficient mouse adenomas can trigger asymmetric division.

To further validate the presence of asymmetric division in clinical samples, we examined 12 pairs of human normal colon and CRC samples. 10.6% of the Lgr5+ and 8.4% of the Ascl2+ dividing pairs were undergoing asymmetric division in CRC samples, in contrast to less than 1% in normal colon samples (Figures 12K-12L and 13I-13J).

Taken together, the *in vitro* and *in vivo* data indicate that, despite being rare in normal tissue, the frequency of asymmetric division can be increased to rein in excessive stem cell proliferation during inflammation-induced regeneration/repair. Loss of miR-34a inhibits asymmetric division and promotes symmetric division that exacerbates stem cell proliferation (Figure 14).

DISCUSSION

Spatial imbalance of cell fate determinants can break symmetry and force bifurcation of cell fate. Here we show that the microRNA cell fate determinant miR-34a and canonical protein cell fate determinant Numb synergize to regulate self-renewal vs. differentiation of early-stage CCSC. miR-34a directly suppresses Numb to form an IFFL, which generates a robust binary switch response from Notch. This switch enhances bimodality of the population and separates CCSCs from non-CCSCs. Undermining this switch via Numb knockdown degrades bimodality and gives rise to an intermediate population of cells that have more ambiguous and plastic cell fate. We further showed that this cell fate determination switch likely provides a safeguard against excessive ISC self-renewal and proliferation in normal tissues. This safeguard mechanism can be triggered during tissue regeneration and repair after inflammation-induced damage, and its inactivation by miR-34a deletion exacerbates Lgr5+ ISC proliferation. The miR-34a-mediated asymmetric division is active in early-stage CCSCs, likely triggered by their excessive proliferationand is eventually subverted by miR-34a silencing in late-stage CCSCs.

Like most microRNAs, miR-34a targets multiple genes. The level of free miR-34a available to bind Notch1 mRNA is subject to variation due to the expression of other miR-34a target genes. The IFFL may provide an additional benefit of buffering Notch and cell fate decision from such miR-34a copy number variation because the binary Notch level and its resulting bimodality are largely insensitive to precise miR-34a concentration as long as it does not cross the transition threshold.

miR-34a and Numb are lower in mouse Lgr5+ ISCs and higher in more differentiated non-ISCs, consistent with their roles of suppressing Notch. However, the fact that miR-34a

deletion generates no obvious intestinal phenotype was puzzling initially. However, the observation that miR-34a curbs excessive ISC proliferation under pro-inflammatory stress provides a potential answer: normal tissues possess seemingly non-essential or redundant mechanisms for robustness [49, 50], and the importance of such mechanisms can become more prominent under stress or disease conditions. CCSCs in late-stage tumors eventually remove this barrier by silencing miR-34a and asymmetric division, contributing to more undifferentiated tumors [24, 51]. The concept of robustness may also provide insights into other microRNAs that are important tumor suppressors but not essential for normal tissue homeostasis.

The subject of ISC division symmetry has been intensely studied, which transformed our view of adult stem cell in mammalian tissue [52]. Previously, ISCs were thought to undergo asymmetric division exclusively to protect their number and genomic integrity [53-55]. However, Lgr5+ CBC cells were identified as actively cycling ISCs, and they perform symmetric division while competing in a neutral drift process [12, 13].

Intriguingly, asymmetric division has been consistently observed in CCSCs, and its abrogation in favor of symmetric division increases their tumor initiating and proliferative capacity [18, 24, 25]. Similar observations have been made in other types of cancer stem cells as well [14-17, 19-21]. Why do CCSCs activate asymmetric division, seemingly *de novo*, which curbs proliferation and promotes differentiation? Our data provide a potential explanation to this paradox: the mechanism of asymmetric division exists in ISC, but is largely silent during normal tissue homeostasis. The rate of asymmetric division is increased to rein in the number of proliferating Lgr5+ stem cells during tissue regeneration after inflammatory damages. It is plausible that asymmetric division may be activated to

counter stem cell proliferation at the onset of oncogenesis and remains active in early-stage CCSCs, until being eventually silenced (e.g., through silencing miR-34a) by tumor progression.

METERIALS AND METHODS

CCSCs Isolation, Culture and Differentiation

CCSCs isolation, culture and differentiation were performed as described as previously [24]. Briefly, CCSCs were isolated from patient tumors by FACS based on markers CD44, CD133 and ALDH1 and functionally validated by serial sphere formation, tumor initiation, and self-renewal assays [24]. CCSCs were cultured as spheres in ultralow-attachment flasks (Corning) in DMEM/F12 (Invitrogen), supplemented with nonessential amino acids (Fisher), sodium pyruvate (Fisher), Penicillin-streptomycin (Fisher), N2 supplement (Invitrogen), B27 supplement (Invitrogen), 4μg/mL heparin (Sigma), 40 ng/mL epidermal growth factor (Invitrogen), and 20 ng/mL basic fibroblast growth factor (Invitrogen) at 37 °C and 5% CO2. To propagate in vitro, spheres were collected by gentle centrifugation, dissociated into single cells, and then cultured to form next generation spheres.

Transgenic Mice and DSS treatment

Lgr5-EGFP-creER^{T2}/miR-34a$^{flox/flox}$ mice were generated by interbreeding *Lgr5-EGFP-creER^{T2}* mice [38] and *miR-34a$^{flox/flox}$* mice [42]. *Lgr5-EGFP-creER^{T2}/APC$^{flox/flox}$* mice were generated by interbreeding *Lgr5-EGFP-creER^{T2}* mice with *APC$^{flox/flox}$* mice [56]. Cre recombinase was induced by intraperitoneal injection of Tamoxifen (Sigma) dissolved in sterile corn oil for 5 consecutive days at a dose of 75mg/kg. For DSS treatment, 6-8-week-old mice were treated with DSS (36,000–50,000 kDa; MP Biomedicals) in daily drinking water for 5 days, followed by plain water for 5 days. All animal experiments were approved by The Cornell Center for Animal Resources and Education (CARE) and followed the protocol (2009-0071 and 2010-0100).

Mouse intestinal organoid culture

Crypt isolation, cell dissociation, and organoid culturing were performed using previously described protocol [38]. For TNFα treatment, organoid cells were cultured in medium containing 10ng/ml TNFα (R&D) for 72 hours.

Immunofluorescence

Pair-cell assay was used to investigate CCSC division. Disassociated single CCSC sphere cells were plated on an uncoated glass culture slide (Corning) and allowed to divide once. After fixed in cold methanol, the cells were blocked in 10% normal goat serum for 1 hour and then incubated with anti-ALDH1 (clone H-4, 1:100, Santa Cruz), anti-CK20 (clone H-70, 1:100, Santa Cruz), anti-Numb (1:100, Abcam) and anti-Notch1 (1:400, Abcam) antibody overnight at 4 °C. For the BrdU incorporation assay, the tissue sections were incubated in 1M HCl for 1 hour at 37 °C after fixation. The sections were then washed, and switched to 100 mM $Na_2B_4O_7$ for 2 minutes. After blocked in 10% normal goat serum for 1 hour, the cells were then incubated with anti-BrdU (1:200, Sigma). The cells were then incubated with Rhodamine Red labeled secondary antibody (Invitrogen) for 1 hour at room temperature. After counterstained with DAPI (Invitrogen), the slides were observed under a fluorescent microscope (Olympus).

Divisions of Lgr5-EGFP ISCs were examined by three methods. First, Lgr5-GFP doublets were directly collected from intestinal organoids by FACS sorting based on GPF signal and cell size. The cells were then immediately fixed in 4% paraformaldehyde, permeabilized in 0.5% Triton-X and stained with anti-GFP-Alexa Fluor 488 (1:500, Abcam), anti-Ascl2 (1:100, Bioss) and anti-β-Tubulin-Cy3 antibodies (1:100, Sigma). In the second method, single Lgr5-GFP cells were plated in Matrigel and allowed to divide once. The cells were then fixed, permeabilized and stained with anti-GFP, anti-Ascl2 and

anti-α-tubulin (1:500, Abcam) antibodies. In the third method, intestines from *LGR5-EGFP-creER^{T2}* and *LGR5-EGFP-creER^{T2}/APC$^{flox/flox}$* mice and human colon and CRC samples were fixed in 4% paraformaldehyde. Frozen sections were then prepared and stained with anti-GFP, anti-Ascl2, anti-PARD3 (1:200, Abcam) and anti-α-tubulin (1:500, Abcam) antibodies. After counterstaining with DAPI (Invitrogen), the slides were observed under a fluorescent microscope (Olympus).

RNA FISH

RNA FISH was performed as described as previously [24]. In brief, CCSCs were fixed with 4% formaldehyde for 30 minutes at room temperature, followed by permeabilization in 70% ethanol at 4 °C overnight. 1-ethyl-3-(3-dimethylaminopropyl) carbodiimide (EDC) fixation was applied to prevent the loss of miRNA. After a 2-hour incubation in prehybridization buffer (25% formamide, 0.05 M EDTA, 4×SSC, 10% dextran sulfate, 1×Denhardt's solution, 0.5 mg/ml Escherichia coli tRNA and 0.5 mg/ml RVC), digoxigenin (DIG)–labeled locked nucleic acid (LNA) probe (Exiqon) was added for hybridization. The slides were then incubated with anti-DIG antibody (1:400, Roche), and the miRNA expression was detected by Rhodamine Red labeled secondary antibody (Invitrogen). DAPI (Invitrogen) was used for nucleic counterstaining. The slide was then observed under a fluorescent microscope (Olympus).

Flow Cytometry

Single CCSC sphere cells were incubated with anti-Notch1 antibody (1:100, Abcam) after fixed with formaldehyde and further permeabilized by methanol. The cells were then incubated with PE labeled secondary antibody (Invitrogen). Notch^{high}, Notch^{low} and Notch^{inter} populations were isolated by FACS using a Notch signaling reporter with tandem

repeats of the RBP-Jk transcriptional response element (TRE) [24]. Lgr5-GFP population was evaluated by directly measuring GFP signal from intestinal organoids. ALDH1 levels were analyzed using the Alde flour kit. The samples were analyzed using a BD LSR II flow cytometer. The raw FACS data were analyzed with the FlowJo software to gate cells according to their forward (FSC) and side (SSC) scatter profiles.

Quantitative Real-time RT-PCR Analysis

Total RNA was extracted from the cells using the TRIzol Reagent (Invitrogen). cDNA was synthesized from 500 ng of total RNA in 20μl of reaction volume using the High Capacity cDNA Archive Kit (Applied Biosystems). Quantitative PCR was carried out using the SYBR Green System (Applied Biosystems) to detect gene expression. All samples were run in triplicate three times. The primer sequences include: Notch1, 5`-GTGACTGCTCCCTCAACTTCAAT-3` and 5`-CTGTCACAGTGGCCGTCACT-3`; Notch2, 5'-AACTGTCAGACCCTGGTGAAC-3' and 5`-CGACAAGTGTAGCCTCCAATC-3`; Numb, 5`-GCTGCCTCTCCAGGTCTCTTC-3` and 5`-CGCTCTTAGACACCTCTTCTAACCA-3`; CK20, 5`- AGGAGACCAAGGCCCGTTA-3` and 5`- ATCAGTTGGGCCTCCAGAGA-3`; actin, 5`-CGCGAGAAGATGACCCAGAT-3` and 5`-ACAGCCTGGATAGCAACGTACAT-3`; The expression of each gene was defined from the threshold cycle (Ct), and the relative expression levels were calculated using the 2-△△Ct method after normalization to the actin expression level.

Western Blot

Whole cell lysate was prepared in a lysis buffer (20 mM Tris pH 7.5, 150 mM NaCl, 1% Nonidet P-40, 0.5% Sodium Deoxycholate, 1 mM EDTA, 0.1% SDS, protease inhibitors). Proteins were first separated by 10% SDS-PAGE and then transferred to a Hybond

membrane (Amersham). The membranes were incubated with primary antibodies either anti-Notch1 (1:1000, Abcam), anti-Numb (1:1000, Abcam), anti-NICD (1:1000, R&D Systems), anti-Hes1 (1:500, Millipore), or anti-Action (1:1000, Abcam) in 5% milk/TBST buffer (25 mM Tris pH 7.4, 150 mM NaCl, 2.5 mM KCl, 0.1% Triton-X100) overnight, and then probed for 1 hour with secondary horseradish peroxidase (HRP)-conjugated anti-mouse or anti-rabbit IgG (Santa Cruz). After extensive wash with PBST, the target proteins were detected on membrane by enhanced chemiluminescence (Pierce).

Lentiviral Vector Constructs and Infection

Lentiviral constructs expressing miR-34a or Numb shRNA have been described previously [24]. The Numb luciferase reporter was generated by cloning the Numb 3`UTR into the pGL3 construct. The QuickChange Site-directed Mutagenesis Kit (Stratagene) was used to mutate the miR-34a binding sequence in Numb 3`UTR. CCSCs and intestinal organoids were infected with the vectors as described previously [24].

Statistical Analysis

Data were expressed as mean ± standard deviation of three biological repeats. Student t-tests were used for comparisons, with $p<0.05$ considered significant.

ACKNOWLEDGEMENTS:

This work was supported by NIH R01GM95990, NIH R01GM114254, NSF 1350659 career award, NSF 1137269, NYSTEM C029543, and DARPA 19-1091726.

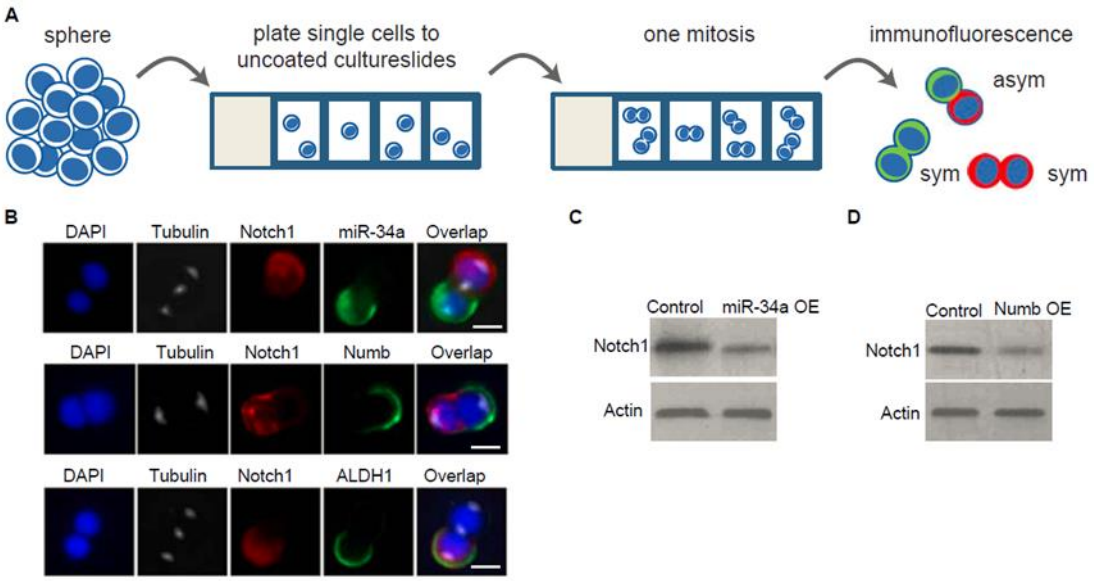

Figure 1. Asymmetric distribution of Notch-targeting miR-34a and Numb during CCSC division.

(A) Schematic illustration of the pair-cell assay. (B) Representative images of pair-cell assay with staining for miR-34a (green) and Notch1 (red), Numb (green) and Notch1 (red), and ALDH1 (green) and Notch1 (red). Tubulin staining indicates dividing pairs in telophase. (C and D) Western blot of Notch1 levels with ectopic miR-34a (B) or Numb (C) expression. Scale bar, 8μm.

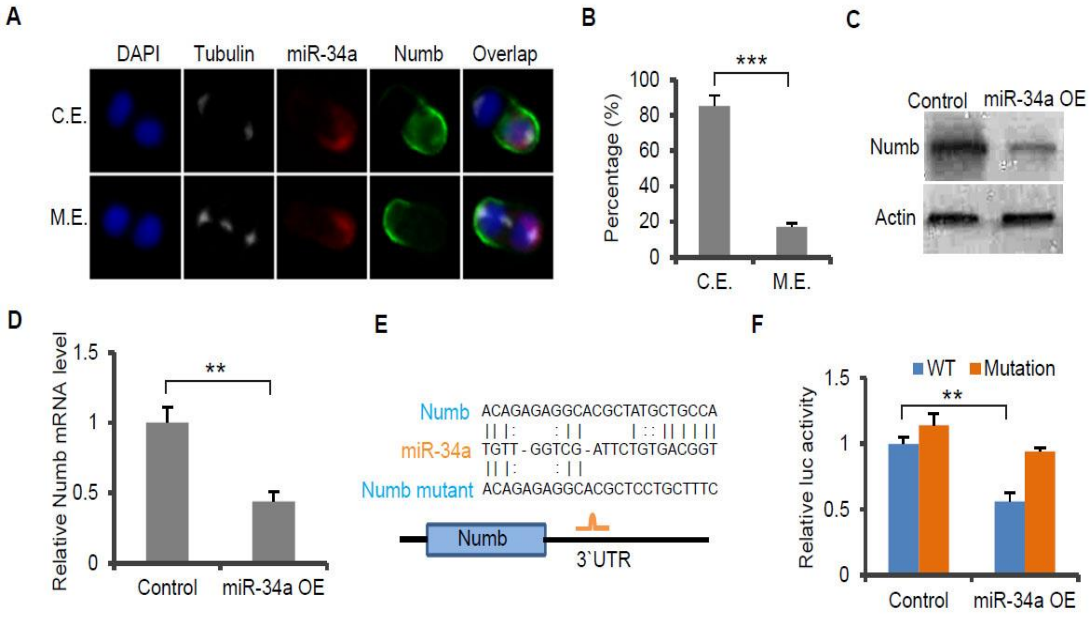

Figure 2. miR-34a directly targets Numb.

(A) Representative images of miR-34a (RNA FISH, red) and Numb (green) distribution during CCSC division. miR-34a and Numb can co-exist (C.E., top row) or be mutually exclusive (M.E., bottom row) in daughter cells. (B) Percentages of CCSC divisions wherein miR-34a and Numb are M.E. or C.E. (C and D) Western blot (C) and RT-qPCR (D) of Numb levels showing ectopic miR-34a expression (miR-34a OE) suppresses Numb expression compared to the control vector. (E) Schematic illustration of predicted binding between miR-34a and Numb 3` UTR, and mutation introduced to the seed region. (F) Luciferase reporter assay confirming the miR-34a binding site in Numb 3`UTR. Numb 3`UTR sequences containing the wild-type (Wt) or mutated (Mut) putative miR-34a binding sites were cloned into the 3`UTR of firefly luciferase (Fluc). Fluc signals were normalized by Renillar luciferase (Rluc) signals. Mutation of the binding site attenuated suppression of Numb by ectopic miR-34a expression (miR-34a OE). Scale bar, 8μm. Error bars denote s.d. of triplicates. **, $p<0.01$; ***, $p<0.001$. p-value was calculated based on Student's t-test.

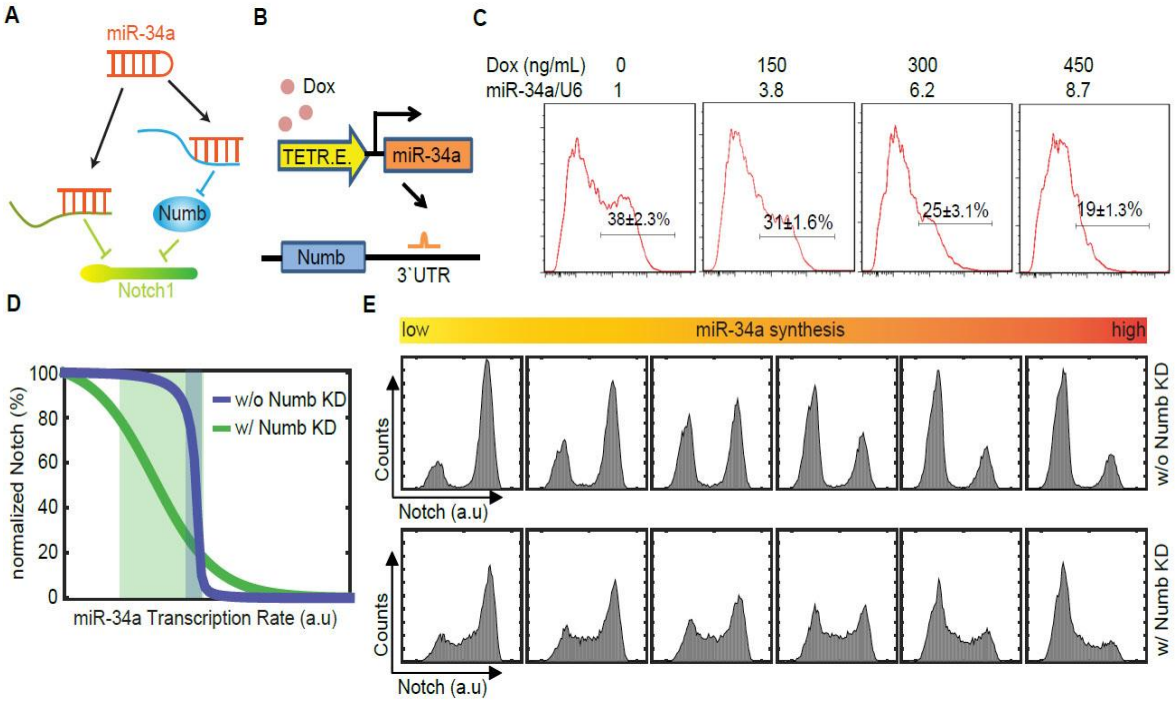

Figure 3. Computational analysis of the incoherent feedforward loop (IFFL).

(A) Schematic of the IFFL formed by miR-34a, Numb, and Notch1. (B) Schematic illustration of the inducible miR-34a construct used in the experiment shown in (C). (C) FACS analysis of Numb expression in CCSC sphere cells when miR-34a expression was incrementally induced by Doxycycline. (D) Simulated Notch1 vs. miR-34a levels from the ODE-based IFFL and Numb knockdown models. Shaded areas are transition regions (80% to 20% of peak Notch level). (E) Simulated Notch1 distributions with IFFL and Numb knockdown models.

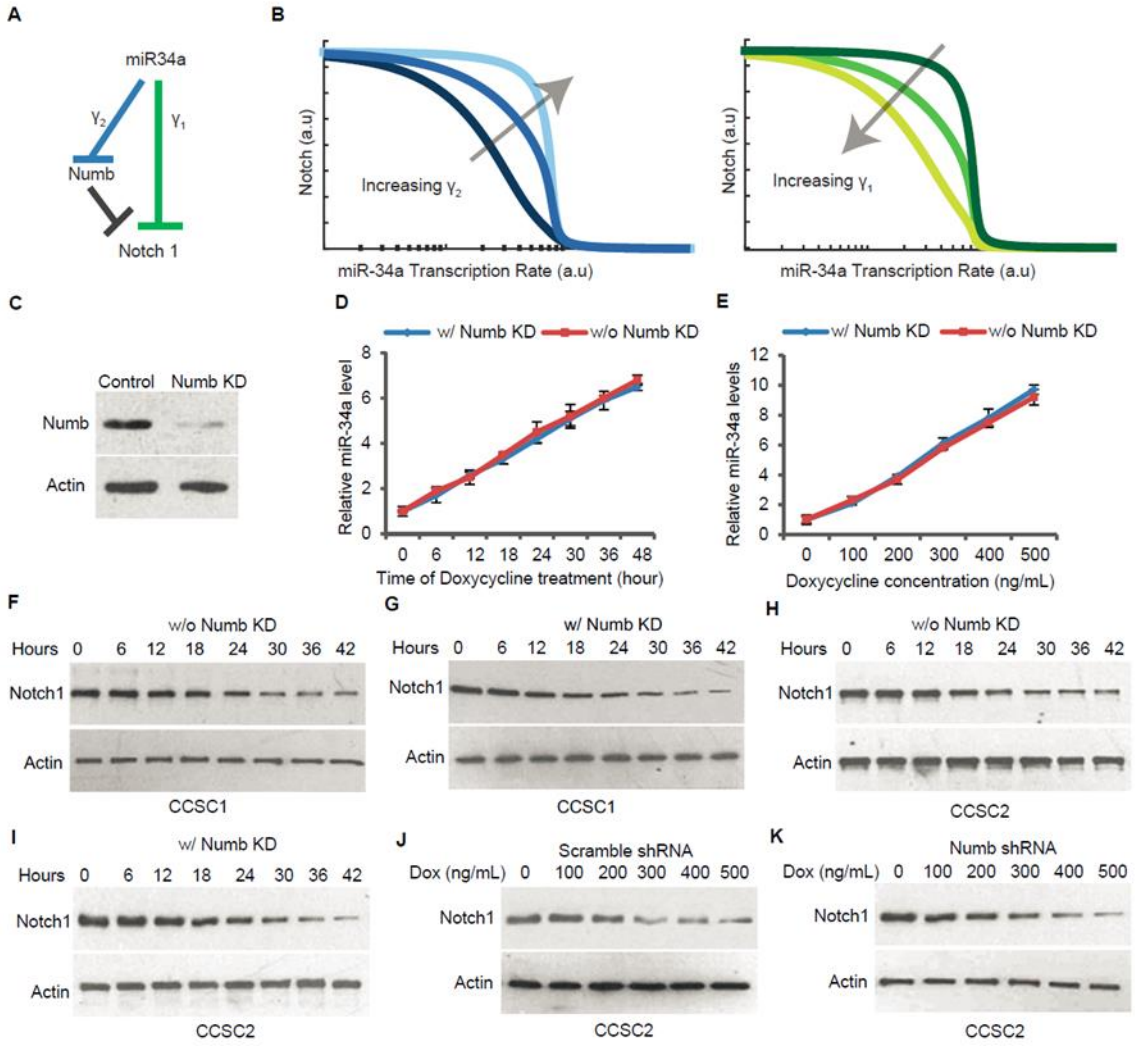

Figure 4. IFFL generates a robust Notch switch.

(A) Schematic of the IFFL. (B) Computational simulation shows the transition (threshold and slope) of the IFFL switch is influenced by the strength of miR-34a suppression of Notch ($\gamma 1$) and Numb ($\gamma 2$). (C) Western blot showing shRNA knockdown of Numb in CCSCs. (D) Time-series RT-qPCR measurements of induced miR-34a levels after addition of Doxycycline. (E) RT-qPCR measurements of miR-34a levels induced by different Doxycycline concentrations. (F and G) Time-series Western blot measurements of Notch1 levels without (F) or with (G) Numb knockdown after miR-34a expression in CCSC1 was induced by 400ng/ml Doxycycline. (H and I) Time-series Western blot measurements of Notch1 levels without (H) or with (I) Numb knockdown after miR-34a expression in CCSC2 was induced by 400ng/ml Doxycycline. (J and K) Western blots of Notch levels in scramble shRNA (J) and Numb shRNA (K) infected CCSC2 spheres with incremental miR-34a induction by Doxycycline.

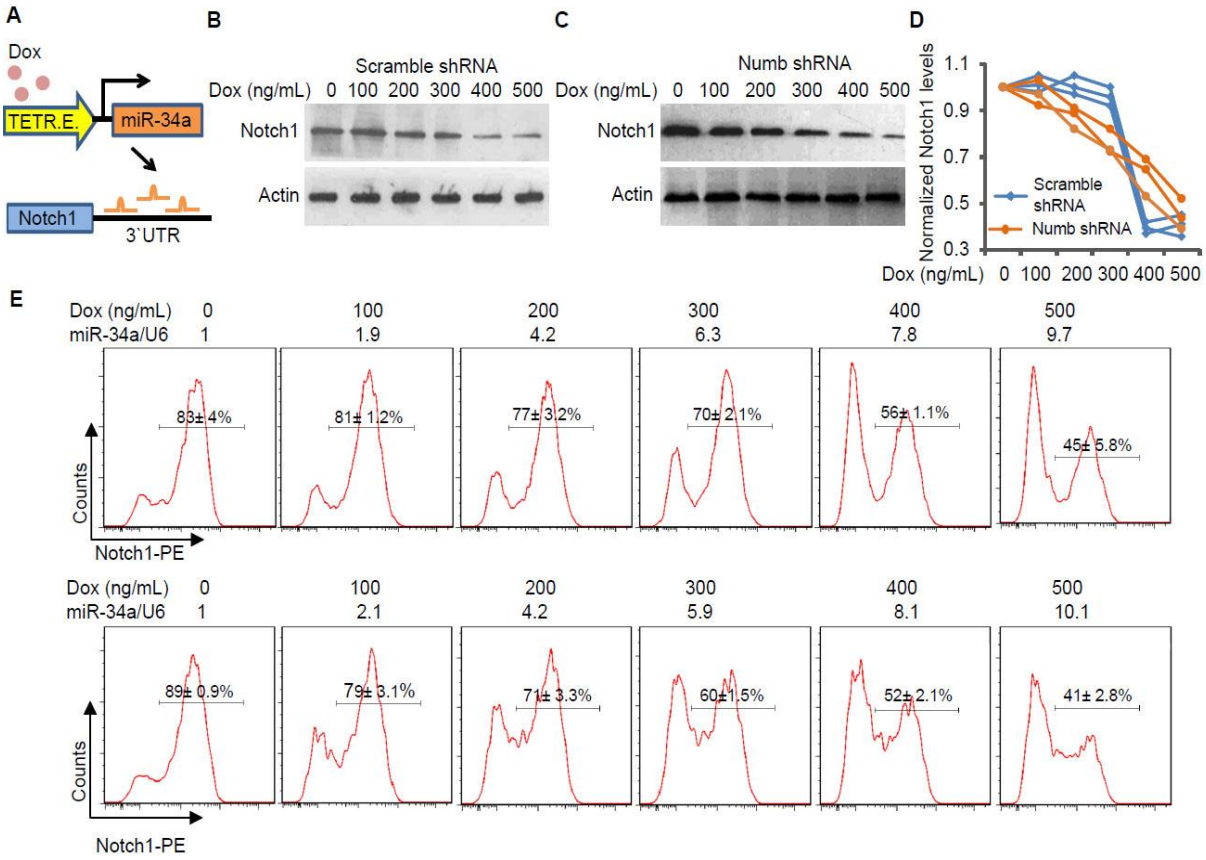

Figure 5. IFFL generates a robust Notch switch.

(A) Schematic illustration of the inducible miR-34a construct used in the experiments shown in (B to E). (B and C) Western blots of Notch levels in scramble shRNA (B) and Numb shRNA (C) infected CCSC spheres with incremental mir-34a induction by Doxycycline. (D) Quantification of Western blots in three independent repeats. (E) FACS analysis of Notch1 bimodality with incremental miR-34a induction by Doxycycline. Top row, intact IFFL; bottom row, Numb knockdown. miR-34a levels were measured by RT-qPCR and shown on top of the FACs plots.

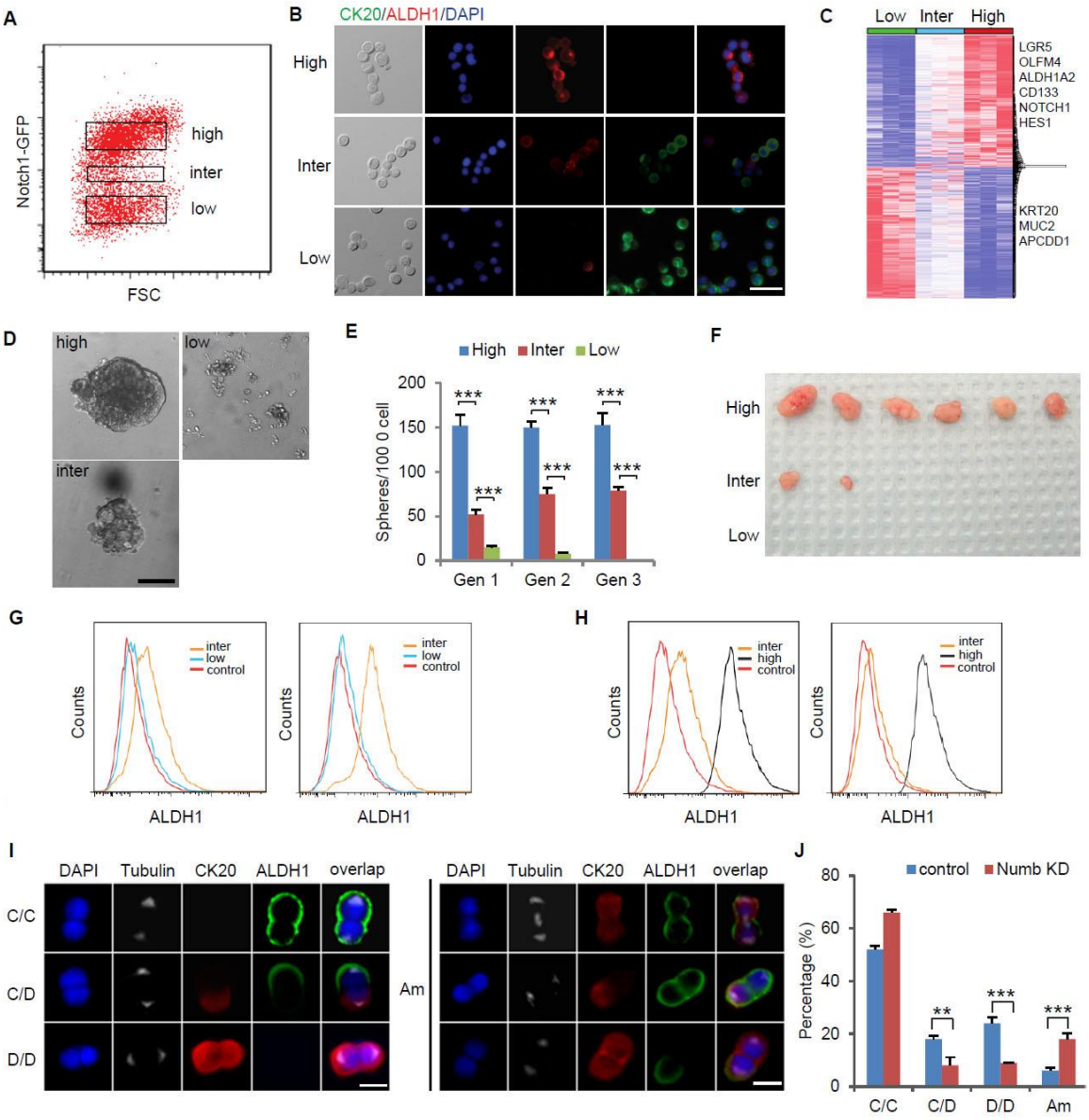

Figure 6. Numb knockdown gives rise to an intermediate population.

(A) FACS plot showing Notch^{high}, Notch^{inter}, and Notch^{low} subpopulations of Numb knockdown sphere cells, treated with 200ng/ml Doxycycline. (B) Immunofluorescence of Notch^{high}, Notch^{inter}, and Notch^{low} cells for CK20 (green) and ALDH1 (red). Scale bar, 20μm. (C) Heat-map of transcriptomes of Notch^{high}, Notch^{inter}, and Notch^{low} cells measured by RNA-seq. (D) Representative images of spheres grown from Notch^{high}, Notch^{inter}, and Notch^{low} cells. Scale bar, 50μm. (E) Serial Sphere propagation of Notch^{high}, Notch^{inter}, and Notch^{low} cells isolated from Numb knockdown sphere cells. Gen, generation. (F) Tumor images showing tumorigenic capability of transplanted Notch^{high}, Notch^{inter}, and Notch^{low} cells. (G) FACS analysis of Notch^{inter} and Notch^{low} cells before (left) and after (right) being under stem cell culture condition for 7 days. Notch^{inter} cells turned

on ALDH1 expression under stem cell culture condition, whereas Notch^{low} cells did not. (H) FACS analysis of Notch^{inter} and Notch^{high} cells before (left) and after (right) being in FBS-containing medium for 24 hours. Notch^{inter} cells lost ALDH1 expression, whereas Notch^{high} cells did not. (I) Representative immunofluorescence images for ALDH1 (red) and CK20 (green) illustrating four types of division: CCSC/CCSC (C/C), CCSC/non-CCSC (C/D), non-CCSC/non-CCSC (D/D) and ambiguous (Am). Scale bar, 8μm. (J) Numb knockdown significantly increased Am divisions besides reducing C/D and D/D. Error bars denote s.d. of triplicates. **, $p<0.01$; ***, $p<0.001$. p-value was calculated based on Student's t-test.

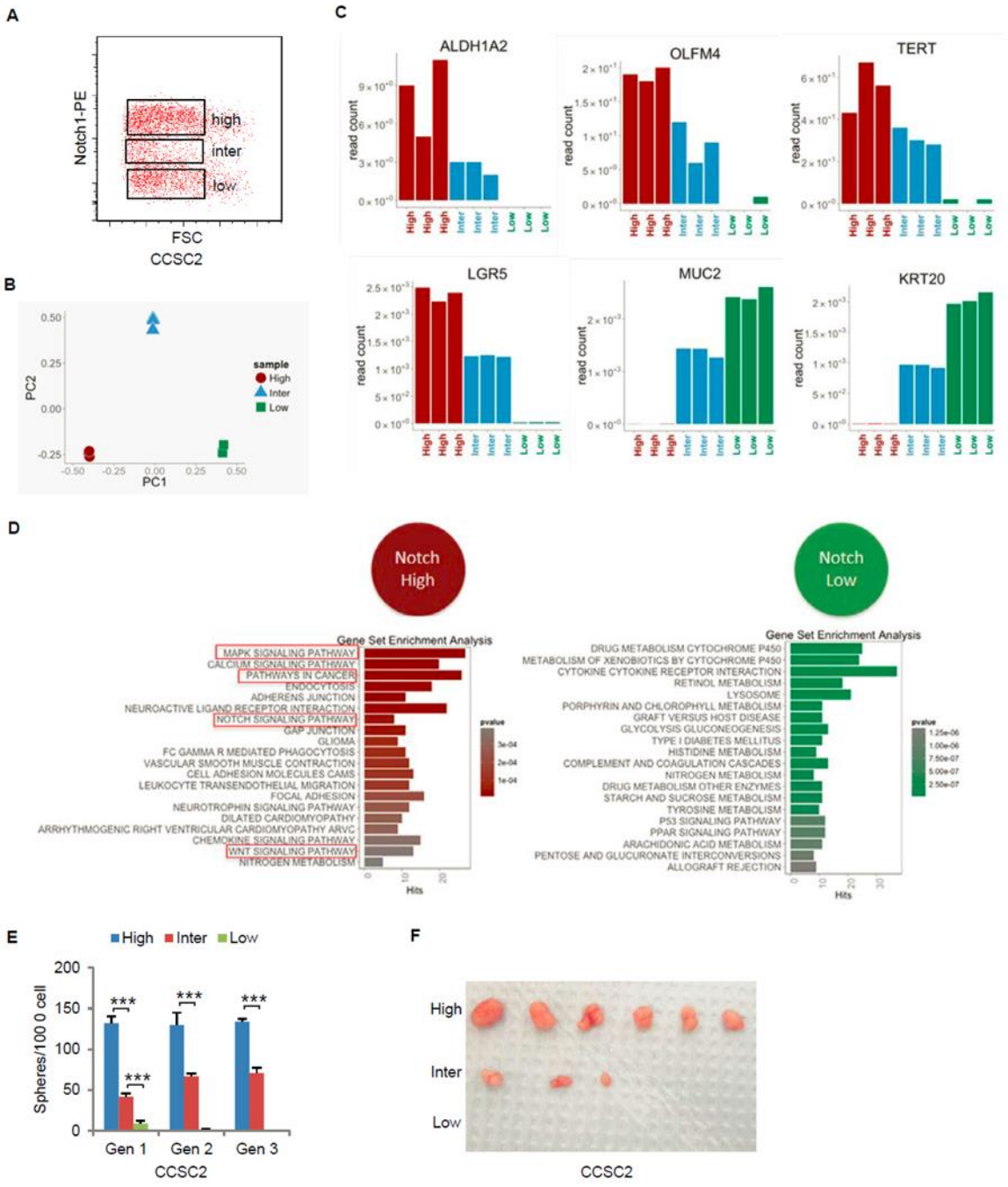

Figure 7. Characterizations of Notch intermediate population in CCSCs generated by Numb knockdown.

(A) FACS plot showing Notch^{high}, Notch^{inter}, and Notch^{low} subpopulations of Numb knockdown CCSC2 sphere cells, treated with 200ng/ml Doxycycline. (B) Principle component analysis (PCA) of transcriptomic profiles of Notch^{high}, Notch^{inter}, and Notch^{low} cells. (C) Marker expression in Notch^{high}, Notch^{inter}, and Notch^{low} cells. (D) Pathways identified by Gene Set Enrichment Analysis (GSEA). (E) Serial Sphere propagation of Notch^{high}, Notch^{inter}, and Notch^{low} cells isolated from Numb Knockdown CCSC2 sphere

cells. Gen, generation. (F) Tumor images showing tumorigenic capability of transplanted Notchhigh, Notchinter, and Notchlow cells. Error bars denote s.d. of triplicates. ***, $p<0.001$. p-value was calculated based on Student's t-test.

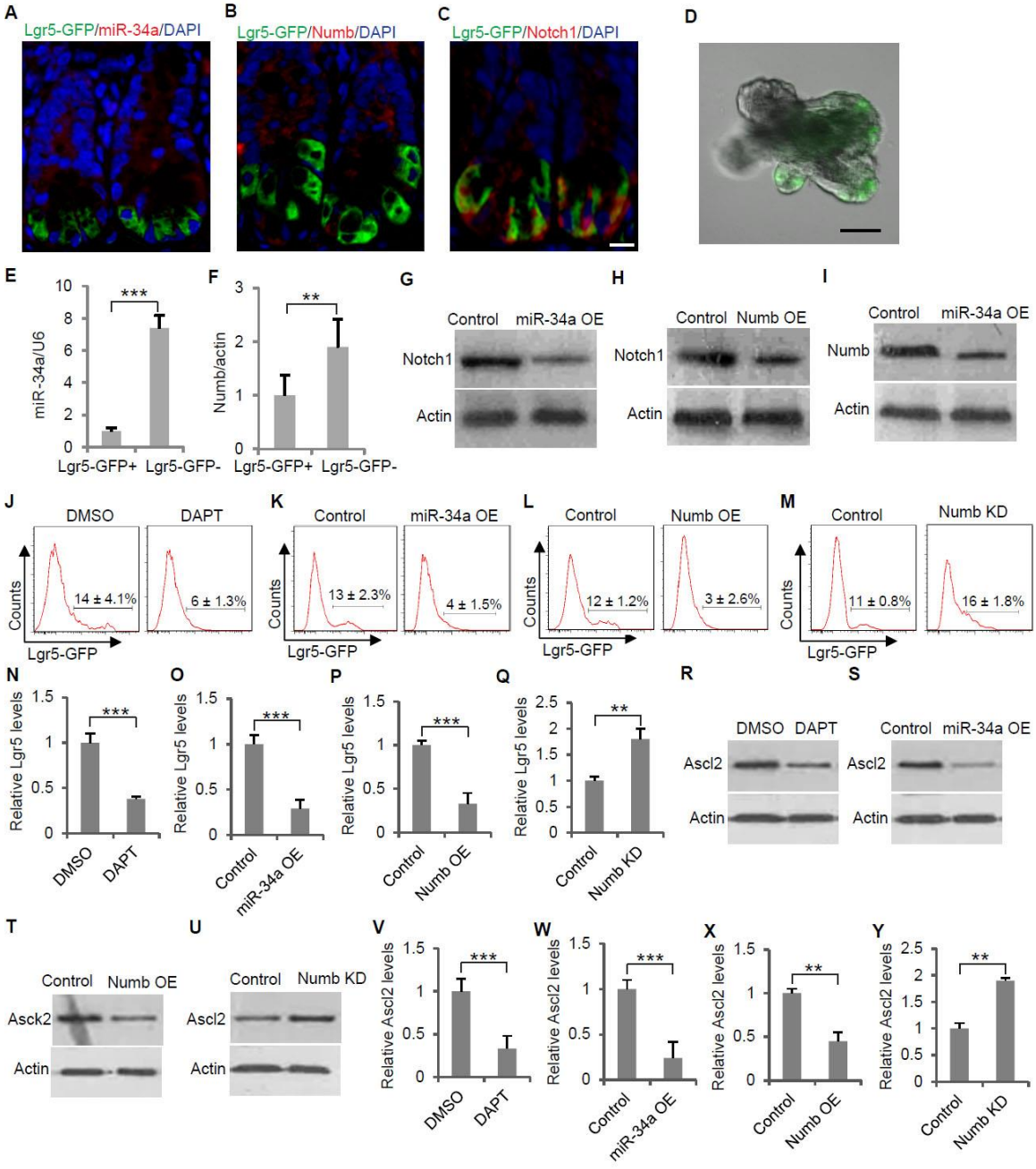

Figure 8. miR-34a and Numb expression in mouse intestinal cells.

(A to C) Immunofluorescence images of intestinal crypts from an Lgr5-EGFP-CreERT2 transgenic mouse. Scale bar, 20μm. (D) A representative image of an intestinal organoid with Lgr5-GFP labeled ISCs. Scale bar, 50μm. (E and F) miR-34a (E) and Numb (F) expression levels in Lgr5-GFP+ and Lgr5-GFP- cells isolated from Lgr5-EGFP-CreERT2 intestinal organoids, measured by RT-qPCR. (G and H) Western blot showing that ectopic miR-34a (G) or Numb (H) expression decreased Notch1 level in organoid cells. (I) Western blot showing that ectopic miR-34a expression decreased Numb level in organoid

cells. (J) DAPT treatment decreased the Lgr5-GFP cell population in Lgr5-EGFP-CreERT2 organoids. (K and L) Ectopic miR-34a (K) or Numb (L) expression decreased the Lgr5-GFP cell population in Lgr5-EGFP-CreERT2 organoids. (M) Numb knockdown gave rise to a subpopulation with intermediate Lgr5-GFP expression. (N to Q) RT-qPCR showing Lgr5 levels in conditions corresponding to J to M. (R to U) Western blot showing Ascl2 levels in conditions corresponding to J to M. (V to Y) RT-qPCR showing Ascl2 levels in conditions corresponding to J to M. Error bars denote s.d. of triplicates. **, $p<0.01$; ***, $p<0.001$. p-value was calculated based on Student's t-test.

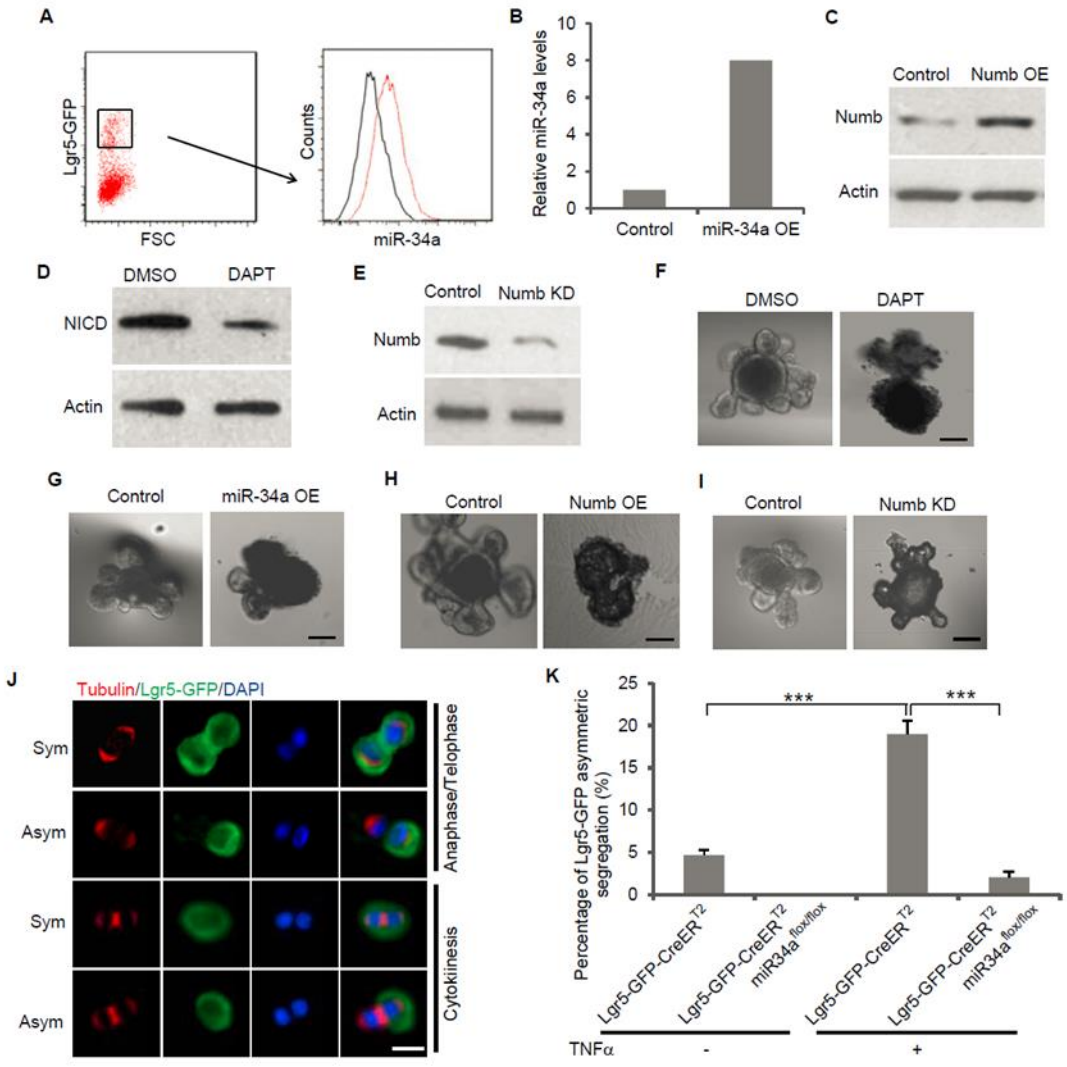

Figure 9. Perturbation of Notch signaling and asymmetric division in mouse intestinal organoids.

(A) miR-34a expression in Lgr5-GFP+ cells by FACS with miR-34a FISH probes. (B) RT-qPCR showing ectopic miR-34 expression. (C) Western blot showing ectopic Numb expression. (D) Western blot showing inhibition of Notch by DAPT. (E) Western blot showing Numb knockdown efficiency. (F-I) Representative images of organoids with DAPT treatment (F), ectopic miR-34a (G) or Numb (H) expression, and with Numb knockdown (I). (J) Representative images of symmetric and asymmetric division of Lgr5-GFP ISCs in intestinal organoids. Tubulin staining indicates stages of mitosis. The anaphase/telophase images were taken from FACS-sorted Lgr5-GFP+ doublets that were fixed and stained immediately without recovery. The cytokinesis images were taken from the pair-cell assay. Scale bar, 8μm. (K) Frequency of asymmetric division of Lgr5-GFP stem cells from Lgr5-EGFP-CreERT2 and Lgr5-EGFP-CreERT2/miR-34aflox/flox intestinal organoids with or without TNFα treatment. Error bars denote s.d. of triplicates. ***, $p<0.001$. p-value was calculated based on Student's t-test.

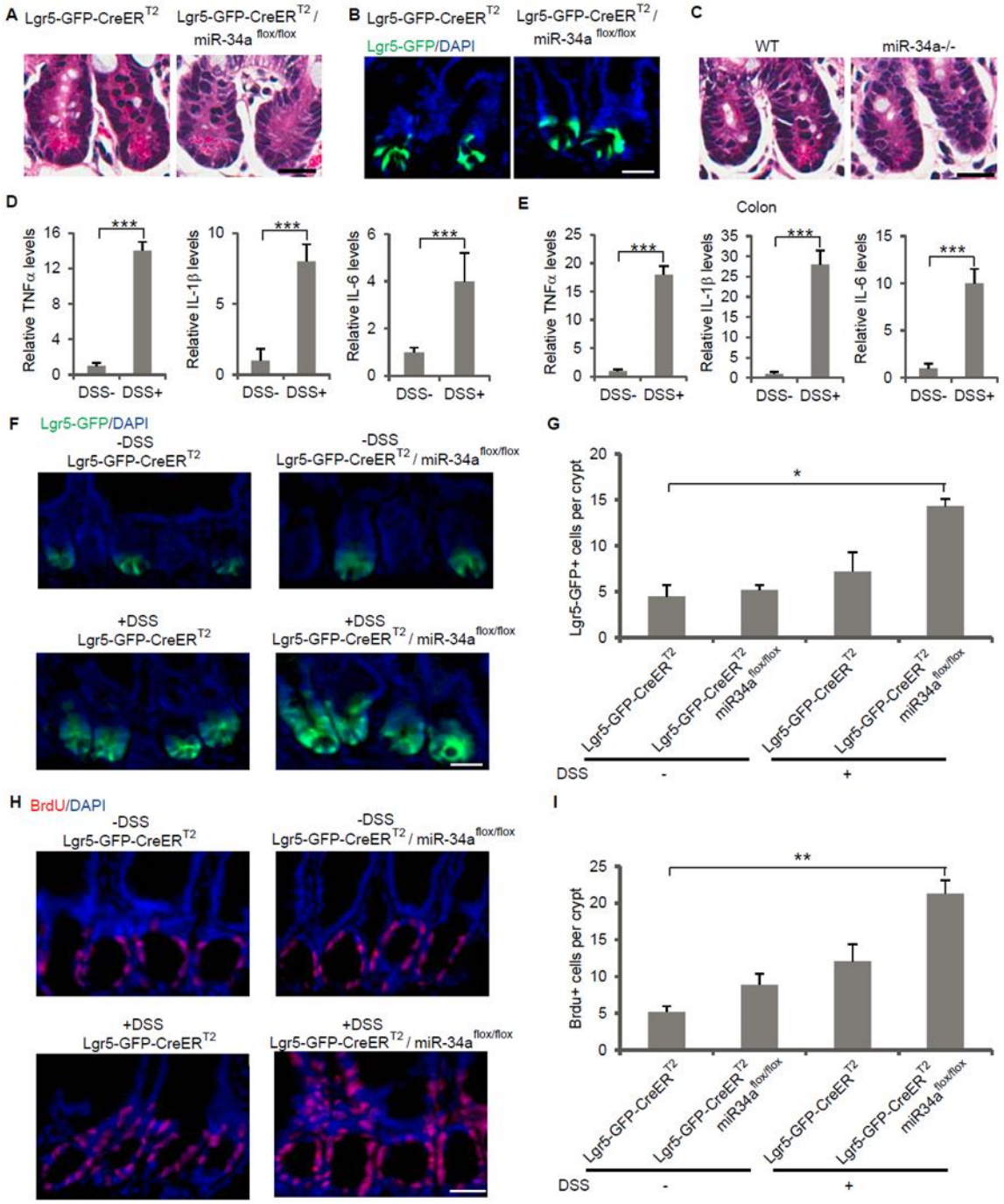

Figure 10. Loss of miR-34a increases DSS-induced proliferation in mouse intestinal crypts.

(A and B) H&E staining (A) and immunofluorescence (B) of intestinal crypts from Lgr5-EGFP-CreERT2 and Lgr5-EGFP-CreERT2/miR-34aflox/flox transgenic mice after Tamoxifen induction. No obvious phenotypes in terms of morphology or Lgr5-GFP (green) ISCs were observed. (C) H&E staining of intestinal crypts from wild type and miR-34a whole-body knockout mice. (D) RT-qPCR showing TNFα, IL-1β and IL-6 expression in

mouse intestine. (E) RT-qPCR showing TNFα, IL-1β and IL-6 expression in mouse colon. (F and G) Representative images (F) and quantification (G) of intestinal crypts from Lgr5-EGFP-CreERT2 and Lgr5-EGFP-CreERT2/miR-34aflox/flox mice administrated with DSS or plain water. DSS treatment followed by recovery increased Lgr5-GFP ISCs in the intestine. (H and I) Representative images (H) and quantification (I) of cell proliferation identified by the BrdU incorporation assay in mouse intestine. DSS and loss-of miR-34a increases proliferation. Scale bar, 50μm. *, $p<0.05$; **, $p<0.001$; ***, $p<0.001$. p-value was calculated based on Student's t-test.

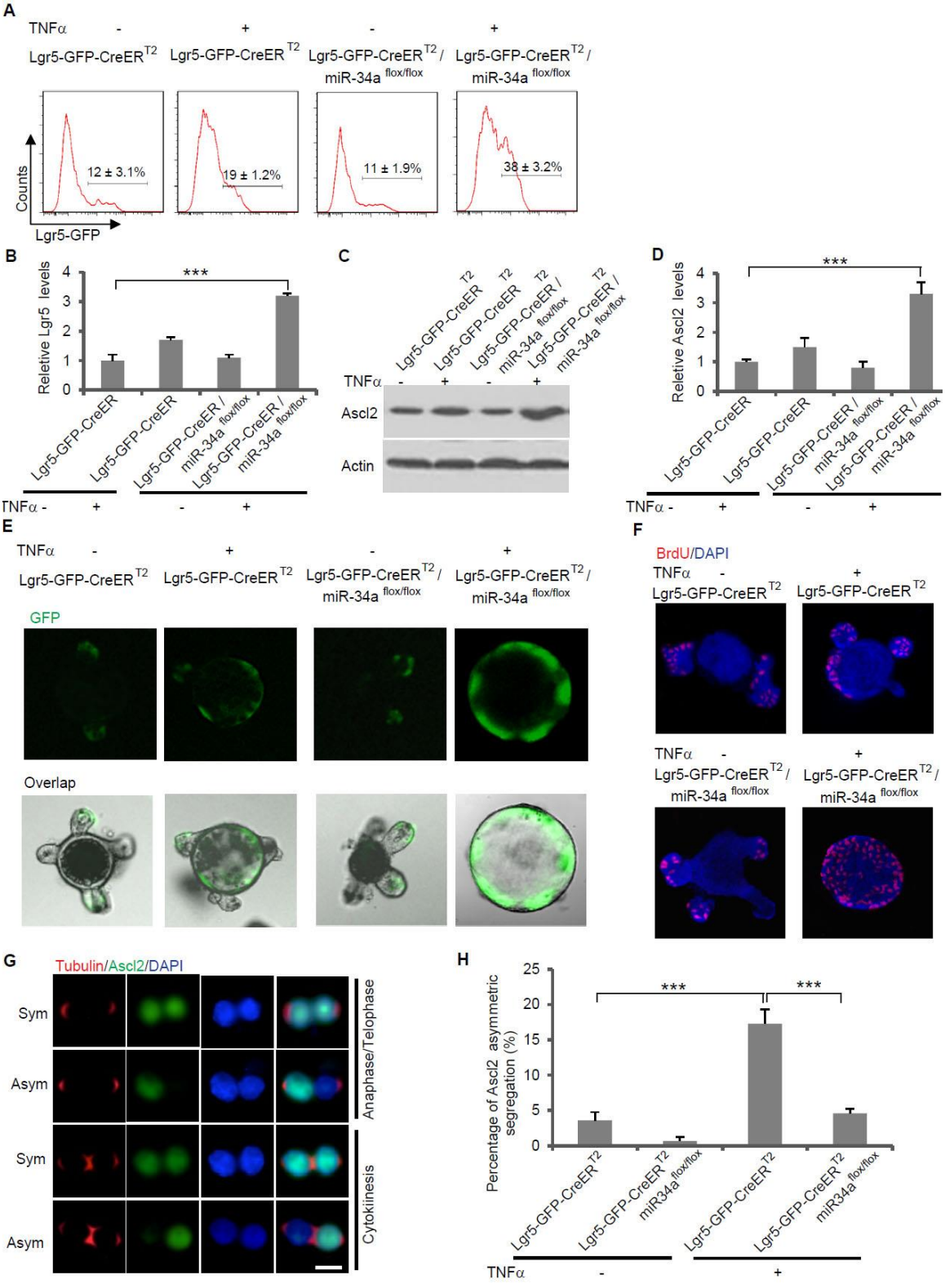
A
TNFα - + - +
Lgr5-GFP-CreER^T2
Lgr5-GFP-CreER^T2
Lgr5-GFP-CreER^T2 / miR-34a flox/flox
Lgr5-GFP-CreER^T2 / miR-34a flox/flox
12 ± 3.1%
19 ± 1.2%
11 ± 1.9%
38 ± 3.2%
Counts
Lgr5-GFP
B
Reletive Lgr5 levels
***
Lgr5-GFP-CreER
Lgr5-GFP-CreER
Lgr5-GFP-CreER / miR-34a flox/flox
Lgr5-GFP-CreER / miR-34a flox/flox
TNFα - + - +
C
Lgr5-GFP-CreER T2
Lgr5-GFP-CreER T2
Lgr5-GFP-CreER T2 / miR-34a flox/flox
Lgr5-GFP-CreER T2 / miR-34a flox/flox
TNFα - + - +
Ascl2
Actin
D
Reletive Ascl2 levels
***
Lgr5-GFP-CreER
Lgr5-GFP-CreER
Lgr5-GFP-CreER / miR-34a flox/flox
Lgr5-GFP-CreER / miR-34a flox/flox
TNFα - + - +
E
TNFα - + - +
Lgr5-GFP-CreER^T2
Lgr5-GFP-CreER^T2
Lgr5-GFP-CreER^T2 / miR-34a flox/flox
Lgr5-GFP-CreER^T2 / miR-34a flox/flox
GFP
Overlap
F
BrdU/DAPI
TNFα - +
Lgr5-GFP-CreER^T2
Lgr5-GFP-CreER^T2
TNFα - +
Lgr5-GFP-CreER^T2 / miR-34a flox/flox
Lgr5-GFP-CreER^T2 / miR-34a flox/flox
G
Tubulin/Ascl2/DAPI
Sym
Asym
Sym
Asym
Anaphase/Telophase
Cytokinesis
H
Percentage of Ascl2 asymmetric segregation (%)
***
***
Lgr5-GFP-CreER^T2
Lgr5-GFP-CreER^T2 miR34a flox/flox
Lgr5-GFP-CreER^T2
Lgr5-GFP-CreER^T2 miR34a flox/flox
TNFα - +

Figure 11. Loss of miR-34a inhibits asymmetric division and promotes ISC proliferation in organoids treated with TNFα.

(A) FACS analysis of Lgr5-EGFP-CreERT2 and Lgr5-EGFP-CreERT2/miR-34aflox/flox organoids with or without TNFα treatment. Percentage of Lgr5-GFP ISCs increased more dramatically in organoids from Lgr5-EGFP-CreERT2/miR-34aflox/flox mice. (B) RT-qPCR showing Lgr5 levels. (C and D) RT-qPCR (C) and Western blot (D) showing Ascl2 levels. (E) Representative images of organoids. Intestinal organoids from Lgr5-EGFP-CreERT2/miR-34aflox/flox mice grew into CCSC-like, undifferentiated spheres with high level of Lgr5-GPF upon TNFα treatment. (F) Cell proliferation measured by BrdU incorporation. (G and H) Representative images (G) and quantification (H) of symmetric and asymmetric division of Ascl2+ ISCs in Lgr5-EGFP-CreERT2 and Lgr5-EGFP-CreERT2/miR-34aflox/flox intestinal organoids with or without TNFα treatment. Tubulin staining indicates stages of mitosis. The anaphase/telophase images were taken from FACS-sorted doublets that were fixed and stained immediately without recovery. The cytokinesis images were taken from the pair-cell assay. Scale bar, 8μm. Error bars denote s.d. of triplicates. ***, $p<0.001$. p-value was calculated based on Student's t-test.

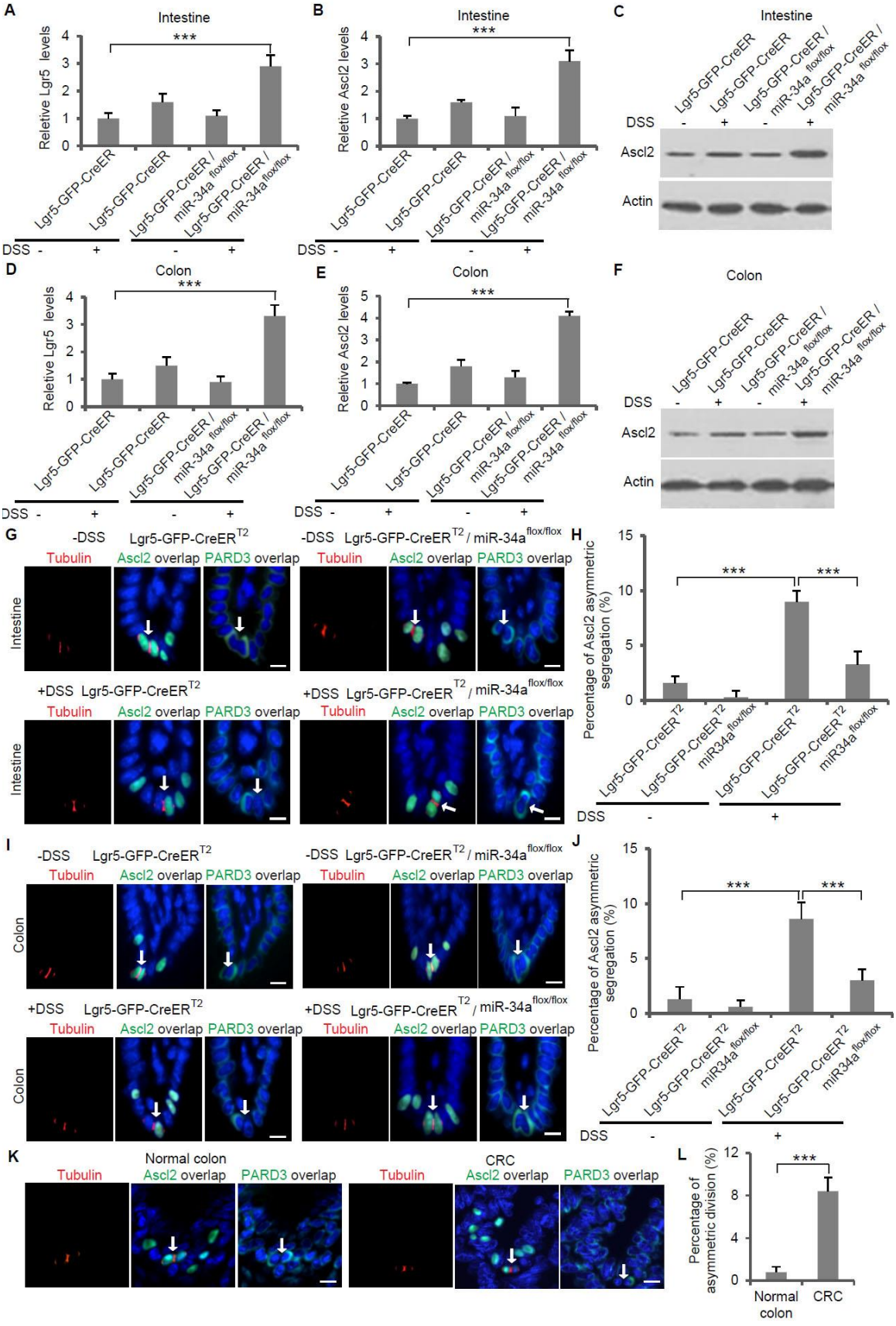
A
Intestine
Reletive Lgr5 levels
***
Lgr5-GFP-CreER
Lgr5-GFP-CreER
Lgr5-GFP-CreER / miR-34a flox/flox
Lgr5-GFP-CreER / miR-34a flox/flox
DSS - + - +
B
Intestine
Relative Ascl2 levels
***
C
Intestine
DSS - + - +
Ascl2
Actin
D
Colon
Reletive Lgr5 levels
***
E
Colon
Relative Ascl2 levels
***
F
Colon
G
-DSS Lgr5-GFP-CreER T2
-DSS Lgr5-GFP-CreER T2 / miR-34a flox/flox
Tubulin Ascl2 overlap PARD3 overlap
Intestine
+DSS Lgr5-GFP-CreER T2
+DSS Lgr5-GFP-CreER T2 / miR-34a flox/flox
H
Percentage of Ascl2 asymmetric segregation (%)
***
***
Lgr5-GFP-CreER T2
Lgr5-GFP-CreER T2 miR34a flox/flox
DSS - +
I
Colon
J
Percentage of Ascl2 asymmetric segregation (%)
K
Normal colon
CRC
L
Percentage of asymmetric division (%)
Normal colon
CRC

Figure 12. Loss of miR-34a inhibits asymmetric division and promotes ISC proliferation in crypts recovering from DSS treatment.

(A) RT-qPCR showing Lgr5 levels in mouse intestine. (B and C) RT-qPCR (B) and Western blot (C) showing Ascl2 levels in mouse intestine. (D) RT-qPCR showing Lgr5 levels in mouse colon. (E and F) RT-qPCR (E) and Western blot (F) showing Ascl2 levels in mouse colon. (G and H) Representative images (G) and quantification (H) of symmetric and asymmetric division of Ascl2+ intestinal stem cells in Lgr5-EGFP-CreERT2 and Lgr5-EGFP-CreERT2/miR-34aflox/flox mice with (+DSS) or without (-DSS) treatment. Cell polarity protein PARD3 was also stained. (I and J) Representative images (I) and quantification (J) of symmetric and asymmetric division of Ascl2+ colon stem cells in Lgr5-EGFP-CreERT2 and Lgr5-EGFP-CreERT2/miR-34aflox/flox mice with (+DSS) or without (-DSS) treatment. PARD3 established cell polarity. (K and L) Representative images (I) and quantification (J) of symmetric and asymmetric division of Ascl2+ cells in human normal colon and CRC tissue. Scale bar, 20μm. Error bars denote s.d. of triplicates. ***, $p<0.001$. p-value was calculated based on Student's t-test.

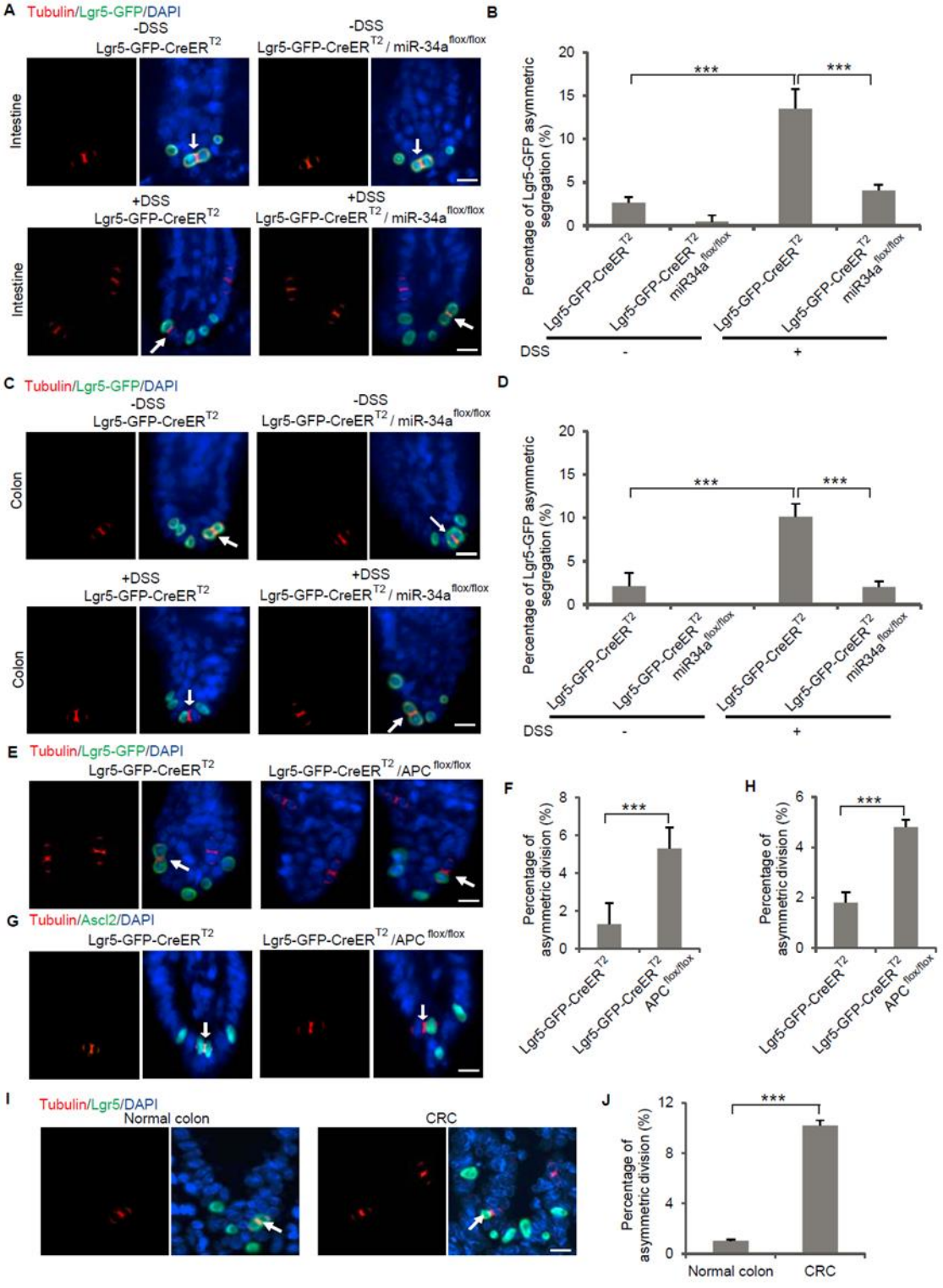

Figure 13. DSS treatment increases asymmetric division and loss-of-miR-34a abrogates asymmetric division in mouse intestine and colon.

(A and B) Representative images (A) and quantification (B) of symmetric and asymmetric division of Lgr5-GFP intestinal stem cells in Lgr5-EGFP-CreERT2 and Lgr5-EGFP-CreERT2/miR-34aflox/flox mice with (+DSS) or without (-DSS) treatment. (C and D) Representative images (C) and quantification (D) of symmetric and asymmetric division of Lgr5-GFP colon stem cells in Lgr5-EGFP-CreERT2 and Lgr5-EGFP-CreERT2/miR-34aflox/flox mice with (+DSS) or without (-DSS) treatment. (E and F) Representative images (E) and quantification (F) of Lgr5-GFP ISC division in Lgr5-EGFP-CreERT2 mice and Lgr5-EGFP-CreERT2/APCflox/flox mice. (G and H) Representative images (G) and quantification (H) of Ascl2+ ISC division in Lgr5-EGFP-CreERT2 mice and Lgr5-EGFP-CreERT2/APCflox/flox mice. (I and J) Representative images (I) and quantification (J) of symmetric and asymmetric division of Lgr5+ cells in human normal colon and CRC tissue. Tubulin staining indicates dividing cell pair. Scale bar, 20μm. Error bars denote s.d. of triplicates. ***, $p<0.001$. p-value was calculated based on Student's t-test.

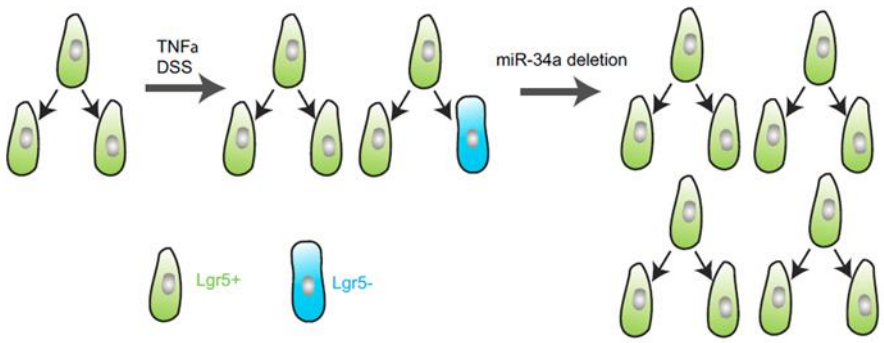

Figure 14. Schematic illustrating the effect of TNF-a/DSS treatment and miR-34a loss.

TNFα or DSS treatment causes cell proliferation. Asymmetric division is increased to curb the number of Lgr5+ ISCs. Loss of miR-34a suppresses asymmetric division, contributing to Lgr5+ ISC proliferation.

REFERENCES

1. Li, R., The art of choreographing asymmetric cell division. Dev Cell, 2013. 25(5): p. 439-50.
2. Williams, S.E., et al., Asymmetric cell divisions promote Notch-dependent epidermal differentiation. Nature, 2011. 470(7334): p. 353-8.
3. Bultje, R.S., et al., Mammalian Par3 regulates progenitor cell asymmetric division via notch signaling in the developing neocortex. Neuron, 2009. 63(2): p. 189-202.
4. Neumuller, R.A. and J.A. Knoblich, Dividing cellular asymmetry: asymmetric cell division and its implications for stem cells and cancer. Genes Dev, 2009. 23(23): p. 2675-99.
5. Jackson, H.W., et al., Expansion of stem cells counteracts age-related mammary regression in compound Timp1/Timp3 null mice. Nat Cell Biol, 2015. 17(3): p. 217-27.
6. Beckmann, J., et al., Asymmetric cell division within the human hematopoietic stem and progenitor cell compartment: identification of asymmetrically segregating proteins. Blood, 2007. 109(12): p. 5494-501.
7. Inaba, M. and Y.M. Yamashita, Asymmetric stem cell division: precision for robustness. Cell Stem Cell, 2012. 11(4): p. 461-9.
8. Knoblich, J.A., Mechanisms of asymmetric stem cell division. Cell, 2008. 132(4): p. 583-97.
9. Katajisto, P., et al., Stem cells. Asymmetric apportioning of aged mitochondria between daughter cells is required for stemness. Science, 2015. 348(6232): p. 340-3.
10. Morrison, S.J. and J. Kimble, Asymmetric and symmetric stem-cell divisions in development and cancer. Nature, 2006. 441(7097): p. 1068-74.
11. Lander, A.D., et al., What does the concept of the stem cell niche really mean today? BMC Biol, 2012. 10: p. 19.
12. Snippert, H.J., et al., Intestinal crypt homeostasis results from neutral competition between symmetrically dividing Lgr5 stem cells. Cell, 2010. 143(1): p. 134-44.
13. Lopez-Garcia, C., et al., Intestinal stem cell replacement follows a pattern of neutral drift. Science, 2010. 330(6005): p. 822-5.
14. Pece, S., et al., Biological and molecular heterogeneity of breast cancers correlates with their cancer stem cell content. Cell, 2010. 140(1): p. 62-73.
15. Pine, S.R., et al., Microenvironmental modulation of asymmetric cell division in human lung cancer cells. Proc Natl Acad Sci U S A, 2010. 107(5): p. 2195-200.
16. Dey-Guha, I., et al., Asymmetric cancer cell division regulated by AKT. Proc Natl Acad Sci U S A, 2011.

17. Lathia, J.D., et al., Distribution of CD133 reveals glioma stem cells self-renew through symmetric and asymmetric cell divisions. Cell Death Dis, 2011. 2: p. e200.
18. O'Brien, C.A., et al., ID1 and ID3 regulate the self-renewal capacity of human colon cancer-initiating cells through p21. Cancer Cell, 2012. 21(6): p. 777-92.
19. Bajaj, J., B. Zimdahl, and T. Reya, Fearful Symmetry: Subversion of Asymmetric Division in Cancer Development and Progression. Cancer Res, 2015. 75(5): p. 792-797.
20. Cicalese, A., et al., The tumor suppressor p53 regulates polarity of self-renewing divisions in mammary stem cells. Cell, 2009. 138(6): p. 1083-95.
21. Sugiarto, S., et al., Asymmetry-defective oligodendrocyte progenitors are glioma precursors. Cancer Cell, 2011. 20(3): p. 328-40.
22. McGill, M.A. and C.J. McGlade, Mammalian numb proteins promote Notch1 receptor ubiquitination and degradation of the Notch1 intracellular domain. J Biol Chem, 2003. 278(25): p. 23196-203.
23. Schweisguth, F., Regulation of notch signaling activity. Curr Biol, 2004. 14(3): p. R129-38.
24. Bu, P., et al., A microRNA miR-34a-regulated bimodal switch targets Notch in colon cancer stem cells. Cell Stem Cell, 2013. 12(5): p. 602-15.
25. Hwang, W.L., et al., MicroRNA-146a directs the symmetric division of Snail-dominant colorectal cancer stem cells. Nat Cell Biol, 2014. 16(3): p. 268-280.
26. He, L., et al., A microRNA component of the p53 tumour suppressor network. Nature, 2007. 447(7148): p. 1130-4.
27. Liu, C., et al., The microRNA miR-34a inhibits prostate cancer stem cells and metastasis by directly repressing CD44. Nat Med, 2011. 17(2): p. 211-5.
28. Boon, R.A., et al., MicroRNA-34a regulates cardiac ageing and function. Nature, 2013. 495(7439): p. 107-10.
29. Choi, Y.J., et al., miR-34 miRNAs provide a barrier for somatic cell reprogramming. Nat Cell Biol, 2011. 13(11): p. 1353-60.
30. Bouchie, A., First microRNA mimic enters clinic. Nat Biotechnol, 2013. 31(7): p. 577.
31. Bader, A.G., miR-34 - a microRNA replacement therapy is headed to the clinic. Front Genet, 2012. 3: p. 120.
32. Kaplan, S., et al., The incoherent feed-forward loop can generate non-monotonic input functions for genes. Mol Syst Biol, 2008. 4: p. 203.
33. Goentoro, L., et al., The incoherent feedforward loop can provide fold-change detection in gene regulation. Mol Cell, 2009. 36(5): p. 894-9.
34. Mangan, S., et al., The incoherent feed-forward loop accelerates the response-time of the gal system of Escherichia coli. J Mol Biol, 2006. 356(5): p. 1073-81.
35. Osella, M., et al., The role of incoherent microRNA-mediated feedforward loops in noise buffering. PLoS Comput Biol, 2011. 7(3): p. e1001101.

36. Mukherji, S., et al., MicroRNAs can generate thresholds in target gene expression. Nat Genet, 2011.
37. Levine, E., et al., Quantitative characteristics of gene regulation by small RNA. PLoS Biol, 2007. 5(9): p. e229.
38. Sato, T., et al., Single Lgr5 stem cells build crypt-villus structures in vitro without a mesenchymal niche. Nature, 2009. 459(7244): p. 262-5.
39. VanDussen, K.L., et al., Notch signaling modulates proliferation and differentiation of intestinal crypt base columnar stem cells. Development, 2012. 139(3): p. 488-97.
40. Fre, S., et al., Notch lineages and activity in intestinal stem cells determined by a new set of knock-in mice. PLoS One, 2011. 6(10): p. e25785.
41. van der Flier, L.G., et al., Transcription factor achaete scute-like 2 controls intestinal stem cell fate. Cell, 2009. 136(5): p. 903-12.
42. Concepcion, C.P., et al., Intact p53-dependent responses in miR-34-deficient mice. PLoS Genet, 2012. 8(7): p. e1002797.
43. Popivanova, B.K., et al., Blocking TNF-alpha in mice reduces colorectal carcinogenesis associated with chronic colitis. J Clin Invest, 2008. 118(2): p. 560-70.
44. Coussens, L.M. and Z. Werb, Inflammation and cancer. Nature, 2002. 420(6917): p. 860-7.
45. Coste, A., et al., LRH-1-mediated glucocorticoid synthesis in enterocytes protects against inflammatory bowel disease. Proc Natl Acad Sci U S A, 2007. 104(32): p. 13098-103.
46. Oh, S.Y., et al., Comparison of experimental mouse models of inflammatory bowel disease. Int J Mol Med, 2014. 33(2): p. 333-40.
47. Yan, Y., et al., Ste20-related proline/alanine-rich kinase (SPAK) regulated transcriptionally by hyperosmolarity is involved in intestinal barrier function. PLoS One, 2009. 4(4): p. e5049.
48. Schepers, A.G., et al., Lineage tracing reveals Lgr5+ stem cell activity in mouse intestinal adenomas. Science, 2012. 337(6095): p. 730-5.
49. Shen, X., et al., Architecture and inherent robustness of a bacterial cell-cycle control system. Proc Natl Acad Sci U S A, 2008. 105(32): p. 11340-5.
50. Ebert, M.S. and P.A. Sharp, Roles for microRNAs in conferring robustness to biological processes. Cell, 2012. 149(3): p. 515-24.
51. Bu, P., et al., Asymmetric division: a marker for cancer stem cells in early stage tumors? Oncotarget, 2013. 4(7): p. 948-9.
52. McHale, P.T. and A.D. Lander, The protective role of symmetric stem cell division on the accumulation of heritable damage. PLoS Comput Biol, 2014. 10(8): p. e1003802.
53. Potten, C.S., G. Owen, and D. Booth, Intestinal stem cells protect their genome by selective segregation of template DNA strands. J Cell Sci, 2002. 115(Pt 11): p. 2381-8.

54. Quyn, A.J., et al., Spindle orientation bias in gut epithelial stem cell compartments is lost in precancerous tissue. Cell Stem Cell, 2010. 6(2): p. 175-81.
55. Goulas, S., R. Conder, and J.A. Knoblich, The par complex and integrins direct asymmetric cell division in adult intestinal stem cells. Cell Stem Cell, 2012. 11(4): p. 529-40.
56. Shibata, H., et al., Rapid colorectal adenoma formation initiated by conditional targeting of the Apc gene. Science, 1997. 278(5335): p. 120-3.

Chapter 3

MicroRNA miR-34a provides a barrier against inflammation-induced colon stem cell proliferation and oncogenesis

This section is adapted from the following publication:

Lihua Wang, Kun Xiang, Gary Zhou, Nikolai Rakhilin, Pengcheng Bu, Xiling Shen. MicroRNA miR-34a provides a barrier against inflammation-induced colon stem cell proliferation and oncogenesis. Under review.

Author contribution: Lihua Wang and Xiling Shen conceived the concept, designed the experiments, and co-wrote the manuscript. Lihua Wang performed the experiments with the assistance from Pengcheng Bu, Kun Xiang, and Gary Zhou for immunofluorescence and Nikolai Rakhilin for animal experiments.

INTRODUCTION

The colon epithelium is one of the fastest generative tissues in the body. Since most of the gut microbiota resides in the colon, pathogenic bacteria often invade the epithelium causing inflammation. Persistent infections can lead to chronic inflammation, which has been linked to diseases such as inflammatory bowel disease (IBD) and recognized as a significant risk factor for colorectal cancer (CRC) development [1-3]. It has been estimated that chronic inflammation and persistent infections contribute to a significant portion of human cancers, especially CRC [2, 4].

Inflammation plays a dual role in tissue homeostasis. On one hand, inflammation is associated with damage to the tissue. On the other hand, it triggers reparative regeneration [5]. Events of damage and inflammation have been associated with regenerative signaling pathways such as Wnt to increase the numbers of intestinal stem cells and Paneth cells, causing intestinal crypts to become hyperplastic [6]. Regeneration of colon epithelium and crypts also involve non-canonical Wnt signaling [7].

Inflammation triggers intestinal and colon epithelial reparative regenerations via inflammatory cytokines including TNF-a, IL-6, IL-17, and IL-22, which stimulate downstream pathways such as MAPK, JAK-STAT3, and NF-κB [5, 8-11]. Deficiency in IL-22 or IL-17 Receptor E (IL-17RE) led to enhanced mucosal damage after infection by pathogenic bacteria such as Citrobacter rodentium [11, 12]. On the other hand, chronic inflammation causes excessive regeneration and the resulting hyperplasia could eventually lead to cancer. TNF-α is associated with CRC progression [13, 14], and blocking TNF-α reduces colorectal carcinogenesis associated with chronic colitis [15]. IL-6 and IL-17 have also been shown to promote colitis-associated early colorectal

carcinogenesis [16, 17], and IL-22 stimulates stem cell growth after injury and promotes CRC stemness [18, 19]. Infiltration of T helper 1 (Th1) cells in CRC tumor specimens is associated with prolonged disease-free survival, whereas infiltration of T helper 17 (Th17) cells, which secrete IL-17 and IL-22, is predictive of poor prognosis for CRC patients [20].

The microRNA miR-34a is an important tumor suppressor targeting pro-growth genes [21, 22], and its mimics are among the first microRNA mimics to reach clinical trial for cancer therapy [23, 24]. miR-34a also limits self-renewal of cancer stem cells [25-27]. miR-34a expression is often silenced in various cancer types [28-30], and methylation of the miR-34a promoter is correlated with CRC progression [31, 32]. Nevertheless, miR-34a deficiency does not increase susceptibility to spontaneous, irradiation-, or c-Myc–induced tumorigenesis [33], which raised a question about the role of miR-34a in tissue homeostasis.

In this study, we demonstrate that miR-34a acts as a checkpoint to protect tissue integrity during inflammation-induced reparative regeneration. miR-34a deficiency led to colon tumorigenesis after *C. rodentium* infection, where Th17 cell infiltration and epithelial stem cell proliferation were observed. During the pro-inflammatory response, miR-34a suppresses Th17 cell differentiation by targeting IL-6R, Th17 cell expansion by targeting IL-23R, Th17 cell recruitment to the colon epithelium by targeting CCL22, and IL-17 induced stem cell proliferation by targeting IL-17RD. Loss of miR-34a results in a reparative regeneration process that goes awry.

RESULTS

C. rodentium infection promotes colon carcinogenesis in miR-34a-/- mice.

Microbial dysbiosys causes chronic inflammation associated with CRC [34-37]. *C. Rodentium* is a mouse mucosal pathogen that shares pathogenic mechanisms and 67% of its genes with enteropathogenic Escherichia coli (EPEC) and enterohaemorrhagic E. coli (EHEC), which are two clinically important human gastrointestinal pathogens [38-43]. *C. Rodentium* has been used as a model to study mucosal immunology including intestinal inflammatory responses during bacteria-induced colitis and colon tumorigenesis [44-46]. *C. rodentium* infection increases the number of colonic adenomas in ApcMin mice but does not cause adenoma formation in wild-type mice [47].

When wild-type and miR-34a-/- mice were infected with *C. rodentium* (4x108 CFU) [48], both developed similar levels of diarrhea and weight loss within 2 weeks, and the symptoms subsided after 4 weeks. Nevertheless, 11 out of the 20 miR-34a-/- mice developed visible colon tumors after 6 months, whereas none of the wild-type mice developed any tumor (Figures 1A-1C).

Marked by Lgr5 and Ascl2, both of which are enhanced by Wnt signaling [49], the colon stem cells that are usually confined at the base of the crypt in wild-type and miR-34a-/- mice became enriched throughout C. *rodentium* induced colon tumors in miR-34a-/- mice (Figure 1D). Enrichment of Lgr5 and Ascl2 expression in the colon tumors of infected miR-34a-/- mice was further confirmed by western blot (Figure 1E).

Th17 cells are enriched in miR-34a-/- colon tumor.

CD4+ T helper (Th) cells are known to infiltrate and accumulate in the inflammatory environment, which can either promote or suppress tissue malignancy [50]. We isolated CD4+ Th cells from the colon epithelium of *C. rodentium*-infected wild-type and miR-34a-/- mice and analyzed the relative abundance of Th1, Th2, Th17, and Treg subpopulations according to their associated expression of INF-γ, IL-4, IL-17 and FoxP3 respectively. INF-γ, IL-4 and FoxP3 levels were similar between wild-type and miR-34a-/-, but IL-17 was significantly upregulated in miR-34a-/- tissue (Figure 2A). Flow analysis confirmed that, although having little effect in uninfected mice, miR-34a deletion significantly enriched the IL17+ Th17 cell population among the CD4+ Th cells in the colon infected with *C. rodentium* (Figure 2B). Immunofluorescence suggested that many of the enriched CD4+IL-17+ Th17 cells were in proximity to Ascl2+ colon stem cells (Figures 2C and 2D).

We then generated a miR-34a conditional knockout mice strain Lgr5-EGFP-CreER^{T2}/miR-34a$^{flox/flox}$ by crossing miR-34a$^{flox/flox}$ mice with Lgr5-EGFP-IRES-CreER^{T2} mice [26]. In this strain, intraperitoneal injection of Tamoxifen deletes miR-34a in Lgr5-EGFP+ stem cells and their progeny. As in the miR-34a-/- mice, Lgr5-EGFP-CreER^{T2}/miR-34a$^{flox/flox}$ mice did not develop colon tumors spontaneously. When infected with *C. rodentium*, 1 out of 7 mice developed colon tumor at the end of our observation (9 months) (Figure 3A). CD4+IL17+ Th17 cells increased in the infected colons of Lgr5-EGFP-CreER^{T2}/miR-34a$^{flox/flox}$ mice compared to wild-type mice (Figure 3B) but not to the degree of miR-34a-/- mice as shown in Figure 2B.

miR-34a suppresses Th17 differentiation and expansion by targeting IL-6R and IL-23R

We then aimed to understand how miR-34a deletion led to accumulation of Th17 cells in the *C. rodentium*-induced colon tumors. IL-6 is critical for initiating the differentiation of native CD4+ T cells into Th17 cells and IL-23 promotes the final step of Th17 cell differentiation, its proliferation and IL-17 expression [51, 52]. Protein levels of IL-6R and IL-23R, the receptors for IL-6 and IL-23, were upregulated in CD4+ T cells isolated from the *C. rodentium*-infected miR-34a-/- colon compared to the wild-type control (Figure 4A). The RNA22 algorithm identified putative miR-34a binding sites in the IL-6R and IL-23R 3`UTR (Figures 4B and 4C), which were then confirmed by the luciferase reporter assay (Figures 4D and 4E).

To evaluate the miR-34a/IL-6R and miR-34a/IL-23R axes for Th17 cell differentiation, we performed the in vitro Th17 differentiation assay [53] using CD4+ T cells isolated from the wild-type and miR-34a-/- mice. Loss of miR-34a significantly enhanced CD4+ T cell differentiation into Th17 cells, which was largely abrogated by knockdown of either IL-6R or IL-23R (Figure 4F and Figure 5). Therefore, miR-34a suppresses Th17 cell differentiation by targeting IL-6R and IL-23R.

miR-34a suppresses Th17 recruitment by targeting CCL22.

Th17 cells express chemokine receptors CCR6 and CCR4 [54], and the CCR6/CCL20 and CCR4/CCL22 axes play important roles in Th17 cell migration [41]. Loss of miR-34a did not affect CCR6 or CCR4 expression in CD4+ T cells (Figure 6A). However, CCL22 expression in the colon epithelium was significantly upregulated in the miR-34a-/- mice compared to the wild-type, while CCL20 expression remained unchanged (Figures 4G and 6B). A miR-34a binding site was identified in the 3`UTR of the CCL22 gene (Figure 4H), which was validated by the luciferase reporter assay (Figure 4I).

Conditioned medium collected from miR-34a-/- colon tumor organoids enhanced the migration of in vitro-differentiated Th17 cells in comparison to medium from the wild-type colon organoids (Figure 4J). The addition of anti-CCL22 neutralizing antibody in the medium or knockdown of CCL22 in miR-34a-/- colon tumor organoids reduced Th17 migration back to the wild-type level (Figure 4J and Figure 5). Therefore, miR-34a suppresses recruitment of Th17 cells by targeting CCL22 production in colon epithelial cells.

Th17 cells promote colon organoid growth via IL-17.

We then tested whether Th17 cells, which were enriched by loss of miR-34a and in proximity to Ascl2+ colon stem cells (Figures 2D and 2E), regulate colon epithelial cell proliferation. Mouse CD4+ T cells were induced to differentiate into Th17 cells and co-cultured with colon organoids. The presence of Th17 cells significantly increased the organoids sizes, which were suppressed by the addition of anti-IL-17 neutralizing antibody, suggesting that the growth effect was via Th17-secreted IL-17 (Figure 7A). In the absence of Th17 cells, recombinant IL-17 in the medium increased organoid growth (Figures 7B-7C) and upregulated Lgr5 and Ascl2 (stem cell marker) expression (Figure 7D). We then grew organoid culture from human colon tissue using an established protocol [55]. Consistent with mouse organoids, addition of human IL-17 into the medium increased the sizes of human colon organoids (Figures 7E-7F). We then examined 8 pairs of matched normal colon and colon tumor tissue samples from CRC patients (Table 1). The expression levels of the two Th17 cell markers, IL-17 and RORC, were consistently higher in tumor tissues than in matched normal colon tissues (Figures 7G-7H).

IL-17 activates STAT3 signaling.

It has been reported that STAT3 activation is involved in Enterotoxigenic E. coli induced colon carcinogenesis in ApcMin mice [56]. We treated mouse colon organoids with recombinant IL-17 and measured STAT3 phosphorylation by western blot. IL-17 activated STAT3, which was abrogated by the STAT3 inhibitor, Stattic (Figure 8A). Inhibition of STAT3 by Stattic impaired colon organoid growth (Figures 8B and 8C).

miR-34a targets IL-17RD to suppress stem cell proliferation.

The IL-17 receptor, IL-17RA, is essential for IL-17 mediated signaling [57]. Immunofluorescence showed that IL-17RA is evenly distributed along the mouse colon crypt axis (Figure 9A). IL-17RD, another IL-17 receptor, has been reported to interact with IL-17RA to mediate IL-17 signaling [58]. Unlike IL-17RA, IL-17RD is specifically expressed at the base of the crypt, largely overlapping with Ascl2+ stem cells (Figure 10A). RT-qPCR showed that the IL-17RA transcript levels were similar between *C. Rodentium*-induced miR-34a-/- colon tumors and the wild-type colon, whereas the IL-17RD transcript levels were significantly increased in miR-34a-/- colon tumors (Figure 9B). Western blot confirmed that the IL17RD protein level was upregulated in the miR-34a-/- colon tumor (Figure 10B).

RNA22 predicted a miR-34a binding site in the IL-17RD 3`UTR (Figure 10C). The luciferase reporter assay confirmed that miR-34a directly targets IL-17RD and suppresses IL-17RD expression (Figure 10D). Co-immunoprecipitation confirmed interaction between IL-17RA and IL-17RD in mouse colon crypts (Figure 10E). Knockdown of either IL-17RA or IL-17RD inhibited IL-17-mediated STAT3 activation (phosphorylation) and colon organoid growth (Figures 10F-10H and Figure 5).

Furthermore, colon organoid growth spurred by loss of miR-34a was largely offset by IL-17RD knockdown (Figure 10I).

DISCUSSION

Our study indicates that miR-34a acts as a checkpoint against pathogen-induced colon malignancy by playing versatile roles (Figure 11). First, miR-34a suppresses Th17 cell differentiation and expansion by targeting IL-6R and IL-23R. Second, miR-34a limits Th17 cell recruitment to the epithelium by targeting CCL22. Lastly, miR-34a hinders IL-17 induced stem cell proliferation by targeting IL-17RD.

Colon stem cells reside at the base of the crypt, relying on the niche to provide necessary signaling cues for self-renewal. cKit+/Reg4+ colonic crypt base secretory cells interdigitate with Lgr5+ stem cells, providing the latter with Notch ligands DLL1 and DLL4, and epidermal growth factor [59, 60]. Ablation of the crypt base secretory cells inhibits self-renewal of stem cells, disrupts the homeostasis of colonic crypts, and suppresses colon organoid growth. Normally, stem cells are constrained to this spatial niche and are forced to differentiate when they leave the niche. However, in human colon adenoma and carcinoma samples, Lgr5+ stem-like cells are highly upregulated and are not confined to the spatial niche as in normal crypts [61]. This is like what we observed in *C. rodentium* induced colon tumors in miR-34a-/- mice. Inflammatory cytokines such as IL-17 potentially provide an enlarged “inflammatory niche” by stimulating receptors such as IL-17RD on the stem cells, enabling them to ignore the constraint of the crypt base and do away with crypt base secretory cells. Interestingly, IL-17RD specifically amplifies IL-17RA signaling in stem cells, analogously to Lgr5 receptor amplification of Wnt signaling in stem cells for self-renewal.

Non-coding RNAs occupy most of the mammalian genome [62, 63]. Evolutionarily, the percentage of genome devoted to the non-coding region is consistently associated with

the complexity of the organism, rising from less than 25% in prokaryotes, 25-50% in simple eukaryotes, more than 50% in fungi, plants and animals, to approximately 98.5% in humans—which have a genome size that is three orders of magnitude larger than prokaryotes [64]. Compared to microRNA, the role of long non-coding RNA (lncRNA) in regulating tumors has just started to be appreciated [65-67]. In fact, lncRNA has been shown to regulate miR-34a in human CRC, especially in cancer stem cells [32]. Like miR-34a, many of the lncRNAs with strong functions in tumors are largely dispensable for normal development and tissue homeostasis [68, 69]. It is possible that the abundance of non-coding RNAs in mammals may provide extra surveillance to protect tissue integrity during stress conditions such as inflammation, which are often not captured by laboratory animal models raised in well-controlled circumstances.

The miR-34a mimic was the first microRNA mimic to reach clinical trial for cancer therapy [23, 24]. Previous studies largely focused on the role of miR-34a to induce cell cycle arrest, senescence, and apoptosis. This study suggests that the miR-34a mimic may have additional benefits of suppressing Th17 cells in the tumor microenvironment. It might be worth paying extra attention to the delivery efficiency into CD4+ Th cells and evaluate therapeutics effects based on CRC classification, especially on the inflammatory subtype [70].

METERIALS AND METHODS

Transgenic Mice and Bacterial Infection

C57/B6 and B6(Cg)-Mir34atm1Lhe/J mice were ordered from the Jackson Laboratory. Lgr5-EGFP-creERT2/miR-34aflox/flox mice were generated as described as previously [26]. Cre recombinase was induced by intraperitoneal injection of tamoxifen (Sigma) dissolved in sterile corn oil at a dose of 75 mg/kg before infection with *C. rodentium*. Mouse maintenance and procedures were approved by Duke University DLAR and followed the protocol (A286-15-10). *C. rodentium* strain DBS100 was purchased from ATCC and cultured according to previously described methods [71]. 4 × 108 C.F.U *C. rodentium* were infected into 6-8 weeks old mice by oral gavage.

Clinical specimen and colon Organoid Culture

Frozen CRC specimens and paired controls were acquired from Weill Cornell Medical College (WCMC) Colon Cancer Biobank for evaluation of Th17 cell related gene expression. Surgically resected fresh normal human colon tissues were obtained from Duke University hospital. The study was approved by the ethical committee of Duke University hospital, Duke University, and WCMC. All samples were obtained with informed consent.

Mouse and human colon crypt isolation and organoid culturing were performed as described previously [55]. To investigate CCL22 regulation on Th17 cell migration, and IL-17RA and IL-17RD regulation on organoids growth, lentiviral vector carrying shRNA against CCL22, IL-17RA or IL-17RD were purchased from Sigma and infected into organoids according to the protocol described previously [72].

CD4+ T cell isolation and Th17 cell differentiation

To investigate Th17 cell enrichment in *C. rodentium*-infected colons, CD4+ T cells were first isolated from mouse colon as described previously [73]. Briefly, after washing with cold PBS, the mouse colon was cut into 0.5-1cm pieces and incubated in Ca2+ and Mg2+ free PBS containing 0.37mg/ml EDTA and 0.145mg/ml DTT in an orbital shaker at 37°C for 15 min. The supernatant was decanted and the remaining tissue was further incubated in RPMI-1640 containing 5% fetal calf serum, 20mM HEPES, 100U/ml each of penicillin and streptomycin and 0.1mg/ml collagenase dispose (Sigma) with shaking at 37°C for 90 min. After filtering through a 70μm cell strainer, the cells were collected by centrifugation and the pellet was suspended in 35% percoll solution (Sigma). The cells were then collected by centrifugation at 2000rpm for 20mins and applied for CD4+ T cell isolation by a mouse CD4+ T cell isolation kit (StemCell Technology). After staining with CD4 and IL-17, Th17 cells were analyzed by Flow cytometry.

To evaluate the effect of IL-6R and IL-23R on Th17 cell differentiation, CD4+ T cells were isolated from mouse spleen as described previously [73]. Briefly, the spleen was minced and squeezed through 70μm cell strainer to get the single cells. After collection by centrifugation, the cells were suspended into 35% percoll solution (Sigma) with heparin, followed by incubation in red cell lysis buffer (Abcam) to get rid of red cells. The cells were then washed and applied for CD4+ T cell isolation using a mouse CD4+ T cell isolation kit (StemCell Technology). Isolated CD4+ T cells were cultured in 24-well plate coated with anti-CD3e and anti-CD28 antibodies in 1640 RPMI medium with 10% FCS and recombinant mouse IL-2 (rmIL2, 20 ng/mL) at 1x106 /mL according to the previous protocol [74]. Lentiviral vector carrying shRNA against IL-6R or IL-23R were purchased

from Sigma and infected into CD4+ T cells followed the protocol [75]. After selection by antibiotics, the cells were induced to differentiate into Th17 cells using the FlowCellect Mouse Th17 Differentiation Kit according to the protocol (EMD Millipore). Th17 cell differentiation efficiency was measured by Flow cytometry by CD4 and IL-17 staining.

Co-culture Th17 cells with Organoids

After differentiation from CD4+ T cells, Th17 cells were co-cultured with colon crypts at a 10:1 ratio in Matrigel. To active and maintain Th17 cells, rmIL-2 (20ng/ml; Pepro-tech), mIL-6 (50ng/ml; Pepro-tech), TGF-β (10ng/ml; Pepro-tech), mIL-23 (30ng/ml; Pepro-tech) were added into the ENR organoids culture medium. A neutralizing monoclonal antibody against IL-17（Abcam）was used to abrogate IL-17 specific effects of Th17 cells.

Chemotaxis assays

The chemotaxis assay was performed as described previously [76]. Briefly, 1×105 Th17 cells were applied to the upper well of the ChemoTex chambers (96-well, 5-μm pore size; NeuroProbe). Conditional medium from miR-34a-/- colon organoids or control organoids was added in the lower chamber. To evaluate CCL22 effect on Th17 migration, a neutralizing monoclonal antibody against CCL22 (R&D) was included in the conditional medium. After 2-hour incubation, the cells in the upper wells were removed and the migrated cells were collected by centrifugation. Migrated cells were counted by a haemocytometer.

Immunofluorescence

Immunofluorescence was performed on paraffin-embedded colon sections. After rehydration and antigen retrieve, the sections were blocked by 2% horse serum in PBS

for 2 hours at RT and incubated with anti-Ascl2 (1:200, Santa Cruz), anti-IL17 (1:200, Abcam), anti-CD4 (1:50, R&D Systems) or anti-GFP (1:500, Abcam) in antibody diluent buffer (DAKO) overnight at 4°C. After washing, the sections were then incubated with Rhodamine Red or Alexa fluor 488 labeled secondary antibodies (Invitrogen) for 1 hour at room temperature. After counterstained with DAPI (Invitrogen), the slides were observed under Axio Imager upright microscope (Zeiss).

Flow Cytometry analysis

Th17 cells were analyzed by CD4 and IL-17 staining. Briefly, single cells were fixed with 4% formaldehyde and further permeabilized by methanol. The cells were then incubated with anti-IL-17 (1:200, Abcam) and anti-CD4 (1:100, R&D Systems) antibody, followed by incubation with APC or FITC labeled secondary antibody (Invitrogen). The samples were analyzed using a Beckman Coulter flow cytometer. The raw FACS data were analyzed with the FlowJo software.

Quantitative real-time PCR

Total RNA was extracted from the tissue using the RNeasy mini kit (Qiagen). cDNA was synthesized from 500 ng of total RNA in 20µl of reaction volume using the High Capacity cDNA Archive Kit (Applied Biosystems). Quantitative PCR was carried out using the SYBR Green System (Applied Biosystems) to detect gene expression. The qPCR primers used are in Table 2. All samples were run in triplicate three times. The expression of each gene was defined from the threshold cycle (Ct), and the relative expression levels were calculated using the 2-△△Ct method after normalization to the actin expression level.

Western Blot

Whole cell lysate was prepared in a RIPA lysis buffer (Millipore) with proteinase inhibitor (Roche). Proteins were first separated by 10% SDS-PAGE and then transferred to a Hybond membrane (Amersham). The membranes were incubated with primary antibodies either anti-lgr5 (1:500 ,Santa Cruz), anti-ASCL2 (1:1000, Bioss), anti-IL6R (1:1000, R&D Systems), anti-IL23R (1:500, R&D Systems), anti-CCL22(1:500, R&D Systems), anti-IL17RD (1:500, R&D Systems), anti-IL17RA (1:500, R&D Systems), anti-pSTAT3 (1:1000, Cell Signaling) or anti-actin (1:2000, Cell Signaling) in 5% milk/TBST buffer (25 mM Tris pH 7.4, 150 mM NaCl, 2.5 mM KCl, 0.1% Triton-X100) overnight, and then probed for 2 hours with secondary horseradish peroxidase (HRP)-conjugated anti-goat or anti-rabbit IgG (Santa Cruz). After extensive wash with PBST, the target proteins were detected on membrane by enhanced chemiluminescence (Pierce).

Statistical Analysis

Data were expressed as mean ± standard deviation of three biological repeats. Student t-tests were used for comparisons, with $p<0.05$ considered significant.

ACKNOWLEDGEMENTS

We thank other lab members of the Shen laboratory for the helpful discussions, materials supplies. This work was supported by NIH R01GM95990, NIH R01GM114254, NSF 1350659, NSF 1137269, NYSTEM C029543.

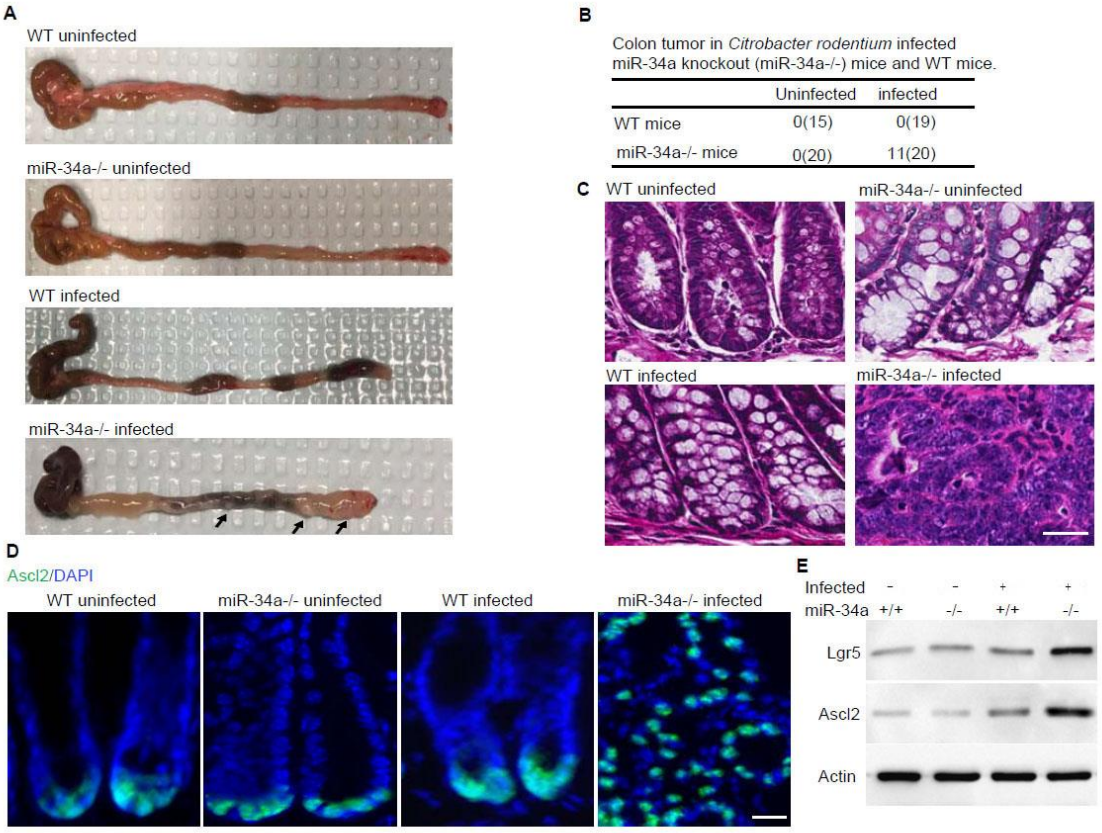

Figure 1 *C. rodentium* infection induces colonic tumor formation in miR-34a-/- mice.

(A) Representative images of mouse colons uninfected or infected with *C. rodentium*. The arrows indicate the visible colon tumors. 4×108 CFU *C. rodentium* were used to infect the mice orally. Six months after the infection, the mice were euthanized and the colons were imaged. (B) Frequencies of colonic tumor formation in infected and uninfected mice. (C) Representative H&E colon staining of infected and uninfected mice. (D) Immunofluorescence of Ascl2 showing enriched colon stem cells in miR-34a-/- colon tumors. Scale bar, 40μm. (E) Western blot of Ascl2 and Lgr5 showing enriched colon stem cells in miR-34a-/- colon tumors.

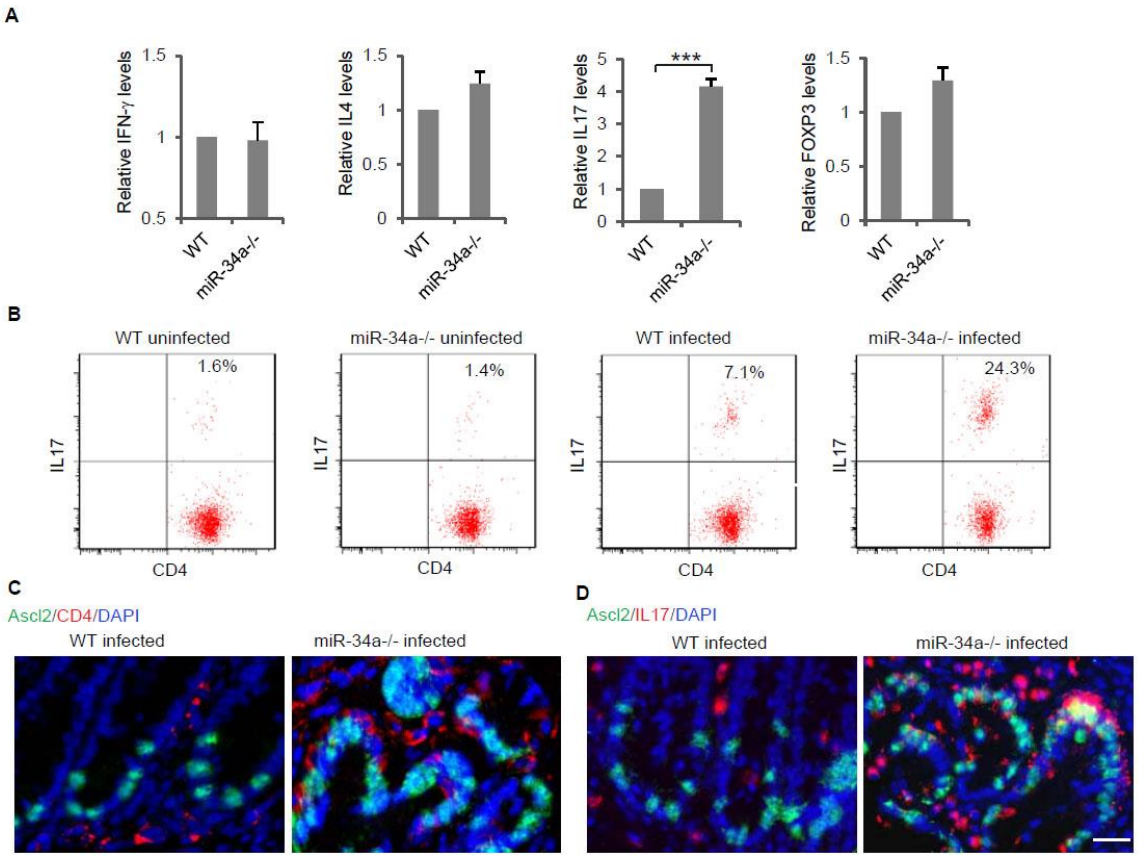

Figure 2. *C. rodentium* infection enhances colon stem cells self-renewal and Th17 cell infiltration in miR-34a-/- colonic tumors.

(A) RT-qPCR showing relative expression of the T lymphocyte genes associated with Th1 (IFN-□), Th2 (IL-4), Th17 (IL-17) and Treg (FOXP3) cells in the colons from *C. rodentium* infected wild-type and miR-34a-/- mice. (B) FACS analyses of Th17 cells (CD4+, IL-17+) in the colons from infected and uninfected mice. (C and D) Immunofluorescence of CD4 (C) and IL-17 (D) showing enhanced Th17 cells infiltrating in miR-34a-/- colonic tumors. Scale bar, 40μm. Error bars denote s.d. of triplicates. ***, $p<0.001$. p-value was calculated based on Student's t-test.

A

Colon tumor in *Citrobacter rodentium* infected miR-34a conditional knockout (Lgr5-GFP-CreER^{T2}/miR-34a$^{flox/flox}$) mice

	Uninfected	infected
Lgr5-GFP-CreER^{T2}/miR-34a$^{flox/flox}$	0(6)	1(7)

B

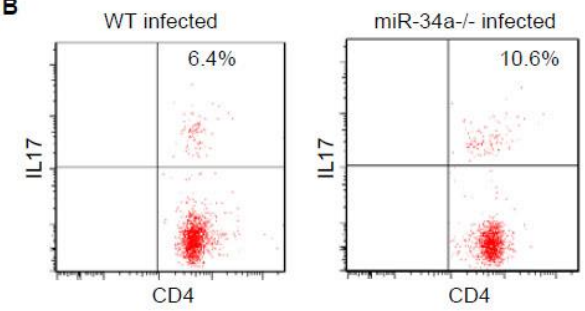

Figure 3. Colon tumorigenesis and Th17 cell accumulation in *C. rodentium*-infected Lgr5-EGFP-CreER^{T2}/miR-34a$^{flox/flox}$ mice.

(A) Frequencies of colon tumor formation in *C. rodentium* infected and uninfected Lgr5-EGFP-CreER^{T2}/miR-34a$^{flox/flox}$ mice. (B) FACS analyses of Th17 cells (CD4+, IL-17+) in *C. rodentium* infected and uninfected Lgr5-EGFP-CreER^{T2}/miR-34a$^{flox/flox}$ mice colon.

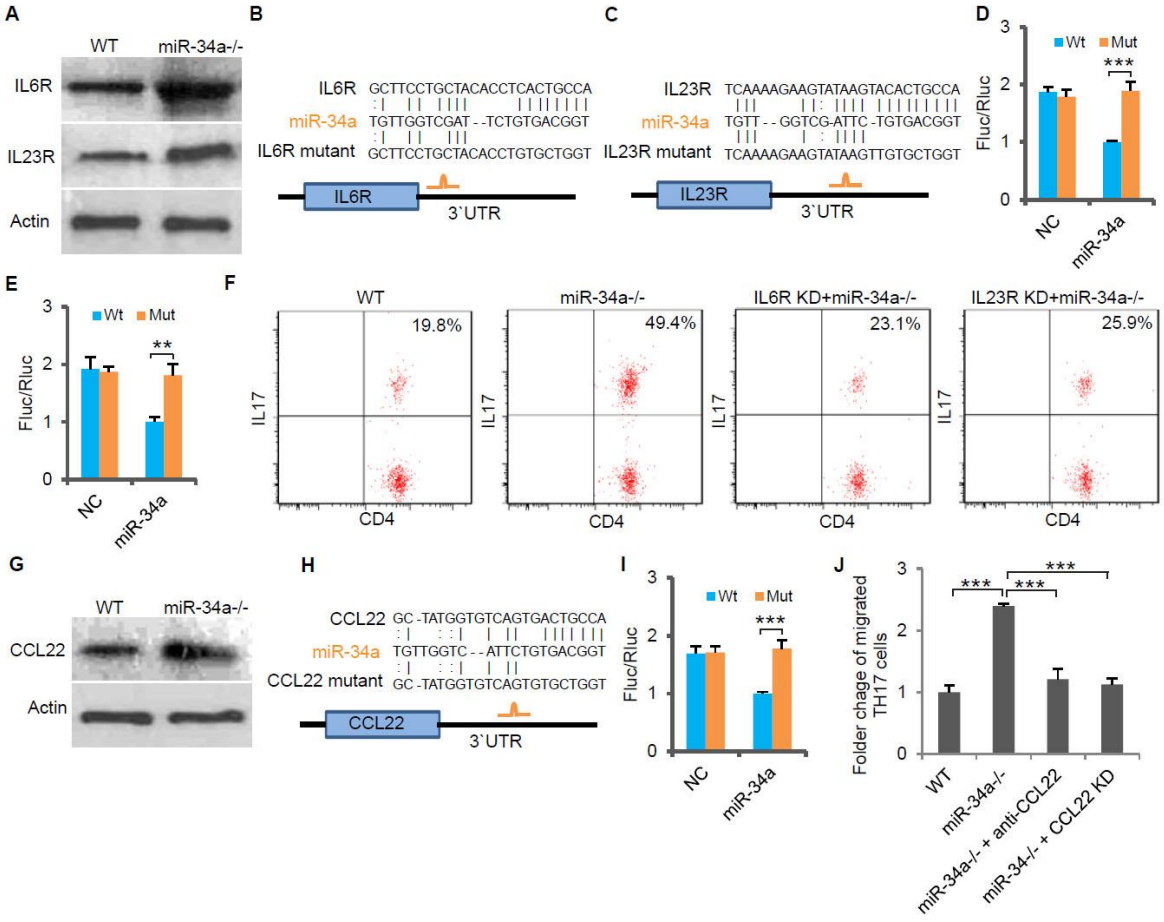

Figure 4. **miR-34a targets IL-6R, IL-23R and CCL22.**

(A) Western blot showing IL-6R and IL-23R expression levels in CD4+ T cells isolated from *C. rodentium* infected wild-type and miR-34a-/- colon. (B and C) Schematic representation of mouse IL-6R (B) and IL-23R (C) 3`UTRs containing the putative miR-34a binding sites. (D-E) Luciferase reporter assays confirming the miR-34a binding sites. 3`UTRs of mouse IL-6R (D) and IL-23R (E) containing wild-type (Wt) or mutated (Mut) putative miR-34a binding sites were cloned into the 3`UTR of firefly luciferase (Fluc). Ectopic miR-34a expression in CT26 cells downregulated luciferase in Wt cells, but not in Mut cells. Fluc signals were normalized by a simultaneously delivered Renillar luciferase (Rluc) expression plasmid. (F) FACS showing knockdown of IL6R or IL-23R in CD4+ T cells largely offsets the effect of miR-34a loss on Th17 cell differentiation. (G) Western blot showing increase of CCL22 expression in miR-34a-/- colon crypts. (H) Schematic representation of miR-34a binding site on the mouse CCL22 3`UTR. (I) Luciferase reporter assays confirming the miR-34a binding sites in mouse CCL22 3`UTR. (J) Chemotaxis assay showing knockdown of CCL22 in colon tumor organoid cells or

neutralization of CCL22 with anti-CCL22 antibody suppresses Th17 cell migration to colon tumor organoid conditioned medium. Error bars denote s.d. of triplicates. **, $p<0.01$; ***, $p<0.001$. p-value was calculated based on Student's t-test.

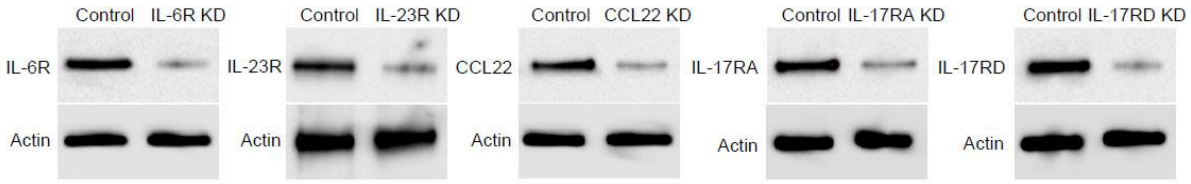

Figure 5. **Validation of gene knockdown efficiency.**

Western blots showing the knockdown efficiency of IL-6R, IL-23R, CCL22, IL-17RA, and IL-17RD.

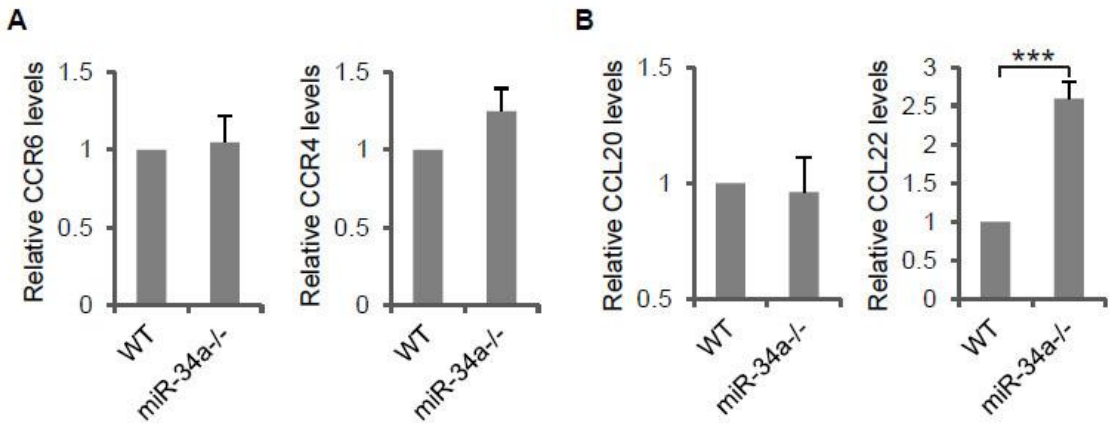

Figure 6. **Loss of miR-34a enhances CCL22 expression in colon epithelium.**

(A) RT-qPCR showing relative expression of CCR6 and CCR4 in CD4+ T cells derived from *C. rodentium* infected miR-34a-/- colon tumors and wild-type controls. (B) RT-qPCR showing relative expression of CCL20 and CCL22 in *C. rodentium* infected miR-34a-/- colon tumors and wild-type controls. Error bars denote s.d. of triplicates. ***, $p<0.001$. p-value was calculated based on Student's t-test.

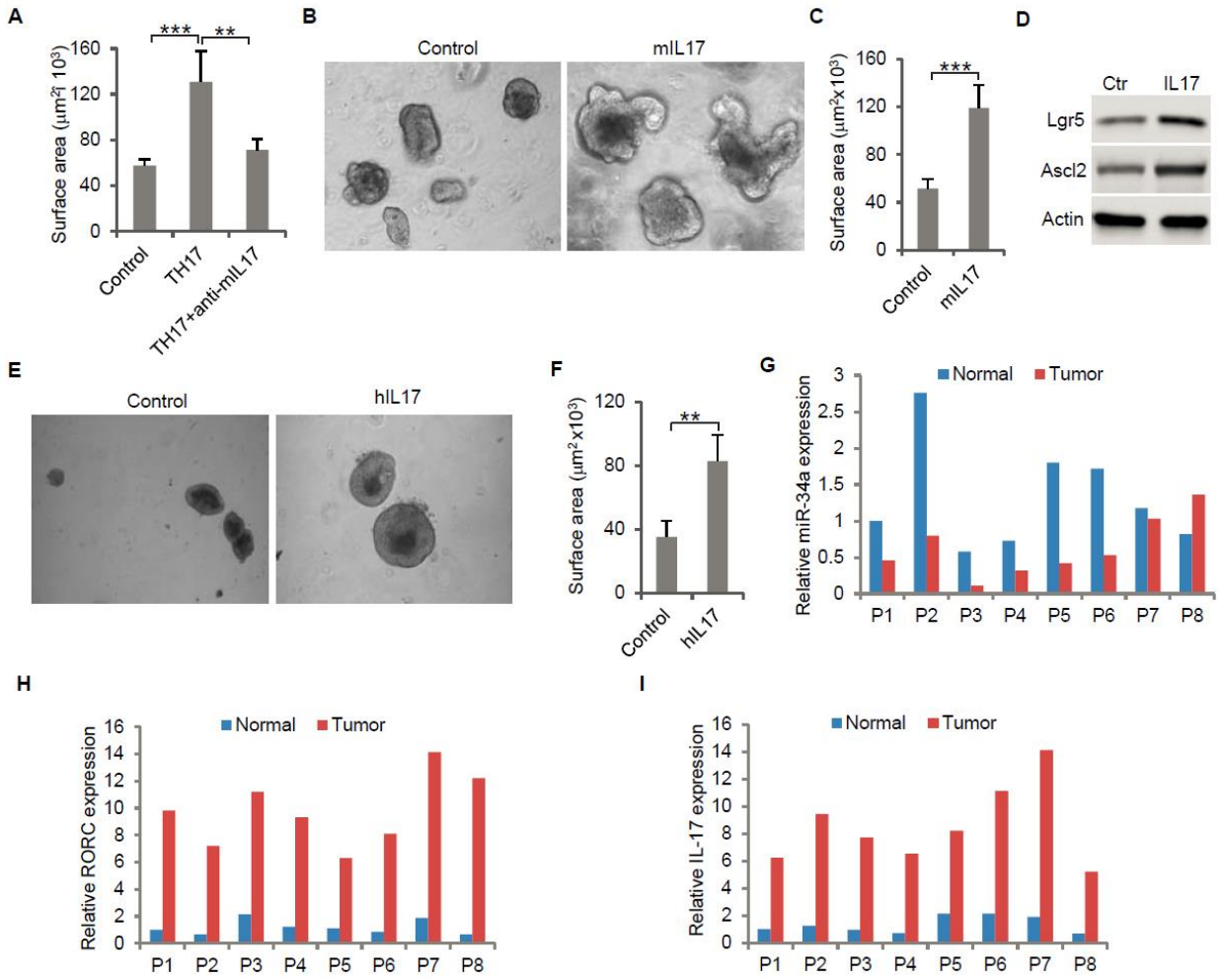

Figure 7. Th17 cells enhance colon organoids growth through IL-17.

(A) Th17 cells enhance colon organoid growth in co-culture. When co-cultured with Th17 cells, colon organoids grow faster with bigger surface area. Anti-IL-17 antibody abrogates Th17 promotion of colon organoids growth. (B and C) Recombinant mouse IL-17 enhances mouse organoids growth as shown by representative mouse colon organoids images (B) and quantitative organoid area (C). (D) Western blot showing that mouse IL-17 increases the expression of colon stem cell markers, Ascl2 and Lgr5, in mouse colon organoids. (E and F) Human IL-17 enhances human colon organoids growth as shown by representative human colon organoids images (E) and quantitative organoids area (F). (G-H) RT-qPCR of 8 paired colon tumor and normal colon tissue samples from CRC patients (Table 1) showing higher expression levels of miR-34a and Th17 associated genes IL-17 and RORC in colon tumors. Error bars denote s.d. of triplicates. **, $p<0.01$; ***, $p<0.001$. p-value was calculated based on Student's t-test.

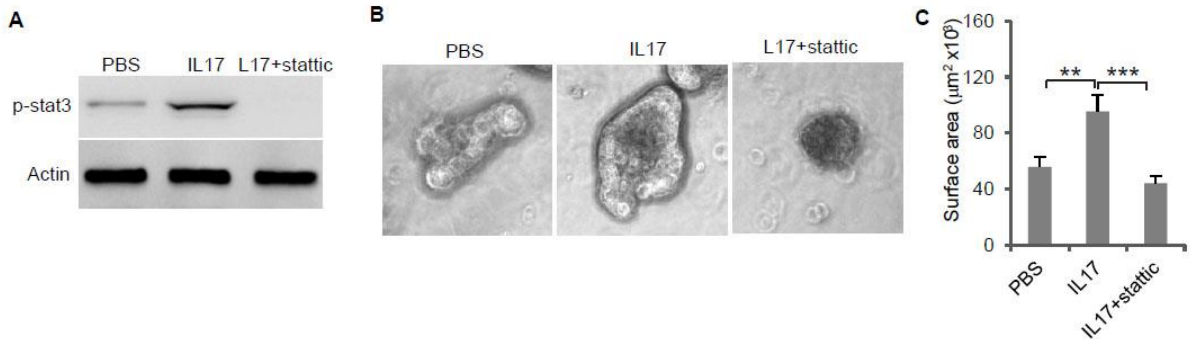

Figure 8. **IL-17 mediated STAT3 activation enhances colon stem cell self-renewal.**

(A) Western blot showing IL-17 promotes STAT3 activation. (B and C) STAT3 activation is required for IL-17 mediated colon organoids growth showing by representative organoids images (B) and quantitative organoids area (C). Error bars denote s.d. of triplicates. **, $p<0.01$; ***, $p<0.001$. p-value was calculated based on Student's t-test.

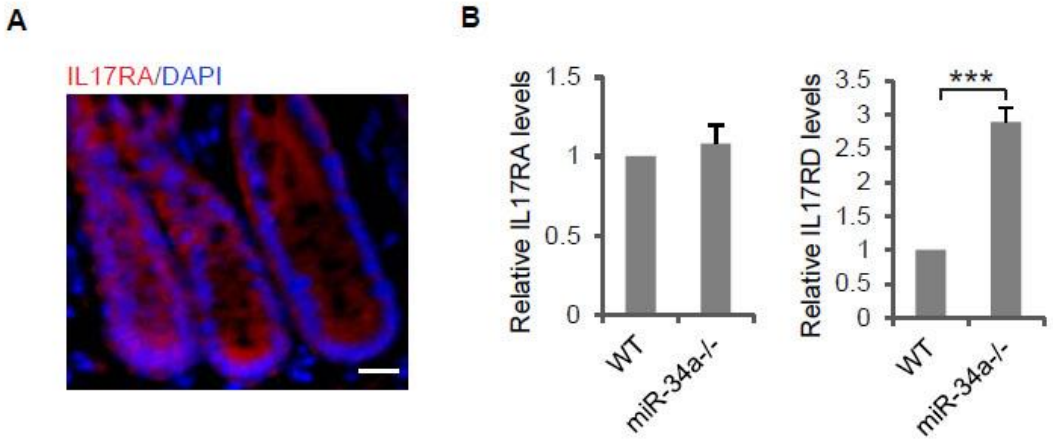

Figure 9. **Expression of IL-17RA and IL-17RD.**

(A) Immunofluorescence showing IL-17RA expression along the colon crypt. (B) RT-qPCR showing relative expression of IL-17RA and IL-17RD in *C. rodentium* infected miR-34a-/- colon tumors and wildtype controls. Scale bar, 40μm. Error bars denote s.d. of triplicates. ***, $p<0.001$. p-value was calculated based on Student's t-test.

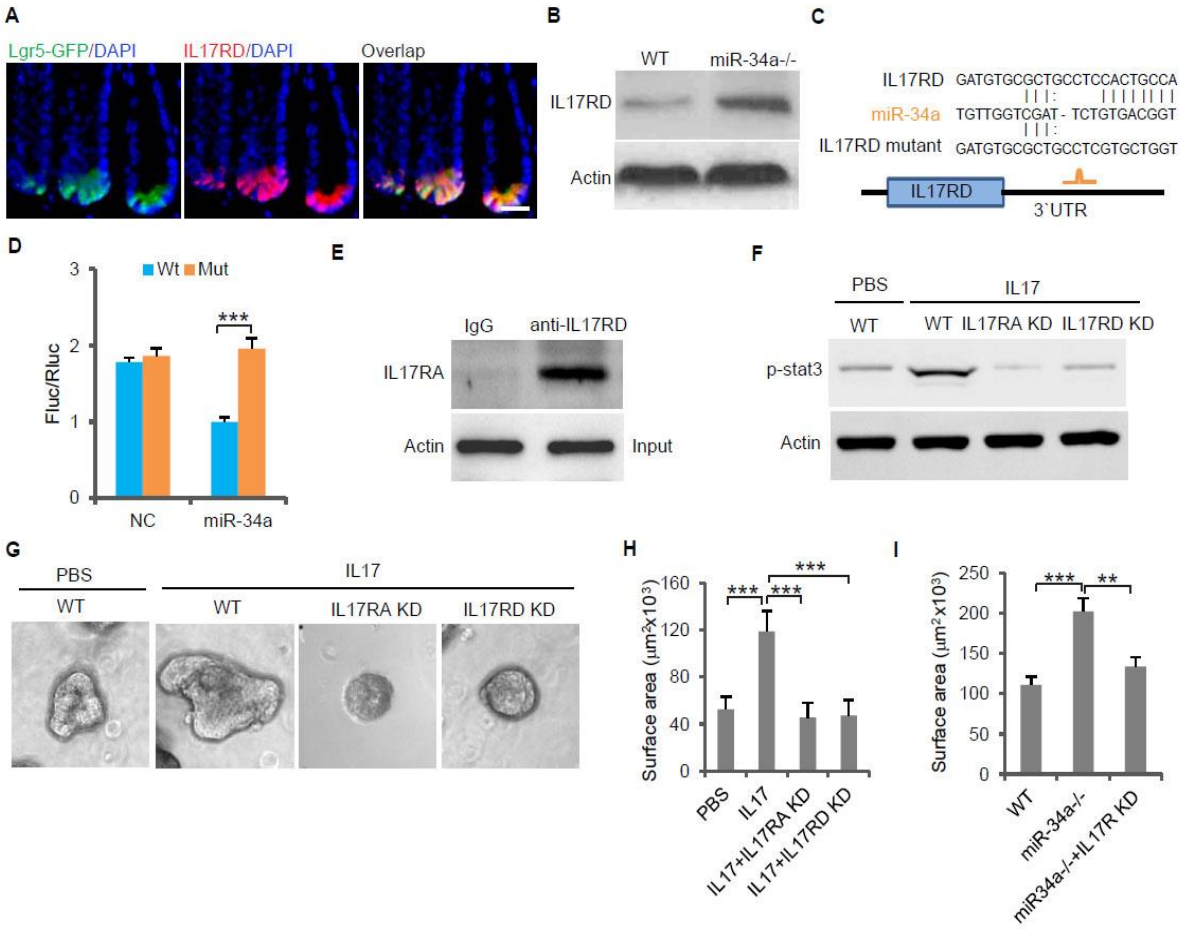

Figure 10. **The IL-17/IL-17RD axis promotes colon organoid growth.**

(A) Immunofluorescence showing IL-17RD expression in Ascl2+ stem cells at the base of the crypt. (B) Western blot showing increase of IL-17RD expression in miR-34a-/- colon tumors. (C) Schematic representation of mouse IL-17RD 3`UTR and the putative miR-34a binding site. (D) Luciferase reporter assays confirming the miR-34a binding sites in mouse IL-17RD 3`UTR. (E) Immunoprecipitation showing the IL-17RA and IL-17RD complex in the colon crypt. (F) Western blot showing IL-17RA and IL-17RD are required for IL-17 mediated STAT3 activation. (G and H) IL-17RA and IL-17RD knockdown suppresses IL-17 mediated colon organoids growth as shown by representative organoids images (G) and quantitative organoids surface area (H). (I) IL-17RD knockdown reduces miR-34a deficiency induced colon organoids growth. Scale bar, 50μm. Error bars denote s.d. of triplicates. **, $p<0.01$; ***, $p<0.001$. p-value was calculated based on Student's t-test.

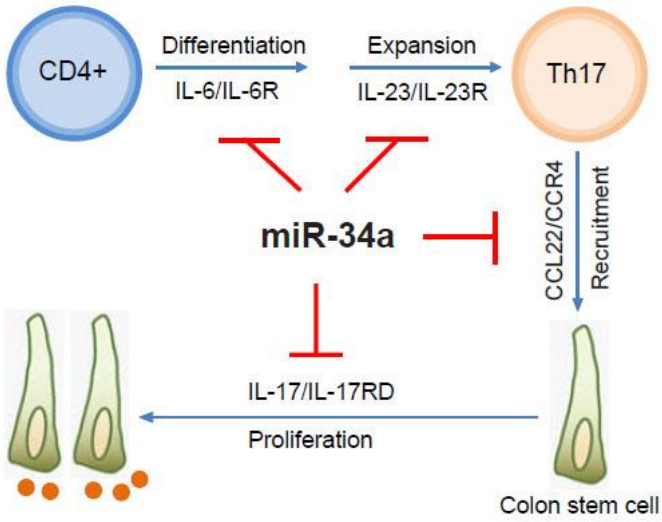

Figure 11. miR-34a regulates Th17 cell-mediated regeneration.

A schematic illustration of the central role of miR-34a in Th17 cell-mediated colon stem cell proliferation. miR-34a suppresses Th17 cell differentiation and expansion by targeting IL-6R and IL-23R in immune cells. miR-34a further inhibits Th17 cells recruitment by targeting CCL22 in the colon epithelium. miR-34a also inhibits IL-17RD expression to suppress IL-17-IL-17RD/IL17-RA mediated colon stem cell proliferation.

Table 1. Information of CRC patients who provided matched tumor and normal colon samples for comparing IL-17 and RORC expression levels.

Patient	Gender	Age at visit	Stage	Differentiation	Lymph nodes
P1	F	59	2B	Poor	N0
P2	F	73	IV	Moderate	N1-3
P3	M	73	IIIA	Well	N1-3
P4	M	56	IV	Poor	N2>3
P5	F	61	IIIC	Poor	N2>3
P6	M	87	IIB	NA	N0
P7	F	74	IIIA	Poor	N1-3
P8	F	68	IIA	Poor	N0

Table 2. RT-qPCR primers.

Primer name	Sequence
mIL-4F	ACTTGAGAGAGATCATCGGCA
mIL-4R	AGCTCCATGAGAACACTAGAGTT
mIL-17F	CTTTCCCTCCGCATTGACAC
mIL-17R	TTTAACTCCCTTGGCGCAAAA
mIFN-γ-F	TCA AGT GGC ATA GAT GTG GAA GAA
mIFN-γ-F	TGG CTC TGC AGG ATT TTC ATG
mFoxp3-F	CCCAGGAAAGACAGCAACCTT
mFoxp3-R	TTCTCACAACCAGGCCACTTG
mCCR4-F	AACAGAGCAGTGCGCATGAT
mCCR4-R	CGTTGTACGGCGTCCAGAA
mCCR6-F	CCTCACATTCTTAGGACTGGAGC
mCCR6-R	GGCAATCAGAGCT CTCGGA
mCCL20-F	ATGGCCTGCGGTGGCAAGCGTCTG
mCCL20-R	TAGGCTGAGGAGGTTCACAGCCCT
mCCL22-F	GTG GCT CTC GTC CTT CTT GC
mCCL22-R	GGA CAG TTT ATG GAG TAG CTT
mIL-17RA-F	AGTGTTTCCTCTACCCAGCAC
mIL-17RA-R	GAAAACCGCCACCGCTTAC
mIL-17RC-F	GGAGCAGGACTTTAGCTTCTT
mIL-17RC-R	GAACCAGGTCTGTGTGGTTTA
mIL-17RD-F	TGATGCAATCAAGAGCCAGACAG
mIL-17RD-R	GGTAGCCACACAGGGCCAATA
mactin-F	GGCTGTATTCCCCTCCATCG
mactin-R	CCAGTTGGTAACAATGCCATGT
hIL-17F	TCAACCCGATTGTCCACCAT
hIL-17F	GAGTTTAGTCCGAAATGAGGCTG
hRORC-F	GAAGTGGTGCTGGTTAGGATGTG
hRORC-R	GCCACCGTATTTGCCTTCAA
hactin -F	CGCGAGAAGATGACCCAGAT
hactin -R	ACAGCCTGGATAGCAACGTACAT

REFERENCES

1. Gagniere, J., et al., Gut microbiota imbalance and colorectal cancer. World J Gastroenterol, 2016. 22(2): p. 501-18.
2. Wang, K. and M. Karin, Tumor-Elicited Inflammation and Colorectal Cancer. Adv Cancer Res, 2015. 128: p. 173-96.
3. Collins, D., A.M. Hogan, and D.C. Winter, Microbial and viral pathogens in colorectal cancer. Lancet Oncol, 2011. 12(5): p. 504-12.
4. Zur Hausen, H., The search for infectious causes of human cancers: where and why. Virology, 2009. 392(1): p. 1-10.
5. Karin, M. and H. Clevers, Reparative inflammation takes charge of tissue regeneration. Nature, 2016. 529(7586): p. 307-15.
6. Ashton, G.H., et al., Focal adhesion kinase is required for intestinal regeneration and tumorigenesis downstream of Wnt/c-Myc signaling. Dev Cell, 2010. 19(2): p. 259-69.
7. Miyoshi, H., et al., Wnt5a potentiates TGF-beta signaling to promote colonic crypt regeneration after tissue injury. Science, 2012. 338(6103): p. 108-13.
8. Chen, L.W., et al., The two faces of IKK and NF-kappaB inhibition: prevention of systemic inflammation but increased local injury following intestinal ischemia-reperfusion. Nat Med, 2003. 9(5): p. 575-81.
9. Taniguchi, K., et al., A gp130-Src-YAP module links inflammation to epithelial regeneration. Nature, 2015. 519(7541): p. 57-62.
10. Sugimoto, K., et al., IL-22 ameliorates intestinal inflammation in a mouse model of ulcerative colitis. J Clin Invest, 2008. 118(2): p. 534-44.
11. Song, X., et al., IL-17RE is the functional receptor for IL-17C and mediates mucosal immunity to infection with intestinal pathogens. Nat Immunol, 2011. 12(12): p. 1151-8.
12. Zheng, Y., et al., Interleukin-22 mediates early host defense against attaching and effacing bacterial pathogens. Nat Med, 2008. 14(3): p. 282-9.
13. Al Obeed, O.A., et al., Increased expression of tumor necrosis factor-alpha is associated with advanced colorectal cancer stages. World J Gastroenterol, 2014. 20(48): p. 18390-6.
14. Zins, K., et al., Colon cancer cell-derived tumor necrosis factor-alpha mediates the tumor growth-promoting response in macrophages by up-regulating the colony-stimulating factor-1 pathway. Cancer Res, 2007. 67(3): p. 1038-45.
15. Popivanova, B.K., et al., Blocking TNF-alpha in mice reduces colorectal carcinogenesis associated with chronic colitis. J Clin Invest, 2008. 118(2): p. 560-70.
16. Grivennikov, S., et al., IL-6 and Stat3 are required for survival of intestinal epithelial cells and development of colitis-associated cancer. Cancer Cell, 2009. 15(2): p. 103-13.

17. Wang, K., et al., Interleukin-17 receptor a signaling in transformed enterocytes promotes early colorectal tumorigenesis. Immunity, 2014. 41(6): p. 1052-63.
18. Lindemans, C.A., et al., Interleukin-22 promotes intestinal-stem-cell-mediated epithelial regeneration. Nature, 2015. 528(7583): p. 560-4.
19. Kryczek, I., et al., IL-22(+) CD4(+) T cells promote colorectal cancer stemness via STAT3 transcription factor activation and induction of the methyltransferase DOT1L. Immunity, 2014. 40(5): p. 772-84.
20. Tosolini, M., et al., Clinical impact of different classes of infiltrating T cytotoxic and helper cells (Th1, th2, treg, th17) in patients with colorectal cancer. Cancer Res, 2011. 71(4): p. 1263-71.
21. He, L., et al., A microRNA component of the p53 tumour suppressor network. Nature, 2007. 447(7148): p. 1130-4.
22. Chang, T.C., et al., Transactivation of miR-34a by p53 broadly influences gene expression and promotes apoptosis. Mol Cell, 2007. 26(5): p. 745-52.
23. Bouchie, A., First microRNA mimic enters clinic. Nat Biotechnol, 2013. 31(7): p. 577.
24. Bader, A.G., miR-34 - a microRNA replacement therapy is headed to the clinic. Front Genet, 2012. 3: p. 120.
25. Bu, P., et al., A microRNA miR-34a-regulated bimodal switch targets Notch in colon cancer stem cells. Cell Stem Cell, 2013. 12(5): p. 602-15.
26. Bu, P., et al., A miR-34a-Numb Feedforward Loop Triggered by Inflammation Regulates Asymmetric Stem Cell Division in Intestine and Colon Cancer. Cell Stem Cell, 2016. 18(2): p. 189-202.
27. Liu, C., et al., The microRNA miR-34a inhibits prostate cancer stem cells and metastasis by directly repressing CD44. Nat Med, 2011. 17(2): p. 211-5.
28. Lodygin, D., et al., Inactivation of miR-34a by aberrant CpG methylation in multiple types of cancer. Cell Cycle, 2008. 7(16): p. 2591-600.
29. Kong, D., et al., Epigenetic silencing of miR-34a in human prostate cancer cells and tumor tissue specimens can be reversed by BR-DIM treatment. Am J Transl Res, 2012. 4(1): p. 14-23.
30. Corney, D.C., et al., Frequent downregulation of miR-34 family in human ovarian cancers. Clin Cancer Res, 2010. 16(4): p. 1119-28.
31. Siemens, H., et al., Detection of miR-34a promoter methylation in combination with elevated expression of c-Met and beta-catenin predicts distant metastasis of colon cancer. Clin Cancer Res, 2013. 19(3): p. 710-20.
32. Wang, L., et al., A long non-coding RNA targets microRNA miR-34a to regulate colon cancer stem cell asymmetric division. Elife, 2016. 5.
33. Concepcion, C.P., et al., Intact p53-dependent responses in miR-34-deficient mice. PLoS Genet, 2012. 8(7): p. e1002797.

34. Sobhani, I., et al., Microbial dysbiosis and colon carcinogenesis: could colon cancer be considered a bacteria-related disease? Therap Adv Gastroenterol, 2013. 6(3): p. 215-29.
35. Candela, M., et al., Human intestinal microbiota: cross-talk with the host and its potential role in colorectal cancer. Crit Rev Microbiol, 2011. 37(1): p. 1-14.
36. Plottel, C.S. and M.J. Blaser, Microbiome and malignancy. Cell Host Microbe, 2011. 10(4): p. 324-35.
37. Tjalsma, H., et al., A bacterial driver-passenger model for colorectal cancer: beyond the usual suspects. Nat Rev Microbiol, 2012. 10(8): p. 575-82.
38. Schauer, D.B. and S. Falkow. The eae gene of Citrobacter freundii biotype 4280 is necessary for colonization in transmissible murine colonic hyperplasia. Infect Immun, 1993. 61(11): p. 4654-61.
39. Schauer, D.B. and S. Falkow, Attaching and effacing locus of a Citrobacter freundii biotype that causes transmissible murine colonic hyperplasia. Infect Immun, 1993. 61(6): p. 2486-92.
40. Papapietro, O., et al., R-spondin 2 signalling mediates susceptibility to fatal infectious diarrhoea. Nat Commun, 2013. 4: p. 1898.
41. Borenshtein, D., M.E. McBee, and D.B. Schauer, Utility of the Citrobacter rodentium infection model in laboratory mice. Curr Opin Gastroenterol, 2008. 24(1): p. 32-7.
42. Borenshtein, D., et al., Development of fatal colitis in FVB mice infected with Citrobacter rodentium. Infect Immun, 2007. 75(7): p. 3271-81.
43. Gibson, D.L., et al., MyD88 signalling plays a critical role in host defence by controlling pathogen burden and promoting epithelial cell homeostasis during Citrobacter rodentium-induced colitis. Cell Microbiol, 2008. 10(3): p. 618-31.
44. Collins, J.W., et al., Citrobacter rodentium: infection, inflammation and the microbiota. Nat Rev Microbiol, 2014. 12(9): p. 612-23.
45. Chandrakesan, P., et al., Utility of a bacterial infection model to study epithelial-mesenchymal transition, mesenchymal-epithelial transition or tumorigenesis. Oncogene, 2014. 33(20): p. 2639-54.
46. Higgins, L.M., et al., Citrobacter rodentium infection in mice elicits a mucosal Th1 cytokine response and lesions similar to those in murine inflammatory bowel disease. Infect Immun, 1999. 67(6): p. 3031-9.
47. Newman, J.V., et al., Bacterial infection promotes colon tumorigenesis in Apc(Min/+) mice. J Infect Dis, 2001. 184(2): p. 227-30.
48. Choi, Y.J., et al., miR-34 miRNAs provide a barrier for somatic cell reprogramming. Nat Cell Biol, 2011. 13(11): p. 1353-60.
49. Schuijers, J., et al., Ascl2 acts as an R-spondin/Wnt-responsive switch to control stemness in intestinal crypts. Cell Stem Cell, 2015. 16(2): p. 158-70.
50. Terzic, J., et al., Inflammation and colon cancer. Gastroenterology, 2010. 138(6): p. 2101-2114 e5.

51. Dong, C., Regulation and pro-inflammatory function of interleukin-17 family cytokines. Immunol Rev, 2008. 226: p. 80-6.
52. Acosta-Rodriguez, E.V., et al., Interleukins 1beta and 6 but not transforming growth factor-beta are essential for the differentiation of interleukin 17-producing human T helper cells. Nat Immunol, 2007. 8(9): p. 942-9.
53. Esplugues, E., et al., Control of TH17 cells occurs in the small intestine. Nature, 2011. 475(7357): p. 514-8.
54. Antonic, V., et al., Significance of infectious agents in colorectal cancer development. J Cancer, 2013. 4(3): p. 227-40.
55. Sato, T., et al., Long-term expansion of epithelial organoids from human colon, adenoma, adenocarcinoma, and Barrett's epithelium. Gastroenterology, 2011. 141(5): p. 1762-72.
56. Kopan, R. and M.X. Ilagan. The canonical Notch signaling pathway: unfolding the activation mechanism. Cell, 2009. 137(2): p. 216-33.
57. Bility, M.T., et al., Hepatitis B virus infection and immunopathogenesis in a humanized mouse model: induction of human-specific liver fibrosis and M2-like macrophages. PLoS Pathog, 2014. 10(3): p. e1004032.
58. Li, Y., et al., MicroRNA-34a inhibits glioblastoma growth by targeting multiple oncogenes. Cancer Res, 2009. 69(19): p. 7569-76.
59. Rothenberg, M.E., et al., Identification of a cKit(+) colonic crypt base secretory cell that supports Lgr5(+) stem cells in mice. Gastroenterology, 2012. 142(5): p. 1195-1205 e6.
60. Sasaki, N., et al., Reg4+ deep crypt secretory cells function as epithelial niche for Lgr5+ stem cells in colon. Proc Natl Acad Sci U S A, 2016. 113(37): p. E5399-407.
61. Baker, A.M., et al., Characterization of LGR5 stem cells in colorectal adenomas and carcinomas. Sci Rep, 2015. 5: p. 8654.
62. Kung, J.T., D. Colognori, and J.T. Lee, Long noncoding RNAs: past, present, and future. Genetics, 2013. 193(3): p. 651-69.
63. Mattick, J.S. and J.L. Rinn, Discovery and annotation of long noncoding RNAs. Nat Struct Mol Biol, 2015. 22(1): p. 5-7.
64. Mattick, J.S., RNA regulation: a new genetics? Nature Reviews Genetics, 2004. 5(4): p. 316-323.
65. Huarte, M., The emerging role of lncRNAs in cancer. Nat Med, 2015. 21(11): p. 1253-1261.
66. Prensner, J.R. and A.M. Chinnaiyan, The emergence of lncRNAs in cancer biology. Cancer Discov, 2011. 1(5): p. 391-407.
67. Schmitt, A.M. and H.Y. Chang, Long Noncoding RNAs in Cancer Pathways. Cancer Cell, 2016. 29(4): p. 452-63.

68. Zhang, B., et al., The lncRNA Malat1 is dispensable for mouse development but its transcription plays a cis-regulatory role in the adult. Cell Rep, 2012. 2(1): p. 111-23.
69. Nakagawa, S., et al., The lncRNA Neat1 is required for corpus luteum formation and the establishment of pregnancy in a subpopulation of mice. Development, 2014. 141(23): p. 4618-27.
70. Sadanandam, A., et al., A colorectal cancer classification system that associates cellular phenotype and responses to therapy. Nat Med, 2013. 19(5): p. 619-25.
71. Shui, J.W., et al., HVEM signalling at mucosal barriers provides host defence against pathogenic bacteria. Nature, 2012. 488(7410): p. 222-5.
72. Koo, B.K., et al., Controlled gene expression in primary Lgr5 organoid cultures. Nat Methods, 2012. 9(1): p. 81-3.
73. Weigmann, B., et al., Isolation and subsequent analysis of murine lamina propria mononuclear cells from colonic tissue. Nat Protoc, 2007. 2(10): p. 2307-11.
74. Zhong, S., et al., Retroviral transduction of T-cell receptors in mouse T-cells. J Vis Exp, 2010(44).
75. Bao, S., et al., Stem cell-like glioma cells promote tumor angiogenesis through vascular endothelial growth factor. Cancer Res, 2006. 66(16): p. 7843-8.
76. Huang, Y., et al., The c-Abl tyrosine kinase regulates actin remodeling at the immune synapse. Blood, 2008. 112(1): p. 111-9.

Chapter 4

miR-1269 Promotes Metastasis and Forms a Positive Feedback Loop with TGF-β

This section is adapted from the following publication:

Pengcheng Bu*, **Lihua Wang***, Kai-Yuan Chen, Nikolai Rakhilin, Jian Sun, Adria Closa, Kuei-Ling Tung, Sarah King, Anastasia Kristine Varanko, Yitian Xu, Joyce Huan Chen, Amelia S Zessin, James Shealy, Bethany Cummings, David Hsu, Steven M. Lipkin, Victor Moreno, Zeynep H. Gümüş, Xiling Shen. miR-1269 Promotes Metastasis through a Positive Feedback Loop with TGF-β. ***Nat* commun**. 2015 Apr 15; 6:6879**.**

* co-first author

Author contributions: Pengcheng Bu, Lihua Wang and Xiling Shen designed the experiments. Pengcheng Bu and Lihua Wang performed the experiments with the assistance from Kuei-Ling Tung, Nikolai Rakhilin and Yitian Xu. Sarah King helped for RNA extraction and H&E staining. Anastasia Kristine Varanko and Bethany Cummings helped for cecum injection. Kai-Yuan Chen, James Shealy, Jian Sun and Zeynep H. Gümüş performed bioinformatics analysis. Adria Closa and Victor Moreno performed Kaplan–Meier relapse analysis. Steven M. Lipkin provided the human samples. Amelia S. Zessin and David Hsu analyzed the data for H&E staining. Pengcheng Bu, Lihua Wang and Xiling Shen wrote the manuscript.

INTRODUCTION

Many solid tumors progress through stages while accumulating genetic alterations and reprogramming microenvironments [1, 2]. Ranked among the most common cancers and a leading cause of cancer-related deaths [3, 4], CRC progresses through an adenoma to carcinoma sequence that eventually leads to metastasis [5, 6]. The stage of CRC is specified by the American Joint Committee on Cancer (AJCC) tumor-node-metastasis (TNM) staging system, which provides the guideline for treatment. Stages I and II are usually considered non-invasive, stage III has spread to lymph nodes, and stage IV involves metastasis. However, although there is consensus to treat stage I CRC with only surgery and stages III/IV CRC with chemotherapy in addition to surgery, the overall benefit of adjuvant chemotherapy after resection of stage II CRC remains unclear [7]. Still, chemotherapy likely improves survival for certain subsets of stage II patients. As patient survival drops from 80~90% for early-stage CRCs to below 10% for late-stage and metastatic CRCs, it is important to identify prognostic markers and therapeutic targets for chemoprevention [8].

microRNAs are small non-coding RNA molecules that suppress gene expression via the 3` untranslated regions (UTRs) of target mRNAs. Individual microRNA can control many target genes and microRNA expression is often altered in cancer cells [9]. Among them, microRNAs that promote relapse and metastasis are of particular interest as potential prognostic biomarkers and therapeutic targets [10，11].

RESULTS

miR-1269 is upregulated in late-stage CRC tumors

To investigate the roles of microRNAs in CRC progression, we systematically compared microRNA expression levels in early- versus late-stage CRC tumors using the latest colon adenocarcinoma (COAD) miRNASeq dataset in TCGA [12]. Differential expression analysis based on read counts identified miR-1269 as a top microRNA candidate that is upregulated in state IV CRCs vs. stage I & II CRCs, with a p-value of 0.01 (Figures 1A-1C, 2 and Table 1). We did not include Stage III CRCs in our TCGA analysis because their metastatic potential was less clear and may vary widely between individuals.

The miR-1269 family has two isoforms, miR-1269a and miR-1269b. To validate the TCGA analysis, we measured miR-1269a and miR-1269b expression levels in 12 early-stage and 17 late-stage CRC tumors acquired from the Weill Cornell Medical College (WCMC) Colon Cancer Biobank (Table 2). Late-stage CRCs have higher miR-1269a expression levels than early-stage CRCs in a statistically significant manner according to RT-qPCR measurements, consistent with the TCGA finding (Figure 1D). On the other hand, miR-1269b level was not statistically different between early- and late-stage CRC samples.

miR-1269 is a marker associated with CRC relapse and metastasis

Generally, it is difficult to predict whether stage II CRC patients will relapse or develop metastasis after surgical removal of their primary tumors, although 10-20% of stage II patients will eventually relapse. To explore whether miR-1269a is a prognostic marker for relapse and metastasis, we performed a clinical study on 100 stage II CRC patients at the Catalan Institute of Oncology (Table 3) [13]. These disease-free patients were

considered “low-risk” for relapse and did not undergo chemotherapy after the surgery. The patients were divided into two cohorts, “miR-1269a^{low}” and “miR-1269a^{high}”, based on the miR-1269a expression levels measured in their surgically removed primary tumors. Based on risk of relapse for stage II CRC, we allocated the top 10% (10 patients) into the miR-1269a^{high} cohort and the rest (90 patients) into the miR-1269a^{low} cohort to see whether miR-1269a expression could distinguish the small subset of patients who actually had high risk of relapse.

Follow-up revealed that high miR-1269a expression was associated with relapse and metastasis of these disease-free patients (log rank p=0.002). The miR-1269a^{high} cohort had a significantly higher recurrence rate than the miR-1269a^{low} cohort, based on disease-free survival curves from Kaplan-Meier analysis (Figure 1E). Distant metastasis developed in only 18% of the patients in the miR-1269a^{low} cohort but in 60% of the patients in the miR-1269a^{high} cohort (Table 3A). The prognostic value of miR-1269a was significant (p=0.015) in a multivariable Cox’ proportional hazards model adjusted for age, sex, sub-site (left/right) and sub-stage (IIa/IIb) (Table 3B). These results indicate that miR-1269a could be a potential marker associated with a small subset of high-risk CRC Stage II patients who were previously deemed low-risk and may benefit from chemotherapy after surgery. We also explored cut points of miR-1269a expression that stratified patients at 15 and 20 upper percentiles, and the miR-1269a^{high} cohort still had higher recurrence rate than the miR-1269a^{low} cohort in a statistically significant way (p=0.009 and 0.022). Similar analysis on miR-1269b showed that miR-1269b was not associated with risk of relapse (Figure 3A).

miR-1269a expression is associated with metastatic potential in CRC cell lines.

We measured miR-1269a expression in 6 commonly used CRC cell lines (Figure 1F). In general, miR-1269a levels are low in cells with relatively low metastatic potential (HT29 and SW480) and are high in cells with relatively high metastatic potential (DLD1, LoVo, LS174T, and SW620). One ambivalent case is the low miR-1269a expression in HCT116 cells, which were derived from primary adenocarcinoma but seem to possess metastatic potential. It is likely that HCT116 cells have accumulated other metastasis-promoting mutations. Notably, the miR-1269a level is 6-fold higher in SW620 cells than in SW480 cells. Originally from the same CRC patient, SW480 was derived from a primary colon adenocarcinoma prior to relapse while SW620 was derived from mesenteric lymph nodes metastases post-relapse [14]. Hence, this controlled comparison between the two patient-matched cell lines supported that miR-1269a levels are associated with metastatic potential. Unlike miR-1269a, miR-1269b exhibited similar expression levels in SW480 and SW620 cells (Figure 3B). Therefore, we decided to focus on miR-1269a for the rest of the study.

miR-1269a promotes CRC metastasis

To evaluate the effect of miR-1269a on SW480 cells, which have low endogenous miR-1269a expression, we ectopically expressed miR-1269a in SW480 cells. Ectopic miR-1269a only slightly increased cell growth in vitro (Figure 4) and subcutaneous xenograft tumor growth in vivo (Figure 5A). However, transwell migration assay (Figure 5B) and Matrigel invasion assay (Figure 5C) showed that ectopic expression of miR-1269a increased migration and invasion of SW480 cells significantly.

To investigate whether miR-1269a promotes metastasis in vivo, we used an established CRC orthotopic model by implanting human CRC cells into cecum terminus of NOD/SCID

mice [15, 16]. SW480 cells were infected with lentiviral vectors to establish two stable lines that either expressed miR-1269a (SW480-miR-1269a) or contained a control vector (SW480-NC). These cells also carry constitutive luciferase and mCherry reporter constructs. After cecal implantation of equal numbers of cells from both lines, metastasis was tracked using the whole-body IVIS bioluminescence imaging system. Once a mouse became moribund, all mice were sacrificed simultaneously and hepatic metastases expressing mCherry were analyzed by imaging the entire liver with a fluorescent microscope. SW480-NC cells failed to metastasize to liver in all 8 mice (0/8). In contrast, 7 out 8 (7/8) mice injected with SW480-miR-1269a cells developed hepatic metastases (Figures 5D-5F, 5J, 6A and 6B). Hence ectopic miR-1269a expression promotes metastasis of SW480 cells in vivo.

To investigate whether silencing of miR-1269a expression in metastatic cells impedes their ability to metastasize, we knocked down endogenous miR-1269a levels in SW620 cells, the metastatic counterpart of SW480 from the same patient. SW620 cells were infected with lentiviral vectors to establish two stable lines that either expressed antisense RNA against miR-1269a (SW620-Anti-miR-1269a) or contained a control vector (SW620-Anti-NC). The miR-1269a knockdown efficiency in SW620-Anti-miR-1269a cells was evaluated by a luciferase reporter (Figure 7). Equal numbers of SW620-Anti-NC and SW620-Anti-miR-1269a cells were implanted into the ceca of NOD/SCID mice. All mice were simultaneously sacrificed for metastasis examination when one became moribund. 6 out of 8 (6/8) mice injected with SW620-Anti-NC cells developed hepatic metastases, whereas only 1 out of 8 (1/8) mice injected with SW620-Anti-miR-1269a cells developed

hepatic metastasis (Figures 5G-I, 5K, 6C and 6D). Thus, miR-1269a knockdown suppressed metastasis of SW620 cells in vivo.

In addition to the cecum-injection model, we performed intravenous injection through tail vein with the same cells. In the group injected with SW480-miR-1269 cells, all 10 mice developed lung metastasis, with a large number of metastatic nodules covering the entire lung. In contrast, only 4 out of 10 mice injected with SW480-NC cells developed lung metastasis, with a small number of metastatic nodules (Figures 8A-8C). miR-1269a also promoted CRC colonization of liver. Only 1 out of the 10 mice injected with SW480-NC cells developed liver metastasis while 5 out of the 10 mice injected SW480-miR-1269a cells developed liver metastasis (Figures 8D-8F). Consistent with SW480 cells, ectopic miR-1269a expression in HCT116 also enhanced lung and liver metastasis, compared with the control vector (Figures 8G and 8H). Therefore, miR-1269a expression promoted colonization of circulating SW480 and HCT116 cells in lung and liver.

Similarly, equal numbers of SW620-Anti-NC and SW620-Anti-miR-1269a were intravenously injected through tail vein. In the control group (SW620-Anti-NC), all 10 mice (10/10) developed lung metastasis, and 4 out of 10 (4/10) developed liver metastasis, which is consistent with the high metastatic potential of SW620. miR-1269a knockdown significantly reduced lung and liver metastasis of SW620 cells. In the SW620-Anti-miR-1269a group, only 3 out 10 (3/10) mice developed lung metastasis, and 1 out 10 (1/10) developed liver metastasis (Figures 8A-8F). The SW620 data were further corroborated by knocking down miR-1269a in LS174T cells, which also have high endogenous miR-1269a expression. Injected LS174T control cells formed extensive metastasis in the lung, lymph nodes in the lateral thoracic region, and the bone. In contrast, miR-1269a

knockdown in LS174T cells significantly reduced metastasis in these regions (Figure 8I). Therefore, silencing of endogenous miR-1269a mitigated colonization of circulating SW620 and LS174T cells.

Collectively, the in vitro migration and invasion assays and in vivo metastasis assays, with ectopic expression of miR-1269a in SW480 and HCT116 cells and knockdown of endogenous miR-1269a in SW620 and LS174T cells, indicate that miR-1269a promotes CRC metastasis.

miR-1269a promotes an EMT-like process

Since an EMT-like process has been associated with colon cancer metastasis [17], we examined whether miR-1269a promotes EMT. We measured the levels of the epithelial marker E-cadherin and the mesenchymal markers N-cadherin and Vimentin in SW480-miR-1269a and SW480-NC cells using both Western blot and immunofluorescence. Compared with the control SW480-NC cells, which had high E-cadherin expression and low N-cadherin and Vimentin expression, SW480-miR-1269a cells had significantly downregulated E-cadherin expression and upregulated N-cadherin and Vimentin expression (Figures 9A and 9B). Consistent with the EMT markers, SW480-miR-1269a cells adopted a spindle-shaped, mesenchymal-like morphology in contrast to the epithelial-like morphology of SW480-NC cells (Figure 9C). Hence ectopic miR-1269a expression causes SW480 cells to undergo EMT.

We then examined whether silencing of miR-1269a could impede the ability of cells to undergo EMT. As the metastatic counterpart of SW480, SW620 cells have higher endogenous miR-1269a expression levels than SW480 cells. miR-1269a knockdown reduced N-cadherin and Vimentin levels in SW620 cells, as shown by

immunofluorescence and Western blot (Figures 9D and 9E). TGF-β treatment turned on N-cadherin and Vimentin expression and turned down E-cadherin expression in the control (SW620-Anti-NC) cells, which started to display a mesenchymal-like morphology (Figure 9F). In contrast, the effect of TGF-β induction was much attenuated by miR-1269a knockdown, as SW620-Anti-miR-1269a cells largely maintained E-cadherin expression and the epithelial-like morphology in the presence of TGF-β (Figures 9D-9F). Therefore, miR-1269a knockdown impedes the ability of SW620 cells to undergo an EMT-like process upon TGF-β induction. Together, the data indicate that miR-1269a not only promotes an EMT-like process but is also involved with TGF-β induced transformation of CRC cells.

TGF-β activates miR-1269a via Sox4.

To explore the crosstalk between miR-1269a and TGF-β, we treated SW480 cells with TGF-β and measured the response of miR-1269a by RT-qPCR. TGF-β treatment upregulated miR-1269a expression, suggesting that TGF-β is an upstream regulator of miR-1269a (Figure 10A). Genomic analysis identified 2 Sox4 binding motifs at -173 to -166 (site 1) and -947 to -940 (site 2) inside the putative miR-1269 promoter region (Figure 10B). Notably, Sox4 is a downstream target gene of TGF-β [18] and has been reported to be a master regulator of EMT and cancer metastasis [19]. Therefore, Sox4 is a potential intermediate between TGF-β and miR-1269a. Notably, Sox4 expression level was higher in SW620 cells than in SW480 cells, similar to miR-1269 (Figure 11)

We then tested whether Sox4 can activate the miR-1269a promoter as suggested by their binding motifs. In SW480 cells, ectopic expression of Sox4 caused a 4-fold increase of miR-1269a expression level, compared with cells transfected with a control vector (Figure

10C). We then tested whether Sox4 is the intermediate regulator that is required for TGF-β induced miR-1269a upregulation. Compared to the control cells, Sox4 knockdown by shRNA (shSox4) completely abolished the effect of TGF-β on miR-1269a expression, consistent with Sox4 as an intermediate regulator between TGF-β and miR-1269a (Figure 10D).

To address whether Sox4 directly activates miR-1269a expression, we performed chromatin immunoprecipitation (ChIP) assays in SW480 and HT29 cells. ChIP confirmed that Sox4 proteins were recruited to both binding sites in the putative miR-1269a promoter, with the majority of Sox4 bound to site 1 (Figures 10E and 10F). To test whether the binding of Sox4 is sufficient to activate miR-1269a expression, we cloned the putative miR-1269a promoter sequence into a pGL4-basic vector, which were subsequently transfected into SW480 and HT29 cells. A dual-luciferase reporter assay revealed that ectopic expression of Sox4 activated the transcription of firefly luciferase that was driven by the wild type miR-1269a promoter. When the binding sequence of site 1 was mutated, firefly luciferase expression dropped 6.8-fold in SW480 cells and 5.4-fold in HT29. When the binding sequence of site 2 was mutated, firefly luciferase expression dropped 4.6-fold in SW480 and 5.7-fold in HT29 (Figures 10G and 10H). Therefore, Sox4 directly binds to these two sites to activate miR-1269a expression.

We then examined whether endogenous Sox4 binding to the miR-1269 promoter increases upon TGF-β induction. We treated SW480 cells with TGF-β and then performed ChIP. As expected, more Sox4 proteins were recruited to both binding sites in the miR-1269 promoter after TGF-β treatment (Figure 10I). Next, to investigate whether Sox4 promotes in vivo metastasis as miR-1269 does, we ectopically expressed Sox4 in SW480

cells and implanted them into mouse cecum. Consistent with ectopic miR-1269 expression, ectopic Sox4 expression significantly enhanced SW480 hepatic metastasis (Figures 10J and 10K).

Taken together, our data indicate that TGF-β upregulates miR-1269a through Sox4, which binds to the two Sox4 binding sites in the miR-1269a promoter to activate miR-1269a expression. Thus, TGF-β□, Sox4, and miR-1269a act synergistically to promote EMT and metastasis.

miR-1269a targets Smad7 and HOXD10.

To determine miR-1269a target genes, we searched for computationally predicted candidates using miRecords, which compiles 11 microRNA targets prediction databases such as PicTar, miRanda, TargetScan, and RNA hybrid (Table 4). We then used RT-qPCR to compare expression levels of the candidate genes between ectopic miR-1269a expression and control in SW480 and HT29 cells. Among the candidates, homeobox D10 (HOXD10) has been reported to suppress tumor invasion and metastasis [20], while Smad7 is a well-known antagonist of TGF-β signaling [21]. Smad7 and HOXD10 were downregulated in both SW480 and HT29 cells by miR-1269a (Figures 12A and 12B). Western blot confirmed that miR-1269a suppresses Smad7 and HOXD10 protein levels (Figures 12C and 12D).

To test whether they are direct targeted by miR-1269a, the 3`UTRs of the two genes were cloned downstream of firefly luciferase. The luciferase reporters were then co-transfected with a miR-1269a expressing construct or an empty control vector into SW480 cells. Cells with ectopic miR-1269a expression had suppressed Smad7 and HOXD10 levels, in contrast to the control cells, whereas mutation in the putative miR-1269a seed regions in

the 3`UTRs of either Smad7 or HOXD10 abrogated the suppression of miR-1269a (Figures 12E and 13). Therefore, miR-1269a directly targets Smad7 and HOXD10 through the identified binding sites in their 3UTR.

HOXD10 has been reported to suppress tumor invasion and metastasis [20]. To test whether miR-1269a suppression of HOXD10 promotes invasion and metastasis, we transfected SW480 cells with vector constructs expressing both miR-1269a and HOXD10 mRNA without its 3`UTR (hence resistant to miR-1269a suppression). Transwell migration and Matrigel invasion assays revealed that ectopic expression of HOXD10 was able to abrogate miR-1269a-induced cell migration and invasion (Figure 12F). We then ectopically expressed HOXD10 in SW620 cells and implanted the cells orthotopically into mouse cecum termini. Consistent with the in vitro migration and invasion assays, ectopic HOXD10 expression dramatically reduced hepatic metastasis in vivo (Figures 12G and 12H).

miR-1269a and TGF-β forms a positive feedback loop.

Smad7 is a well-known antagonist of TGF-β signaling [21], but the effect of HOXD10 on TGF-β signaling is unclear. This raised the question as to whether miR-1269a regulates TGF-β signaling in CRC cells through its direct targets. Western blot showed that ectopic expression of miR-1269 in SW480 cells enhanced Smad2 phosphorylation. Consistently, knockdown of miR-1269 target Smad7 or HOXD10 also promoted Smad2 phosphorylation (Figure 14A). To evaluate the effect of HOXD10 and Smad7 on TGF-β targets gene expression, we established cells lines either expressing Smad7 or HOXD10, or containing a control vector. The cell lines were treated with TGF-β for 96 hours before RT-qPCR and Western blot were performed to measure TGF-β target genes, Slug, Snail

and Sox4. As expected, TGF-β upregulated Slug, Snail, and Sox4 expression in cell lines with the control vector. However, the upregulation was significantly reduced by ectopic expression of Smad7 or HOXD10 (Figures 14B-14E, 15A-15D), suggesting that HOXD10 is also an antagonist of TGF-β signaling in CRC cells. Ectopic expression of Smad7 or HOXD10 also reduced TGF-β induced miR-1269a upregulation, consistent with the fact that Sox4 levels are down (Figures 14F, and 15E). Taken together, these data indicate that Smad7 and HOXD10 are antagonists of TGF-β signaling.

Since miR-1269a directly targets Smad7 and HOXD10, both of which are antagonists of TGF-β signaling, we examined whether miR-1269a upregulates TGF-β signaling. As showed in Figures 14G-14I and 15F-15H, ectopic expression of miR-1269a increased the expression levels of all three target genes of TGF-β signaling, Slug, Snail, and Sox4, in SW480 and HT29 cells. Slug, Snail, and Sox4 are master regulators of EMT, and their expression in SW480 cells downregulated E-cadherin and upregulated N-cadherin (Figure 14J). These data provide an explanation for the strong induction of EMT by miR-1269a in CRC cells – miR-1269a upregulates TGF-β signaling and its target genes, Slug, Snail, and Sox4, via suppression of TGF-β antagonists Smad7 and HOXD10. To examine whether miR-1269a induces TGF-β expression, we performed RT-qPCR in SW480 cells that ectopically express miR-1269a. miR-1269a increased TGF-β1 expression but had little effect on TGF-β2 and TGF-β3 expression (Figure 16). ELISA confirmed that miR-1269a also increased TGF-β1 protein level in SW480 medium (Figure 14K). miR-1269a seems to upregulate TGF-β1 via a regulatory route independent of Smad7 and HOXD10, since knockdown of Smad7 and HOXD10 did not affect TGF-β1 level (Figure 14I). Our studies suggest that TGF-β and miR-1269a form a positive feedback loop, wherein TGF-

β upregulates miR-1269 via Sox4, while miR-1269 upregulates TGF-β and enhances TGF-β signaling by suppressing its antagonists Smad7 and HOXD10 (Figure 17).

DISCUSSION

In this study, we performed differential analysis between early- and late-stage CRCs in TCGA to identify miR-1269 as a top candidate, which was confirmed by additional 29 CRC samples. A study of 100 stage II CRC patients revealed that miR-1269a expression level was associated with risk of relapse and metastasis. Mechanistically, this is because miR-1269a and TGF-β form a positive feedback loop via Sox4, HOXD10, and Smad7 to promote EMT and metastasis.

miR-1269a was a somewhat surprising candidate that emerged from our analysis because very little was known about this microRNA. A global study of 8 paired samples of normal mucosa and CRC tumor reported that miR-1269 was one of the 16 microRNAs that were deregulated in tumor tissues [22]. Nevertheless, a differential expression analysis between normal and tumor tissues in TCGA did not suggest a statistically significant change in miR-1269a expression. Regardless, our analysis suggests that miR-1269a likely plays a more prominent role in CRC relapse and metastasis than in oncogenesis. Hence the practice of grouping CRC tumors of various stages into a single group may mask the complexity of microRNA regulation during tumor progression.

miR-1269a does not promote metastasis alone. Instead, it forms a positive feedback loop with TGF-β. This finding is consistent with the increasing appreciation that microRNAs form regulatory motifs with protein regulators to confer robustness to biological processes, and their subversion can expose cells to elevated risk of malfunction [23]. Therefore, the context is important for understanding the role of microRNAs in regulatory networks. For example, positive feedback is known to amplify a response and commits into a self-sustained mode that is autonomous to the original stimuli. It is tempting to speculate that,

once induced by TGF-β, the miR-1269a-mediated feedback loop allows CRC cells to become more autonomous. This would enhance the ability of CRC cells to invade and metastasize to new microenvironments, which would explain the strong pro-metastasis phenotype we have observed.

Elevated TGF-β production is associated with high risk of CRC relapse and metastasis [24]. Stromal cells in the CRC microenvironment can also produce TGF-β, which increases the efficiency of organ colonization by CRC cells. In a likely scenario, TGF-β released from the microenvironment reaches a certain concentration to activate the positive feedback loop in CRC cells and promote their dissemination. Hence miR-1269a may play an integrated role in the TGF-β -mediated crosstalk between CRC and stromal cells to confer a survival advantage to metastatic cells.

On the other hand, we certainly have to caution against over-simplification of CRC metastasis, which is a complicated process involving many players. Mutations could interfere with this feedback loop, while miR-1269a might also affect metastasis through other targets independent of TGF-β. Neither miR-1269 nor the positive feedback loop is likely to be sufficient or necessary for metastasis.

METERIALS AND METHODS

Cell lines

Human CRC cell lines SW480, SW620, HCT116, HT29, DLD1, LoVo and LS174T were acquired from ATCC and cultured under the conditions recommended by the provider. For TGF-β activation, the cells were treated with 10ng/ml TGF-β for 96 hours, and TGF-β was replaced after 48 hours.

Kaplan-Meier relapse analysis and clinical specimens

The studies followed informed consent and approval of the ethical committees at Catalan Institute of Oncology and Weill Cornell Medical College. Tumor relapse was analyzed by tracking 100 stage II CRC patients. The patients were divided into two groups, "miR-1269^{low}" and "miR-1269^{high}", based on the miR-1269 expression levels measured in their surgically removed primary tumors. microRNA expression was measured using Solid IV small-RNA sequencing and bowtie2 mapped to miRbase [20]. Sample counts were normalized according to the library size using the DESeq bioconductor package (http://genomebiology.com/2010/11/10/r106). The cutoff threshold was set to separate the top 10% miR-1269^{high} patients from the 90% "miR-1269^{low} patients. The disease-free survival curves were estimated using the Kaplan-Meier method and compared with the log-rank test.

To evaluate miR-1269a expression in early- and late-stage CRC tumors, frozen CRC specimens were acquired from Weill Cornell Medical College (WCMC) Colon Cancer Biobank. Total RNA was then isolated from the frozen tissues using the Allprep DNA/RNA kit (Qiagen).

Quantitative real-time RT-PCR analysis

Total RNA was extracted from the cells using the TRIzol Reagent (Invitrogen). cDNA was synthesized from 500 ng of total RNA in 20 µl of reaction volume using the High Capacity cDNA Archive Kit (Applied Biosystems). miR-1269a and miR-1269b levels were measured by quantitative PCR using the TaqMan MicroRNA Assay (Applied Biosystems). Gene expression levels were measured by quantitative PCR using the SYBR Green System (Applied Biosystems). All samples were run in triplicates and were repeated three times. The respective miR-1269a and miR-1269b primers and U6 primer were purchased from Applied Biosystems. Other primer sequences include: HOXD10, 5`-GTGCAGGAGAAGGAAAGCAAAG-3` and 5`-TAACGCTCTTACTGATCTCTAGGC-3`; Smad7, 5'-TGCTCCCATCCTGTGTGTTAAG-3' and 5`-TCAGCCTAGGATGGTACCTTGG-3`; Slug, 5`-CATGCCTGTCATACCACAAC-3` and 5`- GGTGTCAGATGGAGGAGGG-3`; Snail, 5`- GAGGCGGTGGCAGACTAG-3` and 5`-GACACATCGGTCAGACCAG-3`; Sox4, 5`- CACATCAAGCGACCCATGAAC-3` and 5`-CCGGTACTTGTAGTCGGGGTAGT-3`; TGF-β1, 5`-CTCTCCGACCTGCCACAGA-3` and 5`-AACCTAGATGGGCGCGATCT-3`; TGF-β2, 5`-CCGCCCACTTTCTACAGACCC-3` and 5`-GCGCTGGGTGGGAGATGTTAA-3`; TGF-β3, 5`-CTGGCCCTGCTGAACTTTG-3` and 5`-AAGGTGGTGCAAGTGGACAGA-3`; actin, 5`-CGCGAGAAGATGACCCAGAT-3` and 5`-ACAGCCTGGATAGCAACGTACAT-3`. The expression of each gene was defined from the threshold cycle (Ct), and the relative expression levels were calculated using the 2-ΔΔCt method after normalization to the actin expression level.

Lentiviral Vector Constructs and Infection

miR-1269a was ectopically expressed by the GFP hsa-miR-1269a Letivector and silenced by the inhibitor hsa-miR-1269a Letivector. These two vectors and the control vectors were ordered from Applied Biological Material. The Smad7 luciferase reporter, with the Smad7 3`UTR in the pMirtarget Vector, was ordered from OriGene. The HOXD10 luciferase reporter, pMIR-D10 UTR, was order from Addgene. miR-1269a binding sequences in the Smad7 and HOXD10 luciferase reporters were mutated using the QuickChange Site-directed Mutagenesis Kit (Stratagene). In order to construct the reporter for miR-1269a promoter activity, the miR-1269a promoter sequence was amplified from human genomic DNA and cloned into the pGL4.10 vector (Promega). The putative Sox4 binding site in the miR-1269a promoter sequence was further mutated using the QuickChange Site-directed Mutagenesis Kit (Stratagene). Expression vectors for HOXD10, Smad7, Sox4, Slug, and Snail (HOXD10-pcDNA, pBabe-puro-Smad7-HA, pWPXL-Sox4, pBabe-puro-Slug and pBabe-puro-Snail) were ordered from Addgene. shRNA constructs against HOXD10 and Smad7 were ordered from Sigma. The reporter construct carrying luciferase and mCherry was order from Addgene. The lentiviral vectors were co-transfected with helper plasmids into 293T cells. The retroviral vectors were transfected into phoenix cells. The viral supernatant was collected 48 hours after transfection and was used to infect CRC cells.

Luciferase reporter assay

To validate the Sox4 binding sites in the miR-1269a promoter, miR-1269a promoter reporter construct with wide-type or mutated Sox4 binding sites was transfected with the pRL-SV40 Renilla luciferase vectors into SW480 and HT29 cells using the LT1 Transfection Reagent (Mirus). To validate whether HOXD10 and Smad7 are direct targets

of miR-1269a, HOXD10 and Smad7 luciferase reporter constructs with wide-type or mutated miR-1269a binding sites were transfected with the pRL-SV40 Renilla luciferase vector into SW480 and HT29 cells. 48 hours after transfection, Luciferase assays were performed using the dual luciferase reporter assay system (Promega). Measurements from triplicate transfections were analyzed after normalization to the Firefly luciferase activity.

Immunofluorescence

Cells were grown on glass culture slides (BD Biosciences) and fixed with 4% cold methanol at -20 °C for 10 minutes. Subsequently, cells were blocked with 10 % goat serum for 1 hour and incubated with primary antibodies against E-cadherin (24E10, 1:200, Cell Signaling), N-cadherin (1:100, BD Biosciences) and Vimentin (D21H3, 1:100, Cell Signaling) at 4 °C for 1 hour and then incubated with Rhodamine Red or Alexa Fluor 488 labeled secondary antibody (Invitrogen) for 1 hour at room temperature. After counterstained with DAPI (Invitrogen), the slide was observed under a confocal microscope (Zeiss).

Chromatin immunoprecipitation (ChIp) assay

ChIP was performed using a ChIP assay kit (Millipore) according to the manufacturer's instructions. Briefly, SW480 and HT29 cells either infected with a vector expressing Sox4 or treated with TGF-β1 were incubated in 1% formaldehyde for 10 minutes at room temperature to crosslink their DNA. The cells were lysed in lysis buffer, sonicated to generate DNA fragments less than 500 base pairs in length and then diluted by 10 folds in ChIP Dilution Buffer. Before immunoprecipitation, nuclear extracts were pre-cleared with 50% protein G–Sepharose slurry, goat normal serum and sheared salmon sperm

DNA for 2 hours at 4 ºC. Anti-Sox4 antibody (H-90, 1:50, Santa Cruz) was then added to form complexes with Sox4 protein and associated chromatin. These immunocomplexes were recovered by protein G–Sepharose beads, and the associated DNA was purified by extraction with phenol/chloroform. PCR Primers 5`-CAGTGGATTGAGTGAGGAAGATTCT-3` and 5`-TGAGCCCCAGAGTCCAAGAG-3` for site 1 and primers 5`-CCCTCACAGCAATTTTATAGCATCT-3` and 5`-TCAAACAAATATGCCAGTCACTTCA-3` were used to measure the enrichment of the putative Sox4 binding site in the miR-1269a promoter.

Western Blot

Whole cell lysate was prepared in a lysis buffer (20 mM Tris pH 7.5, 150 mM NaCl, 1% Nonidet P-40, 0.5% Sodium Deoxycholate, 1 mM EDTA, 0.1% SDS, protease inhibitors). Proteins were first separated by 10% SDS-PAGE and then transferred to a Hybond membrane (Amersham). The membranes were incubated with primary antibodies either anti-E-cadherin (24E10, 1:1000, Cell Signailing), anti-N-cadherin (1:1000, BD Biosciences), anti-HOXD10 (H-80, 1:1000, Santa Cruz), anti-Smad7 (B-8, 1:500, Santa Cruz), anti-Snail (C15D3, 1:1000, Cell Signaling), anti-Slug (C19G7, 1:1000, Cell Signaling), anti-Sox4 (C20, 1:100, Santa Cruz) anti-Phospho-Smad2 (1:1000, Cell Signaling) or anti-□-actin (13E5, 1:1000, Cell Signaling) in 5% milk/TBST buffer (25 mM Tris pH 7.4, 150 mM NaCl, 2.5 mM KCl, 0.1% Triton-X100) overnight, and then probed for 1 hour with secondary horseradish peroxidase (HRP)-conjugated anti-mouse or anti-rabbit IgG (Santa Cruz). After extensive wash with PBST, the target proteins were detected on membrane by enhanced chemiluminescence (Pierce).

Analysis of Proliferation, migration and invasion

SW480 cells were infected with either the control or miR-1269a expression lentiviral vectors. The infection efficiency was measured by GFP expression from the vectors. Cell proliferation under differentiating condition was analyzed using the WST-1 Cell Proliferation Reagent (Clontech). Migration assay and invasion assay were performed as previously described. Briefly, 1×105 cells were plated in the serum-free medium in the upper chamber with the non-coated membrane (24-well insert; pore size, 8 mm; BD Biosciences) for migration assay and with Matrigel-coated membrane (24-well insert; pore size, 8 mm; BD Biosciences) for invasion assay. The lower chamber was filled with medium containing 20% FBS. The cells were incubated for 24 hours at 37°C. The cells that did not traverse the membrane were removed by a cotton swab, and the cells on the lower surface of the membrane were stained with crystal violet and observed under a microscope.

In Vivo experiments

All animal experiments were approved by The Cornell Center for Animal Resources and Education (CARE) and followed the protocol (2009-0071 and 2010-0100). For subcutaneous injection, 8×106 cancer cells were injected into the lower back region of 5-week-old female nude mice, with 5 mice per group. The mice were sacrificed and the tumors were collected and weighed when one of the mice had developed severe tumor burden.

For intravenous injection, 2×106 cancer cells were injected into 5-week-old female NOD/SCID mice, with 10 mice per group. The mice were sacrificed and lung/liver metastasis was evaluated when one of them became moribund.

For cecum injection, cells were carrying a reporter construct expressing luciferase and mCherry. After FACS sorting, 4×106 cells were injected into 5-week-old female NOD/SCID mice, with 8 mice per group. After injection, luciferase signal was tracked in vivo using the IVIS luciferase imaging system 200 (Xenogen). When one of the mice became moribund, all mice were sacrificed and liver metastases were evaluated based on mCherry signals by an OV100 microscope (Olympus).

Immunohistochemistry

Lung and liver tissue from mice injected with CRC cells with miR-1269a expression or silencing vectors were removed and fixed in 4% paraformaldehyde overnight. Paraffin-embedded sections were processed for H&E staining.

Bioinformatics analysis

microRNA expression profiles of CRC tumors at different stages were compared by analyzing miRNASeq data from the TCGA COlon ADenocarcinoma (COAD) dataset. A total of 409 samples were grouped according to AJCC TNM staging. Stage I (68 samples) and Stage II (162 samples) CRCs were combined to form the early-stage CRC cohort, which was compared with stage IV samples (59 samples) as the late-stage cohort. DESeq was used for differential analysis of the microRNA expression profiling between early- (stage I and II) and late-stage (stage IV) CRC cohorts.

Statistical Analysis

Data were expressed as mean ± standard deviation of no smaller than three biological repeats, unless otherwise noted. Student t tests were used for comparisons, with $p<0.05$ considered significant. Survival curves were estimated using the Kaplan-Meier method and compared using the logrank test. The multivariate analysis was performed

with a Cox's proportional hazards model. Hazard ratios and 95% confidence intervals were derived from the model.

Acknowledements

We thank Robert Weiss and members of the Shen laboratories for discussions. We also thank the investigators and institutions of the TCGA research network that have contributed to the TCGA data used for this study. This work was supported by NIH R01GM95990, NSF 1350659 career award, NSF 1137269, DARPA 19-1091726, Instituto de Salud Carlos III grant PI11-01439, CIBERESP CB07/02/2005, the Spanish Association Against Cancer (AECC) Scientific Foundation, the Catalan Government DURSI grant 2009SGR1489, and the European Commission FP7-COOP-Health-2007-B HiPerDART.

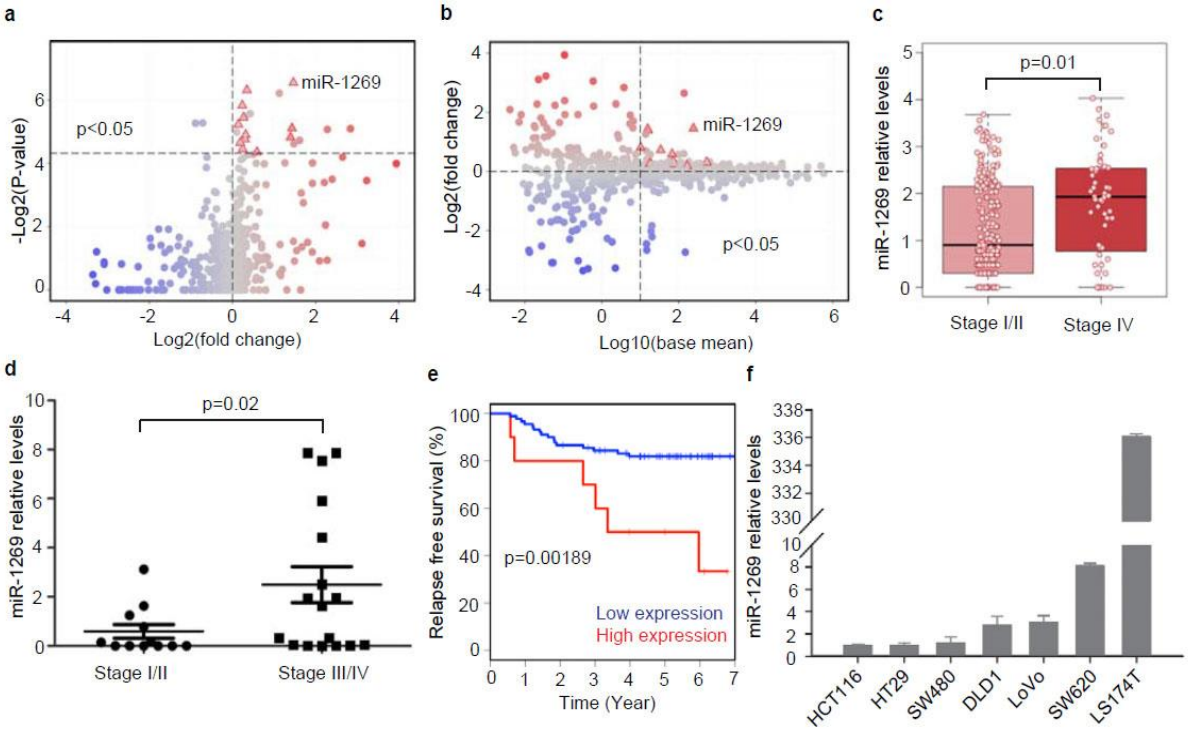

Figure 1. miR-1269 level is associated with CRC progression, relapse and metastasis.

(**a**) Volcano plot comparing miRNASeq data between Stage I/II CRCs and Stage IV CRCs from the TCGA COAD dataset. Each dot represents a microRNA. Dots in the upper right quadrant represent microRNAs that are upregulated in Stage IV CRCs with enough statistical significance (p-value < 0.05). (**b**) MA plot comparing miRNASeq data between Stage I/II CRCs and Stage IV CRCs. Dots in the upper right quadrant represent microRNAs that are abundant and upregulated in Stage IV CRCs. (**c**) miR-1269 expression in early- (Stage I/II, n=230) and late-stage (Stage IV, n=59) CRCs. Each dot represents a CRC sample from COAD. (**d**) RT-qPCR measurements of miR-1269a expression in early- (Stage I/II, n=12) and late-stage (Stage III/IV, n=17) CRC samples from WCMC Colon Cancer Biobank. (**e**) Kaplan-Meier analysis of relapses of Stage II CRC patients with high (red, n=10) and low (blue, n=90) miR-1269a levels in their surgically removed primary tumors. (**f**) RT-qPCR measurements of miR-1269a expression in various CRC lines. Error bars denote s.d. of triplicates.

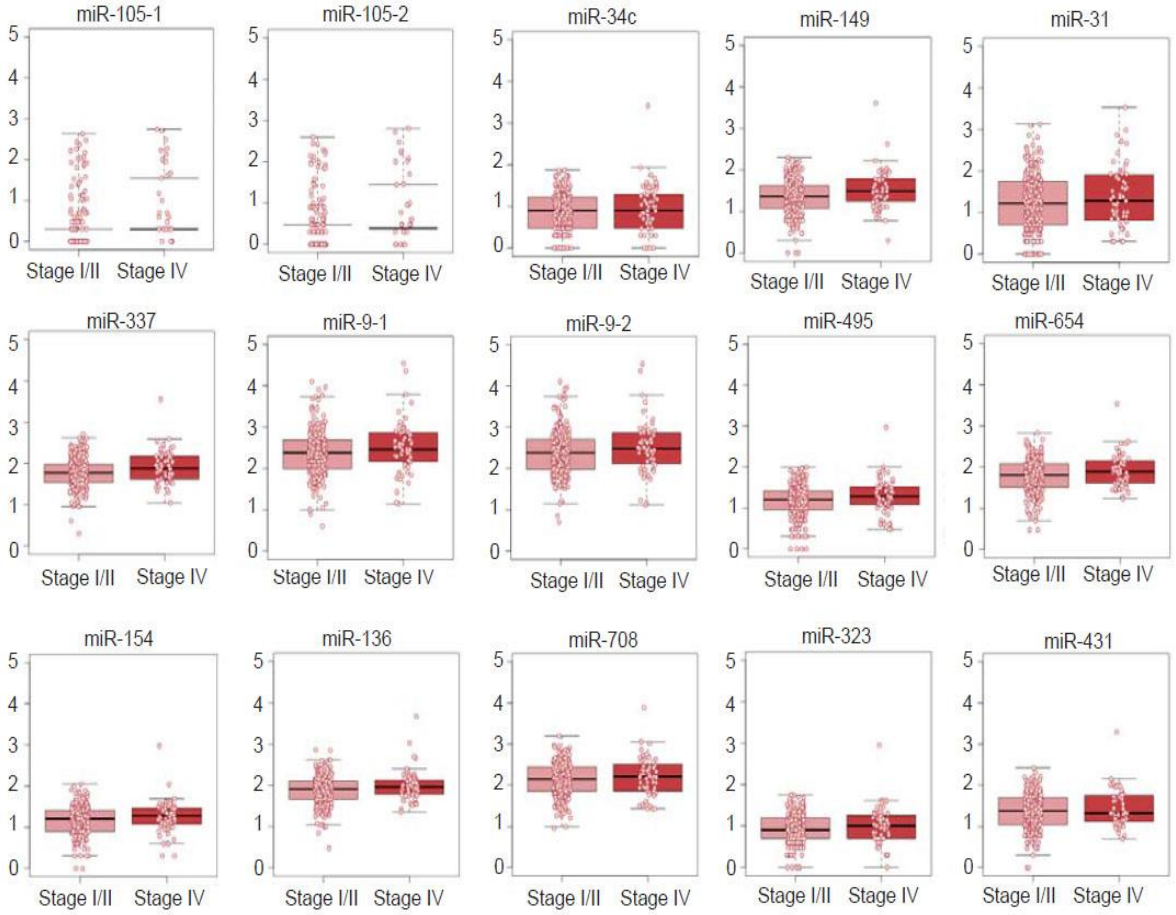

Figure 2. microRNAs upregulated in late-stage CRCs according to TCGA.

Expression levels of micoRNAs from Table 1 in individual early-(stageI/II, n=230) and late-stage (stage IV, n=59) CRCs according to miRNASeq data from COAD.

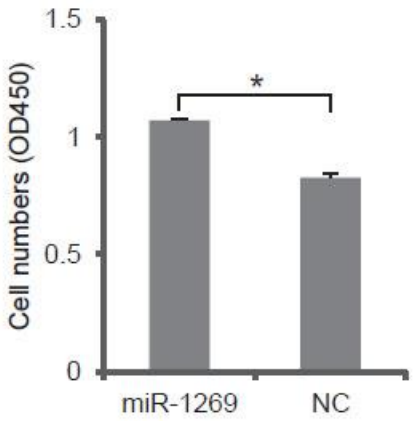

Figure 3. The effect of miR-1269 on cell growth in *vitro*.

SWT-1 assay measuring the growth of SW-480 cells with a control (NC) or a miR-1269 expression vector. Error bars denote the s. d. between triplicates. *. $p<0.05$.

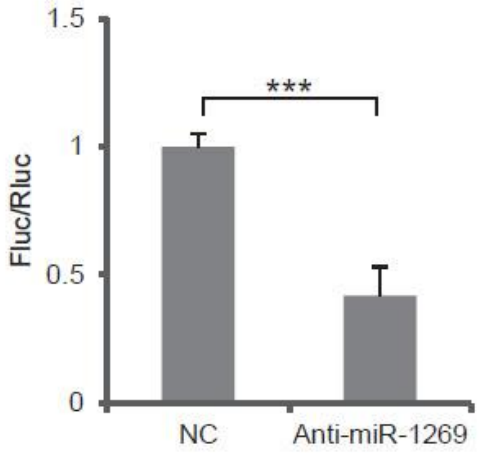

Figure. 4. Efficiencies of ectopic expression and silencing of miR-1269.

Luciferase reporter assay showing the efficiency of an anti-miR-1269 construct in SW480 cells. Error bars denote the s. d. between triplicates. ***, $p<0.001$.

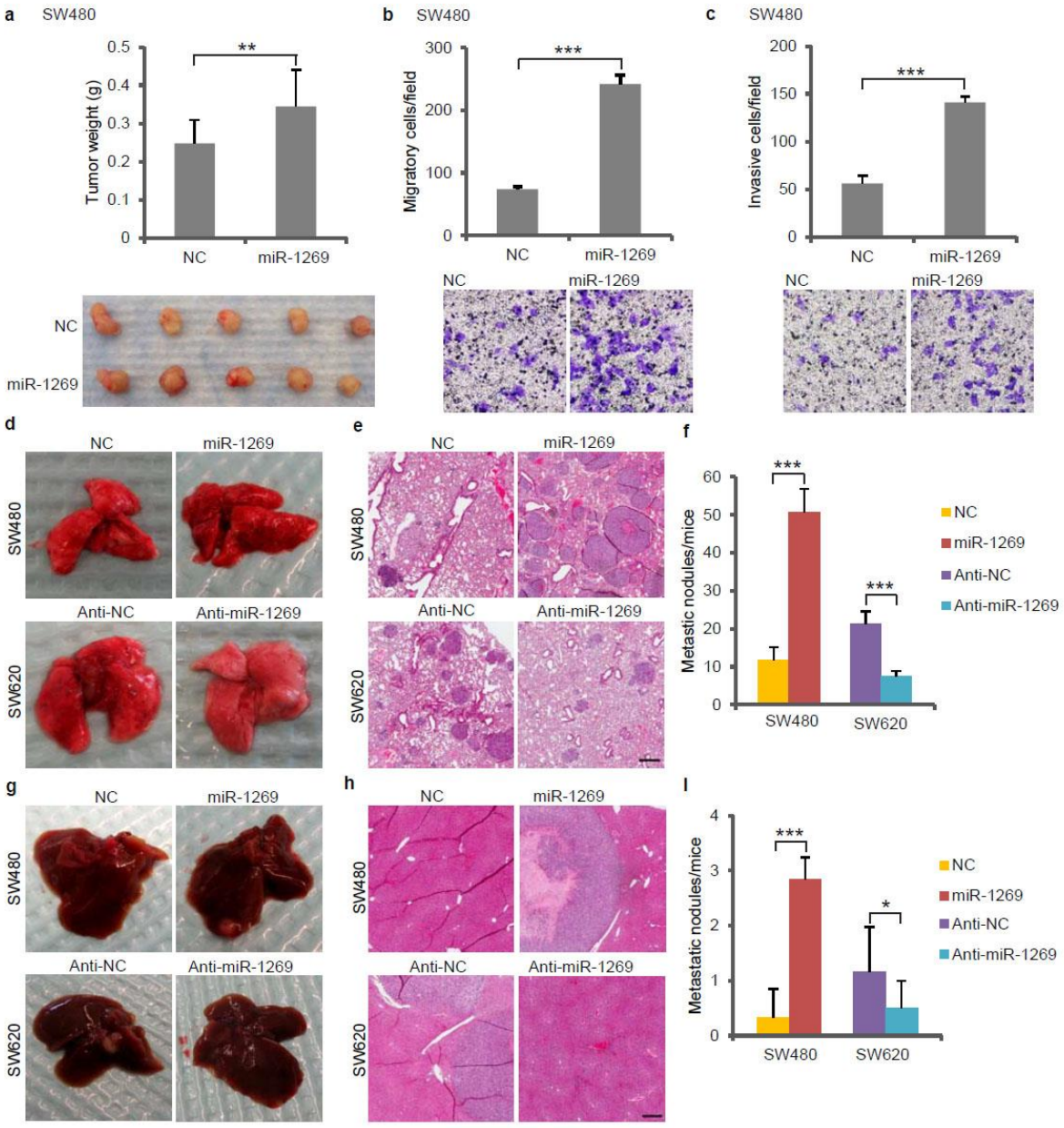

Figure 5. miR-1269a promotes CRC metastasis

(**a**) Growth of subcutanous xenograft CRC tumor, as shown by tumor weight (upper panel) and representative tumor images (lower panel), with a control vector (NC) or with ectopic miR-1269a expression (miR-1269a). Error bars denote s.d. of 5 mice in each group. (**b,c**) Transwell assay measuring CRC cell migration (b) and invasion (c) with a control vector (NC) or with ectopic miR-1269a expression (miR-1269a). Error bars denote s.d. of triplicates. (**d-f**) Analysis of CRC liver metastasis in mice with orthotopic (cecal) injection of SW480-NC and SW480-miR-1269a cells carrying luciferase and mCherry reporter constructs. Representative IVIS luciferase in vivo images (d), bright field and fluorescent (mCherry) images of livers isolated from mice (e), and number of liver metastatic nodules

(f) show ectopic miR-1269a expression promoted liver metastasis of SW480 cells. (**g-i**) Analysis of CRC liver metastasis in mice with orthotopic (cecal) injection of SW620-Anti-NC and SW620-Anti-miR-1269a cells carrying luciferase and mCherry reporter constructs. Representative IVIS luciferase in vivo images (g), bright field and fluorescent (mCherry) images of livers (h), and number of liver metastatic nodules (i) show knockdown of endogenous miR-1269a by antisense RNA suppressed liver metastasis of SW620 cells. Error bars denote s.d. of 8 mice in each group. (**j-k**) H&E staining of liver sections isolated from mice orthotopically injected with SW480-NC or SW480-miR-1269a cells (j) or SW6200-Anti-NC or SW620-Anti-miR-1269a cells (k). Error bars denote s.d. of 8 mice in each group. *, $p<0.05$; **, $p<0.01$; ***, $p<0.001$. Scale bar, 15 μm.

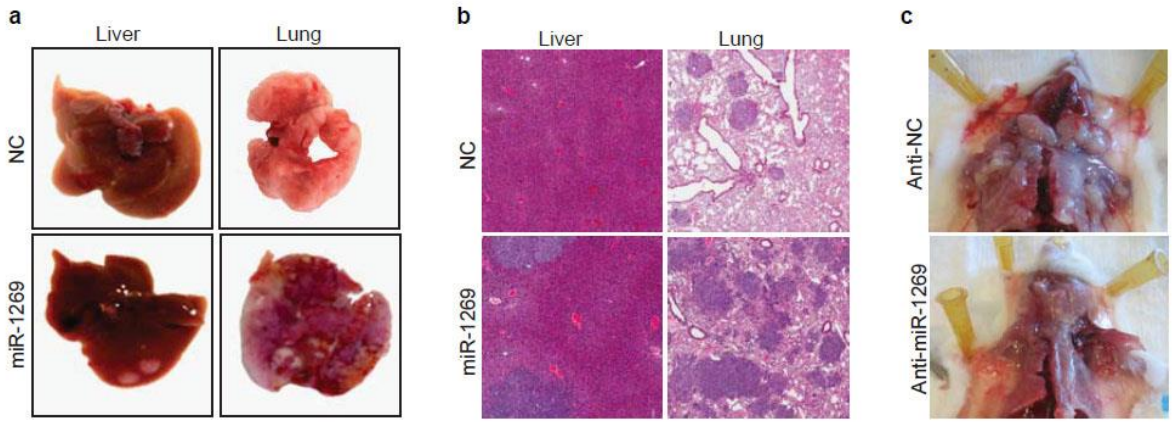

Figure 6. miR-1269 promotes CRC metastasis

(**a**) Ectopic miR-1269 expression in HCT116 cells enhanced their liver and lung metastasis. (**b**) Representative H&E images of liver and lung metastasis from HCT116 cells with a control (NC) or a miR-1269 expression (miR-1269) vector. (**c**) Representative images showing miR-1269 knockdown by antisense RNA in LS174T cells reduced lymph node metastasis.

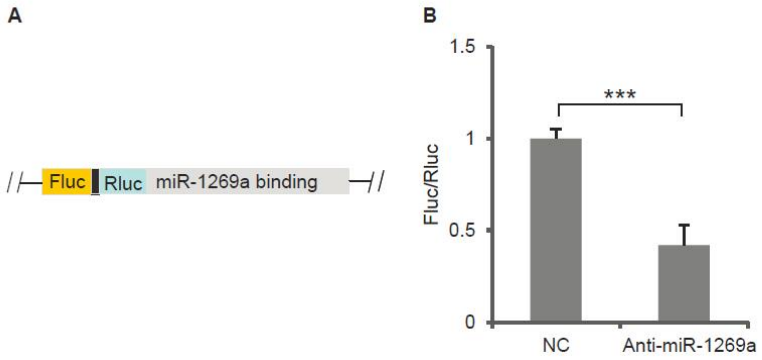

Figure 7. shRNA silencing of miR-1269a.
(**a**) Schematic illustration of the reporter vector used in (b). (**b**) Luciferase reporter assay showing the knockdown efficiency of an anti-miR-1269a construct in SW620 cells. Error bars denote s.d. of triplicates. ***, p<0.001.

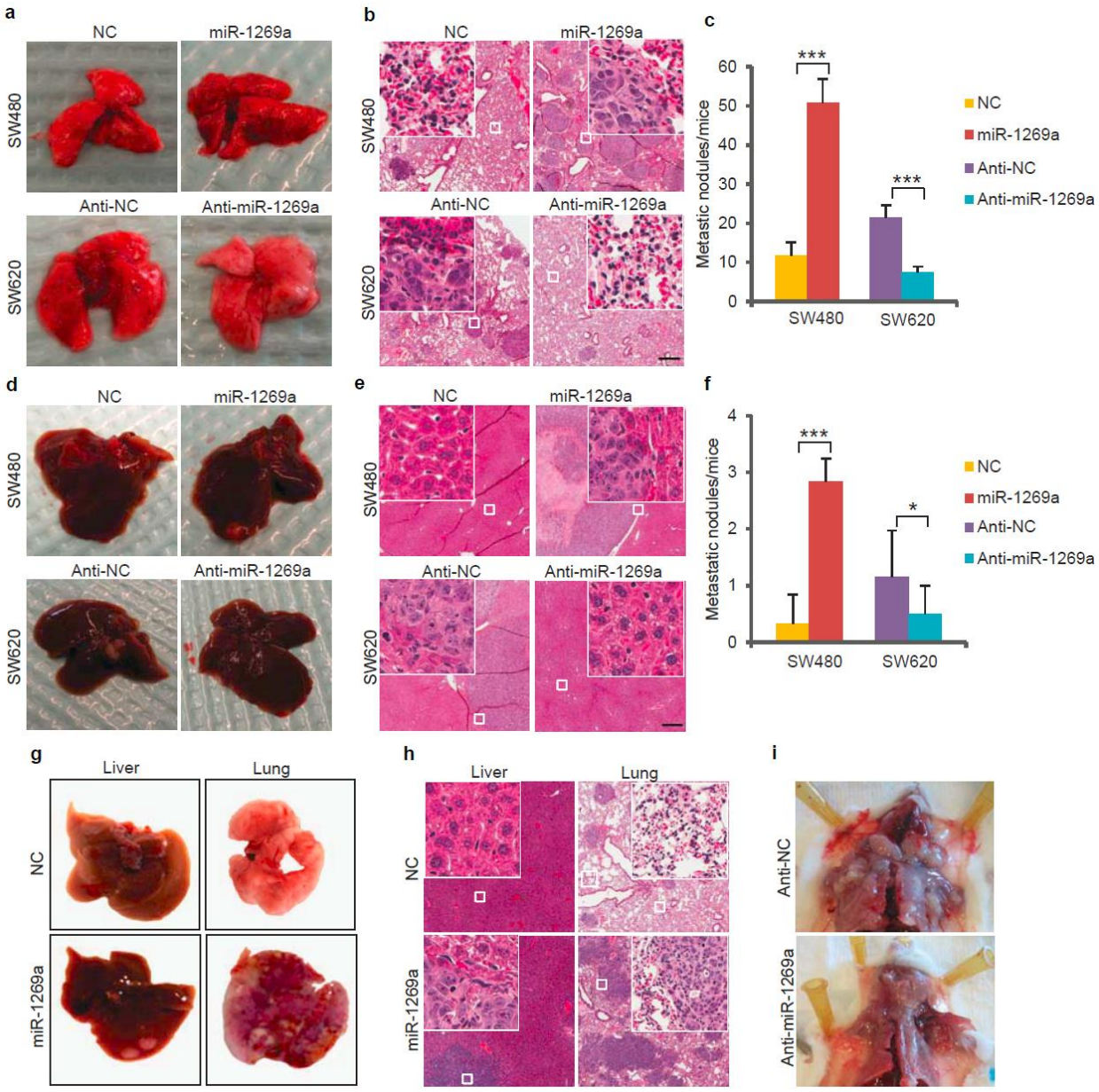

Figure 8. miR-1269a promotes CRC cell colonization of liver and lung after intravenous injection.

(a-c) Representative images (a), H&E staining (b), and number of metastatic nodules (c) of lung metastasis. Ectopic miR-1269 expression promoted lung metastasis of SW480 cells (upper panel). Knockdown of endogenous miR-1269 by antisense RNA suppressed lung metastasis of SW620 cells (lower panel). **(d-f)** Representative images (d), H&E staining (e), and number of metastatic nodules (f) of liver metastasis. Ectopic miR-1269 expression promoted liver metastasis of SW480 cells (upper panel). Knockdown of endogenous miR-1269 by antisense RNA suppressed liver metastasis of SW620 cells (lower panel). **(g-h)** Representative images (g), H&E staining of liver and lung metastasis. Ectopic miR-1269 expression in HCT116 cells enhanced their liver and lung metastasis. **(i)** Representative images showing miR-1269 knockdown in LS174T cells reduced lymph

node metastasis. In the H&E staining, inserts highlight big magnification of the indicated regions. Error bars denote s.d. of triplicates. *, $p<0.05$; ***, $p<0.001$.

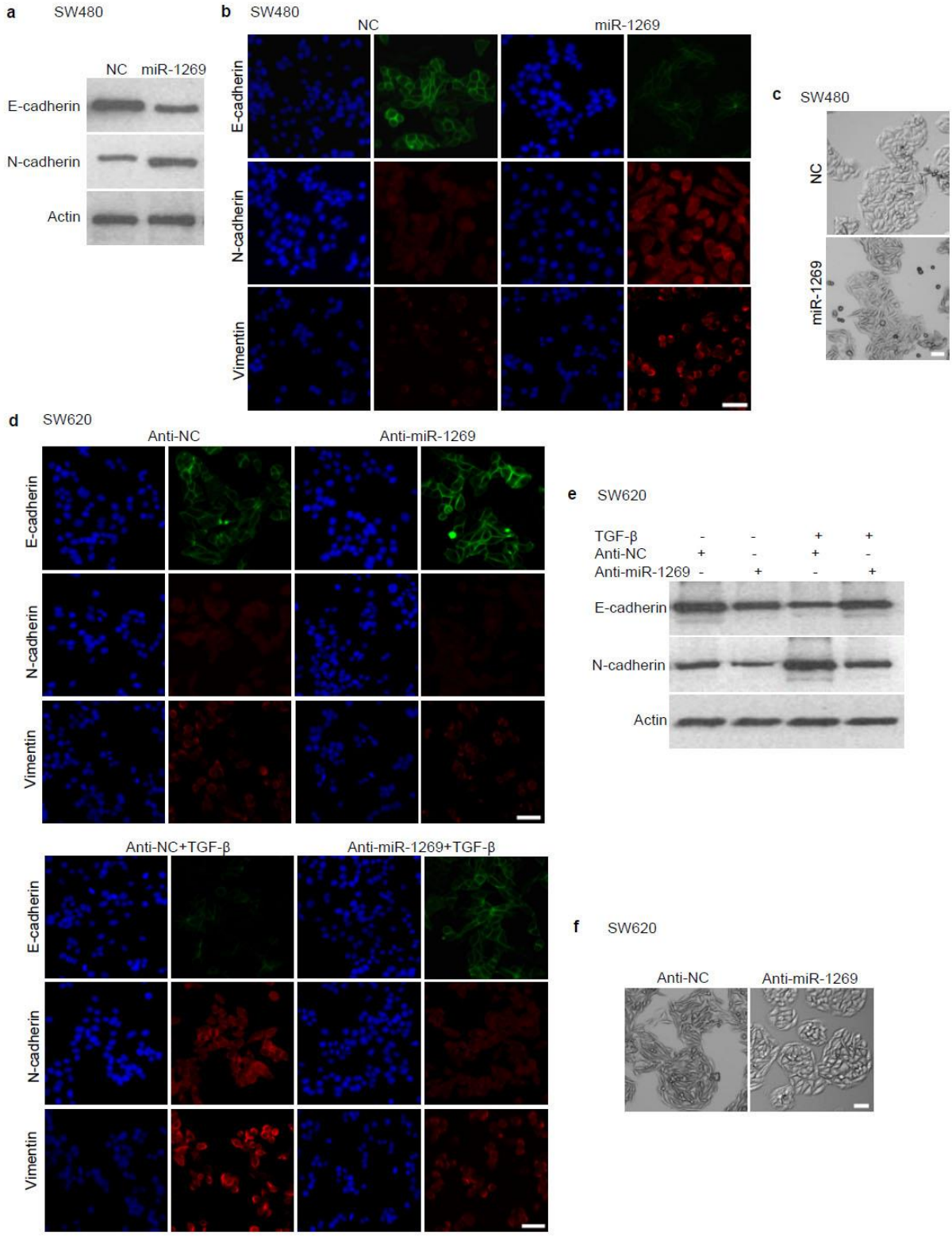
a
SW480
NC
miR-1269
E-cadherin
N-cadherin
Actin
b
SW480
NC
miR-1269
E-cadherin
N-cadherin
Vimentin
c
SW480
NC
miR-1269
d
SW620
Anti-NC
Anti-miR-1269
E-cadherin
N-cadherin
Vimentin
Anti-NC+TGF-β
Anti-miR-1269+TGF-β
E-cadherin
N-cadherin
Vimentin
e
SW620
TGF-β - - + +
Anti-NC + - + -
Anti-miR-1269 - + - +
E-cadherin
N-cadherin
Actin
f
SW620
Anti-NC
Anti-miR-1269

Figure 9. miR-1269a regulates EMT.

(**a-c**) Western blot (a), Immunofluorescence (b), and phase-contract images (c) of SW480 cells with a control vector (NC) or with ectopic miR-1269a expression (miR-1269a). Ectopic miR-1269a downregulated the epithelial marker E-cadherin, upregulated the mesenchymal markers N-cadherin and Vimentin, and changed cell morphology. (**d-f**) Immunofluorescence (d), Western blot (e), and phase-contract images (f) of SW620 cells with a control vector (Anti-NC) or with antisense RNA against endogenous miR-1269a (Anti-miR-1269a). SW620 cells are either untreated (d, upper panel) or treated with TGF-β (d, lower panel). miR-1269a knockdown suppressed TGF-β induction of EMT, as indicated by downregulation of N-cadherin and Vimentin, upregulation of E-cadeherin, and reversion from a mesenchymal-like morphology to an epithelial-like morphology. Scale bar, 15 μm.

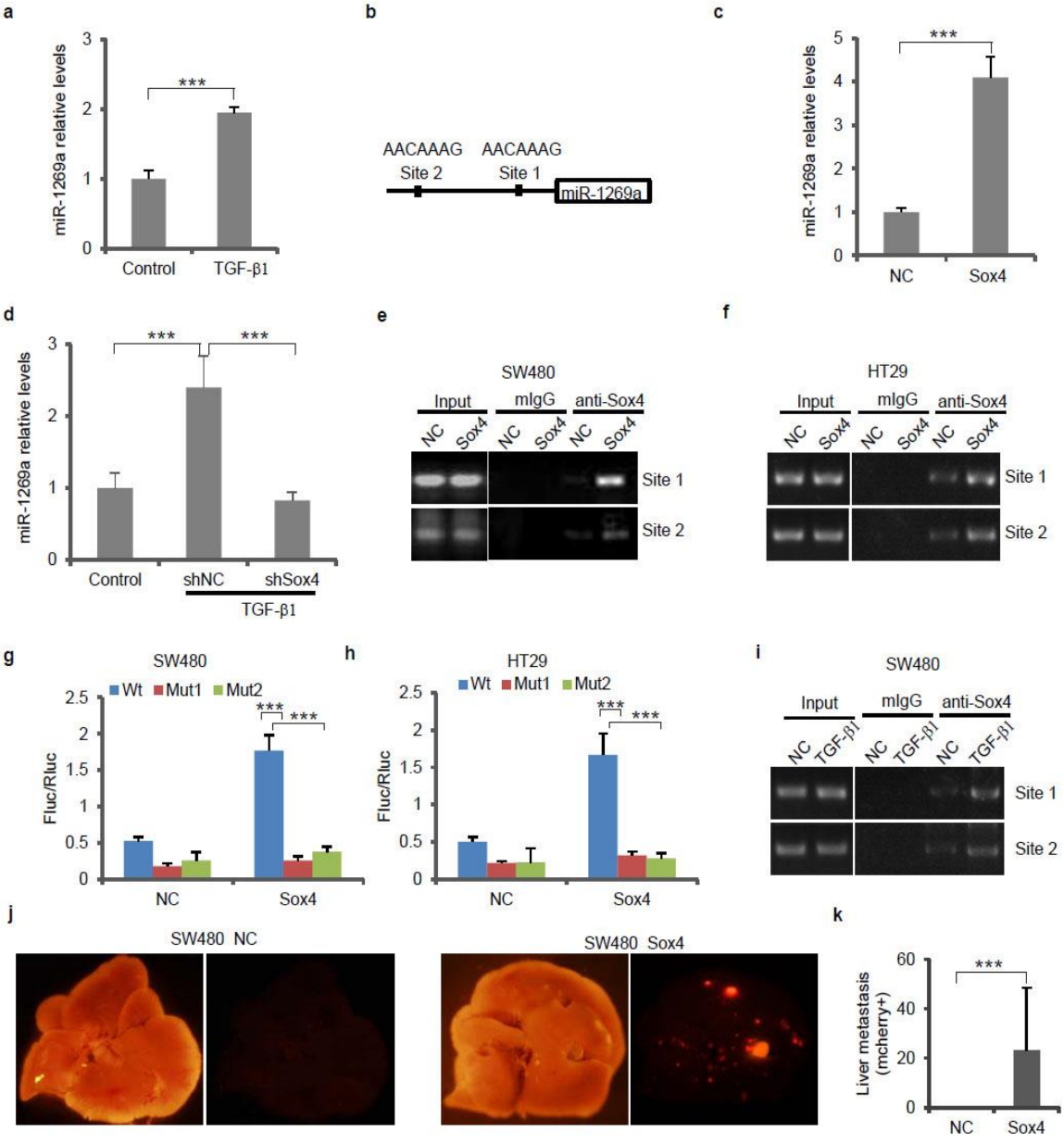
a
miR-1269a relative levels
***
Control
TGF-β1
b
AACAAAG
Site 2
AACAAAG
Site 1
miR-1269a
c
miR-1269a relative levels
***
NC
Sox4
d
miR-1269a relative levels
***
***
Control
shNC
shSox4
TGF-β1
e
SW480
Input
mIgG
anti-Sox4
NC
Sox4
Site 1
Site 2
f
HT29
Input
mIgG
anti-Sox4
Site 1
Site 2
g
SW480
Wt
Mut1
Mut2
Fluc/Rluc
NC
Sox4
h
HT29
i
SW480
Input
mIgG
anti-Sox4
NC
TGF-β1
Site 1
Site 2
j
SW480 NC
SW480 Sox4
k
Liver metastasis (mcherry+)
NC
Sox4

Figure 10. Sox4 activates miR-1269a expression directly.

(**a**) RT-qPCR showing TGF-β□treatment induces miR-1269a expression in SW480 cells. (**b**) A schematic diagram illustrating the two putative Sox4 binding sites in the miR-1269a promoter. (**c**) RT-qPCR showing ectopic Sox4 expression upregulates miR-1269a expression in SW480 cells. (**d**) RT-qPCR showing Sox4 knockdown by a shRNA abolishes TGF-β□induction of miR-1269a. (**e, f**) ChIP assay of SW480 (e) and HT29 (f) cells infected with a control (NC) or a Sox expression (Sox4) vector. Binding of Sox4 to the two sites was confirmed by PCR with primers specific for the two sites. (**g, h**) Luciferase reporter assays confirming Sox4 activation of the miR-1269a promoter through the two Sox4 binding sites in SW480 (g) and HT29 (h) cells. Expression of firefly luciferase (Fluc) was driven by miR-1269a promoter sequences containing either wild-type (Wt) or mutated (Mut1, Mut2) Sox4 binding sites. Ectopic expression of Sox4 upregulates luciferase in Wt cells, but not in Mut1 and Mut2 cells. Fluc signals were normalized by a simultaneously delivered Renillar luciferase (Rluc) expression plasmid. (**i**) ChIP assay of SW480 cells treated with TGF-β. Sox4 binding to the two sites was confirmed by PCR with primers specific for the two sites. (**j, k**) Bright field and fluorescent (mCherry) images of livers isolated from mice orthotopically injected with SW480-NC and SW480-Sox4 cells (j), and number of liver metastatic nodules. Ectopic Sox4 expression promoted liver metastasis of SW480 cells. Error bars in (k) denote s.d of each group (8 mice). In remaining cases, error bars denote s.d. of triplicates. ***, $p<0.001$.

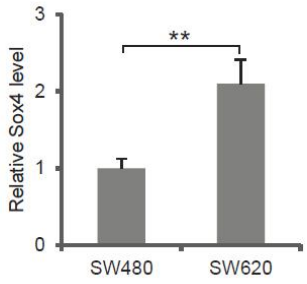

Figure 11. Sox4 expression in SW480 and SW620 cells.
Sox4 expression levels in SW620 and SW480 cells, measured by RT-qPCR. Error bars denote s.d. of triplicates. **, $p<0.01$.

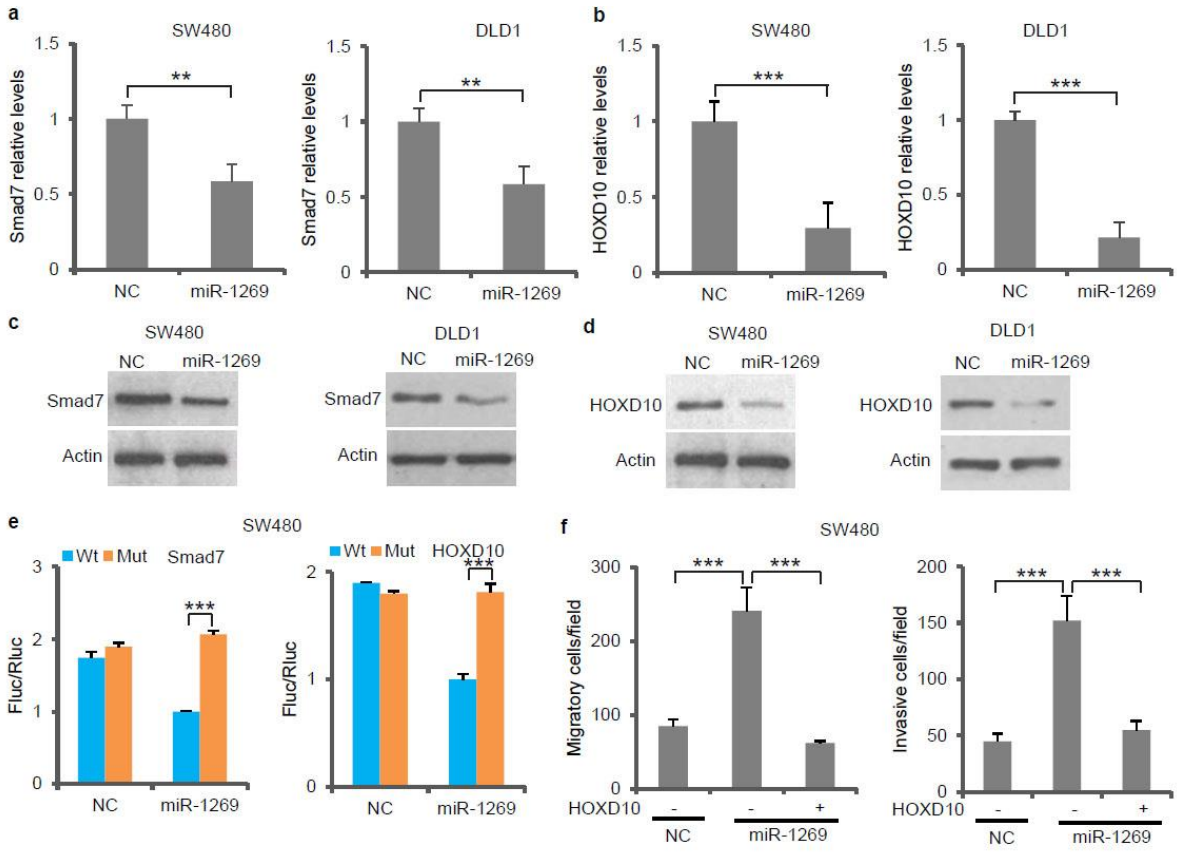

Figure 12. HOXD10 and Smad7 are direct targets of miR-1269a.

(**a,b**) RT-qPCR of Smad7 (a) and HOXD10 (b) mRNA levels in SW480 and HT29 cells with a control vector (NC) or with an ectopic miR-1269a expression vector (miR-1269a). (**c,d**) Western blot of Smad7 (c) and HOXD10 (d) protein levels in SW480 and HT29 cells with a control vector (NC) or with an ectopic miR-1269a expression vector (miR-1269a). (**e**) Luciferase reporter assays confirming the miR-1269a binding sites in Smad7 and HOXD10 3`UTRs. 3`UTRs of Smad7 (left) and HOXD10 (right) containing wild-type (Wt) or mutated (Mut) putative miR-1269a binding sites were cloned into the 3`UTR of firefly luciferase (Fluc). Ectopic miR-1269a expression in SW480 cells downregulated luciferase in Wt cells, but not in Mut cells. Fluc signals were normalized by a simultaneously delivered Renillar luciferase (Rluc) expression plasmid. (**f**) Transwell migration assay (left) and Matrigel invasion assay (right) of SW480 cells carrying control (NC) or miR-1269a expression (miR-1269a) vectors. Transient expression of HOXD10 abrogated miR-1269a induced migration and invasion. Error bars denote the s.d. between triplicates. (**g,h**) Bright field and fluorescent (mCherry) images of livers isolated from mice orthotopically injected with SW620-NC and SW620-HOXD10 cells (j), and number of liver metastatic nodules (h). Ectopic HOXD10 expression reduced liver metastasis of SW620 cells. Error bars in (h) denote s.d. of each group (8 mice). In remaining cases, error bars denote s.d. of triplicates. ***, p<0.001; **, p<0.01; ***, p<0.001.

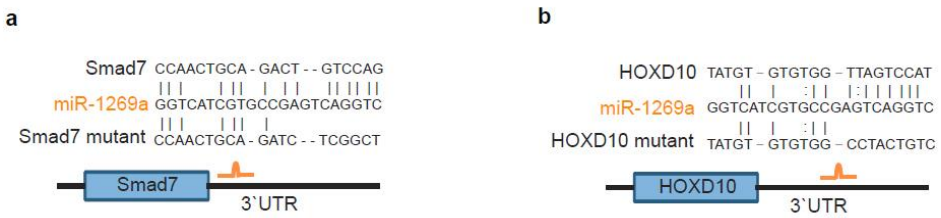

Figure 13. Schematic representation of miR-1269a binding sites in the Smad7 and HOXD10 3`UTR.

(**a**) The predicted duplex formations between Smad7 3` UTR and miR-1269a, and mutation introduced to the seed region. (**b**) The predicted duplex formations between HOXD10 3` UTR and miR-1269a, and mutation introduced to the seed region.

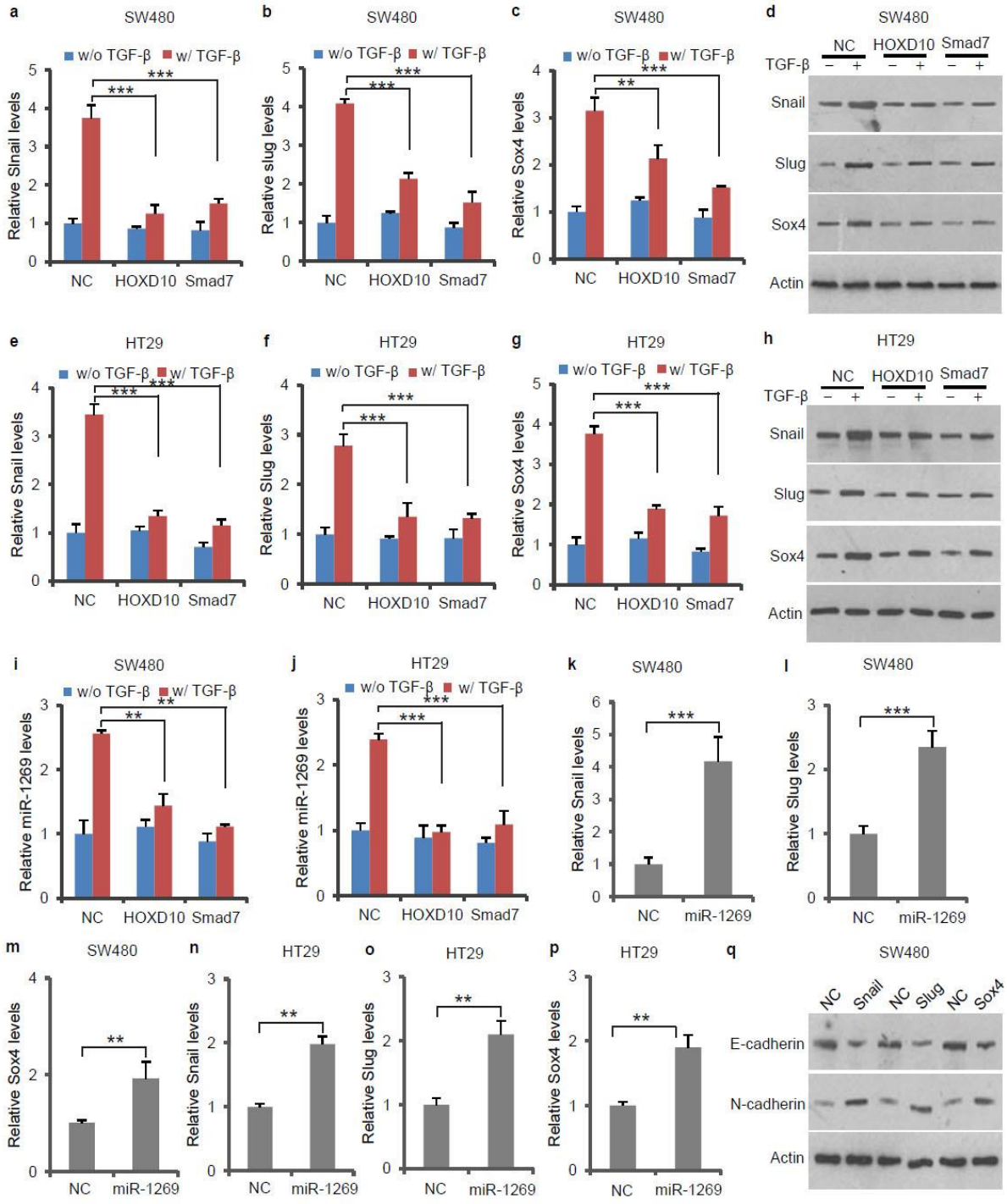

Figure 14. miR-1269a upregulates TGF-β signaling by targeting Smad7 and HOXD10.

(**a**) Western blot of phosphorylated Smad2, levels of which were increased by ectopic miR-1269a expression or knockdown of Smad7 or/and HOXD10. (**b-e**) RT-qPCR and Western blot showing ectopic expression of HOXD10 or Smad7 significantly reduced

TGF-β induction of Snail, Slug and Sox4 expression in SW480. (**f**) RT-qPCR showing ectopic expression of HOXD10 or Smad7 significantly reduced TGF-β induction of miR-1269a in SW480 cells. (**g-i**) RT-qPCR showing ectopic expression of miR-1269a upregulated Snail, Slug, and Sox4 in SW480 cells. (**j**) Western blot showing ectopic Snail, Slug or Sox4 upregulated E-cadherin and downregulated N-cadherin in SW480 cells. (j) ELISA assay showing that ectoptic miR-1269a expression increased TGF-β1 level in SW480 medium. (k) ELISA assay showing that knockdown of Smad7 and HOXD10 had little effect on TGF-β1 level in SW480 medium. In all case, error bars denote s.d. of triplicates. **, $p<0.01$; ***, $p<0.001$.

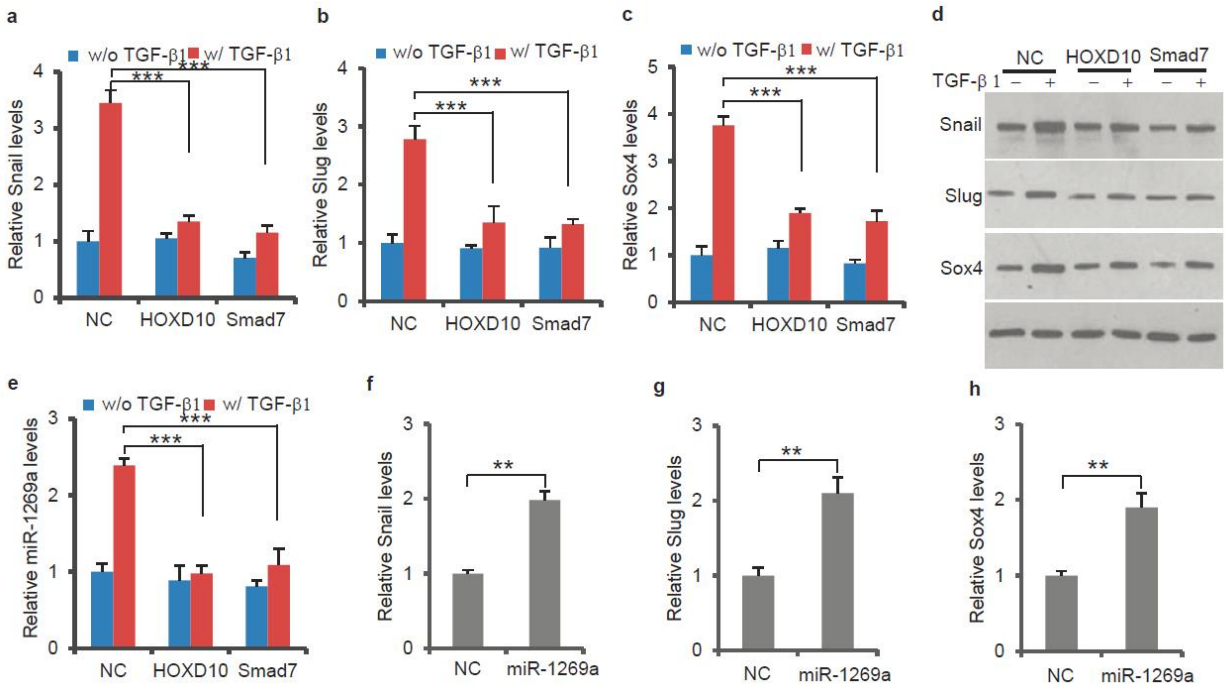

Figure 15. miR-1269a upregulates TGF-β1 signaling by targeting Smad7 and HOXD10.

(**a**-**d**) RT-qPCR (a-c) and Western blot (d) showing ectopic expression of HOXD10 or Smad7 reduced TGF-β1 induction of Snail (a), Slug (b) and Sox4 (c) expression HT29 cells. (**e**) RT-qPCR showing ectopic expression of HOXD10 or Smad7 reduced TGF-β1 induction of miR-1269a in HT-29 cells. (**f-h**) RT-qPCR showing ectopic expression of miR-1269a upregulated Snail (f), Slug (g), and Sox4 (h) in HT29 cells. Error bars denote the s.d. of triplicates. **, p<0.01; ***, p<0.001.

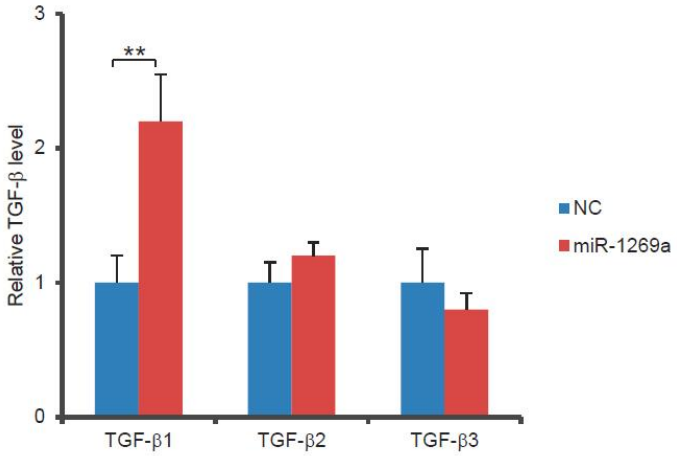

Figure 16. The effect of miR-1269a on TGF-β expression.

RT-qPCR showing that ectoptic expression of miR-1269a increased TGF-β1 expression with little effect on TGF-β2 and TGF-β3 expression. Error bars denote the s.d. of triplicates. **, $p<0.01$.

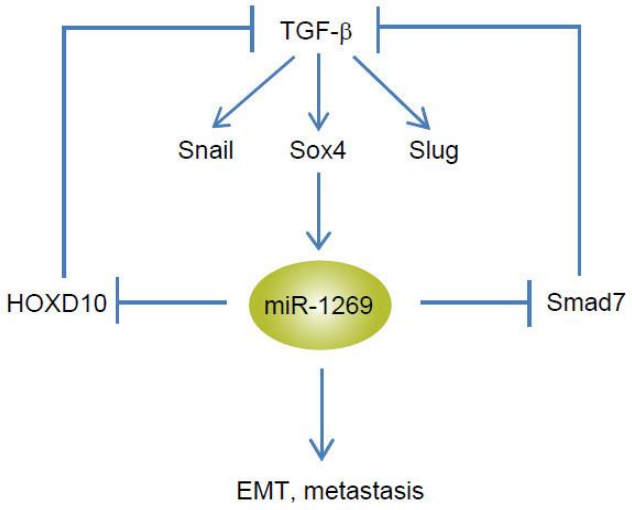

Figure 17. A positive feedback loop between TGF-β and miR-1269a.

A schematic illustration of the positive feedback loop. miR1269a upregulates TGF-β1 and TGF-β signaling by suppressing its antagonists Smad7 and HOXD10. TGF-β in turn upregulates miR-1269 through Sox4.

Table 1. Top 16 microRNAs upregulated in stage IV CRCs vs. stage I/II CRCs.

Rank	MicroRNA	Means of read counts	Fold change	p value
1	hsa-mir-1269	240.56	2.74	1.12E-02
2	hsa-mir-105-1	15.60	2.69	2.89E-02
3	hsa-mir-105-2	16.10	2.63	3.53E-02
4	hsa-mir-34c	10.23	1.75	2.13E-05
5	hsa-mir-149	33.99	1.65	2.83E-06
6	hsa-mir-31	67.06	1.51	4.88E-02
7	hsa-mir-337	72.28	1.27	1.25E-02
8	hsa-mir-9-1	530.79	1.25	3.34E-02
9	hsa-mir-9-2	529.92	1.23	3.68E-02
10	hsa-mir-495	17.81	1.20	2.29E-02
11	hsa-mir-654	77.74	1.19	4.56E-02
12	hsa-mir-154	19.61	1.18	1.76E-02
13	hsa-mir-136	105.70	1.16	5.30E-03
14	hsa-mir-708	165.49	1.14	3.98E-02
15	hsa-mir-323	11.29	1.11	1.25E-03
16	hsa-mir-431	29.40	1.10	2.67E-02

Table 2. Information of patients who provided tissue samples for comparing miR-1269 expression levels in early- vs. late – stage CRC tumors.

Patient	Gender	Age at visit	Stage	Differentiation	Lymph nodes
P1	M	52	I	Well	N0
P2	M	70	I	Poor	N0
P3	M	54	I	Moderate	N0
P4	F	84	I	Moderate	N0
P5	F	65	I	Moderate	N0
P6	M	43	IIA	NA	N0
P7	F	59	IIB	Poor	N0
P8	M	87	IIB	NA	N0
P9	F	62	IIB	Well	N0
P10	F	44	I	Moderate	N0
P11	M	85	I	NA	N0
P12	F	81	IIA	Moderate	N0
P13	F	74	IIIA	Poor	N1
P14	M	73	IIIA	Well	N1
P15	F	55	IIIA	NA	N1
P16	M	77	IIIC	Poor	N2
P17	F	68	IV	Poor	N2
P18	M	56	IV	Poor	N2
P19	F	21	IV	Moderate	N1
P20	F	46	IV	NA	N1
P21	F	73	IV	Moderate	N1
P22	M	66	IV	Poor	N1
P23	M	88	IV	Poor	N2
P24	F	73	IV	Poor	N1
P25	F	71	IIIC	NA	N2
P26	F	50	IIIC	Poor	N2
P27	F	39	IIIA	NA	N1
P28	M	37	IV	Poor	N2
P29	F	74	IIIC	Poor	N1

Table 3. Relationship between miR-1269 and clinic pathological features of 100 stage II CRC patients.

Variable	miR-1269 expression		P value
	Low (N=90) N (%)	High (N=10) N (%)	
Median age, years	70.3	73.3	0.35[a]
Age category, years			0.52[b]
=<70	44 (48.9%)	3 (30%)	
>70	46 (51.1%)	7 (70%)	
Sex			0.28[b]
Male	65 (72.2%)	9 (90%)	
Female	25 (27.8%)	1 (10%)	
Event[c]			
Liver metastasis	10 (11.1%)	4 (40%)	
Liver+other metastasis	1 (1.1%)	1 (10%)	
Other metastasis	4 (4.4%)	0	
Locoregional	1 (1.1)	1 (10%)	
No events	74 (82.3)	4 (40%)	

a, Mann-Whitney test

b, Fisher exact test

c, Metastasis occurred after surgery

REFERENCES

1. Yokota, J. Tumor progression and metastasis. Carcinogenesis 21, 497-503 (2000).
2. Quail, D. F. & Joyce, J. A. Microenvironmental regulation of tumor progression and metastasis. Nat Med 19, 1423-1437, doi:10.1038/nm.3394 (2013).
3. Siegel, R. et al. Cancer treatment and survivorship statistics, 2012. CA: a cancer journal for clinicians 62, 220-241, doi:10.3322/caac.21149 (2012).
4. Siegel, R., Naishadham, D. & Jemal, A. Cancer statistics, 2012. CA: a cancer journal for clinicians 62, 10-29, doi:10.3322/caac.20138 (2012).
5. Fearon, E. R. & Vogelstein, B. A genetic model for colorectal tumorigenesis. Cell 61, 759-767 (1990).
6. Valastyan, S. & Weinberg, R. A. Tumor metastasis: molecular insights and evolving paradigms. Cell 147, 275-292, doi: 10.1016/j.cell.2011.09.024 (2011).
7. Benson, A. B., 3rd et al. American Society of Clinical Oncology recommendations on adjuvant chemotherapy for stage II colon cancer. J Clin Oncol 22, 3408-3419 (2004).
8. Chun, P. & Wainberg, Z. A. Adjuvant Chemotherapy for Stage II Colon Cancer: The Role of Molecular Markers in Choosing Therapy. Gastrointestinal cancer research: GCR 3, 191-196 (2009).
9. Croce, C. M. Causes and consequences of microRNA dysregulation in cancer. Nat Rev Genet 10, 704-714, doi:10.1038/nrg2634 (2009).
10. Kasinski, A. L. & Slack, F. J. Epigenetics and genetics. MicroRNAs en route to the clinic: progress in validating and targeting microRNAs for cancer therapy. Nat Rev Cancer 11, 849-864, doi:10.1038/nrc3166 (2011).
11. Valeri, N. et al. MicroRNA-135b Promotes Cancer Progression by Acting as a Downstream Effector of Oncogenic Pathways in Colon Cancer. Cancer Cell 25, 469-483, doi: 10.1016/j.ccr.2014.03.006 (2014).
12. The Cancer Genome Atlas Network. Comprehensive molecular characterization of human colon and rectal cancer. Nature 487, 330-337, doi:10.1038/nature11252 (2012).
13. Colonomics.org. http://bioinfo.iconcologia.net/colonomics/. (2014).
14. Leibovitz, A. et al. Classification of human colorectal adenocarcinoma cell lines. Cancer research 36, 4562-4569 (1976).
15. Fu, X. Y., Besterman, J. M., Monosov, A. & Hoffman, R. M. Models of human metastatic colon cancer in nude mice orthotopically constructed by using histologically intact patient specimens. Proceedings of the National Academy of Sciences of the United States of America 88, 9345-9349 (1991).

16. Cespedes, M. V. et al. Orthotopic microinjection of human colon cancer cells in nude mice induces tumor foci in all clinically relevant metastatic sites. The American journal of pathology 170, 1077-1085, doi:10.2353/ajpath.2007.060773 (2007).
17. Brabletz, T. et al. Invasion and metastasis in colorectal cancer: epithelial-mesenchymal transition, mesenchymal-epithelial transition, stem cells and beta-catenin. Cells, tissues, organs 179, 56-65, doi:10.1159/000084509 (2005).
18. Kuwahara, M. et al. The transcription factor Sox4 is a downstream target of signaling by the cytokine TGF-beta and suppresses T(H)2 differentiation. Nature immunology 13, 778-786, doi:10.1038/ni.2362 (2012).
19. Tiwari, N. et al. Sox4 is a master regulator of epithelial-mesenchymal transition by controlling Ezh2 expression and epigenetic reprogramming. Cancer Cell 23, 768-783, doi: 10.1016/j.ccr.2013.04.020 (2013).
20. Ma, L., Teruya-Feldstein, J. & Weinberg, R. A. Tumour invasion and metastasis initiated by microRNA-10b in breast cancer. Nature 449, 682-688, doi:10.1038/nature06174 (2007).
21. Yan, X., Liu, Z. & Chen, Y. Regulation of TGF-beta signaling by Smad7. Acta biochimica et biophysica Sinica 41, 263-272 (2009).
22. Hamfjord, J. et al. Differential expression of miRNAs in colorectal cancer: comparison of paired tumor tissue and adjacent normal mucosa using high-throughput sequencing. PLoS One 7, e34150, doi: 10.1371/journal.pone.0034150 (2012).
23. Ebert, M. S. & Sharp, P. A. Roles for microRNAs in conferring robustness to biological processes. Cell 149, 515-524, doi: 10.1016/j.cell.2012.04.005 (2012).
24. Calon, A. et al. Dependency of colorectal cancer on a TGF-beta-driven program in stromal cells for metastasis initiation. Cancer Cell 22, 571-584, doi: 10.1016/j.ccr.2012.08.013 (2012).

Chapter 5

CONCLUDING REMARKS AND FUTURE DIRECTIONS

5.1 Conclusion

We have previously reported that asymmetric distribution of miR-34a determines colon cancer stem cell (CCSC) asymmetry by creating bimodal Notch signaling in daughter cells. However, it remained unknown how miR-34a asymmetry in cancer stem cells is initiated and how miR-34a is eventually silenced in many types of cancer. My thesis described a novel lncRNA, lnc34a, that is capable of initiating CCSC asymmetric division. Lnc34a directly targets the miR-34a promoter to epigenetically silence miR-34a expression through recruitment of epigenetic regulators HDAC1 and DNMT3a via PHB2. Clinical data has confirmed a strong correlation between the upregulation of the lncRNA and epigenetic miR-34a silencing along colorectal cancer (CRC) progression. This study elucidated that lncRNAs not only target protein-coding genes but also target microRNAs such as miR-34a via epigenetic silencing. Furthermore, the finding that spatial imbalance of a lncRNA can initiate cancer stem cell asymmetric division highlights the versatility of ncRNA regulation. Given that miR-34a regulates cell division in both colon cancer stem cells and normal intestine/colon stem cells.

Further studies revealed that miR-34a-mediated asymmetric divisions also occur in normal intestine/colon stem cells. Normal intestine/colon stem cells normally divide symmetrically, but switch to asymmetric division when trigged by inflammation. Loss of miR-34a abolishes stem cell asymmetric division and further induces stem cell

proliferation. We showed that inflammation promotes intestine/colon stem cell proliferation for regeneration, but miR-34a-mediated asymmetric division limits excessive colon stem cell proliferation, serving as a safeguard against hyperplasia.

Infection of gut pathogens and microbial dysbiosys causes chronic inflammation that has been associated with CRC. In the thesis, we described that miR-34a deficiency led to colon tumorigenesis after *Citrobacter rodentium* infection while wildtype mice treated by *C. rodentim* only resulted in inflammation. Mechanistically, loss of miR-34a systematically increased IL-6R and IL-23R expression in immune cells to facilitate Th17 cell differentiation from CD4 T cells. By targeting chemokine CCL22 and IL-17RD in epithelial cells, miR-34a blocks Th17 cells recruitment to colon epithelium and inhibits colon stem cell proliferation. Thus, miR-34a targets both immune and epithelial cells to restrain inflammation-induced reparative regeneration. This study provided a novel insight into colon stem cell niche and inflammation-mediated colon tumorigenesis.

Cancer metastasis continues to account for most of cancer-related deaths and remains a clinical challenge. Current chemotherapy for advanced CRC does not target metastases specifically. Discovery and targeting CRC metastasis biomarker could be a promising approach for CRC therapy. miRNAs may be utilized as prognostic indicators and therapeutic targets due to their stability and robust expression pattern. In this study, a novel miRNA, miR-1269, was discovered by analyzing the colon adenocarcinoma (COAD) miRNASeq dataset in TCGA. miR-1269 promotes colorectal cancer (CRC) metastasis through a positive feedback loop with TGF-β signaling. miR-1269 is upregulated in late-stage CRCs, and long-term monitoring of 100 stage II CRC patients revealed that miR-

1269 expression in their surgically removed primary tumors correlates strongly with risk of CRC relapse and metastasis.

5.2 Future directions

1. A Long Non-Coding RNA Targets MicroRNA miR-34a to Regulate Colon Cancer Stem Cell Asymmetric Division

In this study presented in my thesis, we discovered a novel lncRNA, Lnc34a. Lnc34a silences miR-34a by recruiting Dnmt3a via PHB2 and HDAC1 to methylate and deacetylate the miR-34a promoter. Spatial imbalance of Lnc34a regulates asymmetric division of colon cancer stem cells (CCSCs), and high lnc34a expression promotes CCSC self-renewal and colon cancer growth. It is also important to know whether Lnc34a also regulates normal intestine/colon stem cell fate like miR-34a does. If Lnc34a does function in normal stem cells, does it share the same mechanism as it does in CCSCs?

Lnc34a is highly expressed in CCSCs and low in non-CCSCs. In addition, Lnc34a expression is closely correlated with CRC progression with higher level in late stage of CRC in contrast to early stage of CRC. However, it is still unknown how lnc34a expression is regulated. RNA FISH showed Lnc34a co-localized with ALDH1 while mutually exclusive with miR-34a during the CCSC division, which raised an important question: What is the mechanism causing Lnc34a asymmetric distribution? Also, do Lnc34a asymmetric distribution and upregulation share the same mechanism?

2. MicroRNA miR-34a provides a barrier against inflammation-induced colon stem cell proliferation and oncogenesis

This study demonstrates that the miR-34a plays a central role in protecting tissue integrity during inflammation-induced reparative regeneration. miR-34a deficient mice develop colon tumors after infection of the pathogenic *Citrobacter* bacteria, whereas wild-type mice always recover without tumor formation. It turned out that miR-34a controls both pro-inflammatory immune cells and the colon epithelial cells. miR-34a suppresses the differentiation and expansion of Th17 cells by targeting IL-6R and IL-22R, hinders recruitment of Th17 cells to the colon epithelium by targeting CCL22, and limits stem cell proliferation by targeting IL-17RD. However, this conclusion primarily arises from data collected from a colorectal cancer mouse model. The clinical relevance of these findings has not been compellingly demonstrated. The RNA22 algorithm identified putative miR-34a binding sites of human IL-6R, IL-23R, CCL22, and IL-17RD. Experiments need to be performed to validate the miR-34a potential targets and regulation mechanism in humans.

3. miR-1269 Promotes Metastasis and Forms a Positive Feedback Loop with TGF-β

The study presented in my thesis provides evidence that miR-1269 forms feedback loop with TGF-β to induce CRC cell EMT and metastasis. In the feedback loop, activation of TGF-β signaling upregulates miR-1269 expression. miR-1269 in turn amplifies TGF-β signaling activity by directly targeting TGF-β signaling inhibitor, Hoxd10 and Smad7. miR-1269 is upregulated in late-stage CRCs and correlates strongly with relapse and metastasis of stage II CRC patients after surgical removal of their primary tumors. However, there are remaining issues that need to be further investigated. For instance, TGF-β is required for initiation of the feedback loop. However, it is largely unknown where the TGF-β are from. It has been reported that tumor cells could produce TGF-β to sustain

TGF-β signaling activity. Alternatively, TGF-β could also be provided by tumor environment such as stroma cells. Investigation of the role of TGF-β in the tumor microenvironment will enhance our understanding of the TGF-β/miR-1269 axis in the context of CRC metastasis and prognosis.